https://ntrs.nasa.gov/search.jsp?R=19660024916 2020-03-16T20:19:12+00:00Z

CR 65458

July 28, 1966
Project No. 303260
Copy No. _____

THIN FILM PIEZOELECTRIC RESONATING DEVICE

Final Report

May 28, 1965, through July 28, 1966

Contract No. NAS 9-4373
National Aeronautics and Space Administration
Manned Spacecraft Center

GPO PRICE $ _____

CFSTI PRICE(S) $ _____

Hard copy (HC) 2.50

Microfiche (MF) .75

ff 653 July 65

FACILITY FORM 602

N66 34206 (ACCESSION NUMBER)

(THRU)

88 (PAGES)

1 (CODE)

CR-65458 (NASA CR OR TMX OR AD NUMBER)

09 (CATEGORY)

By: T. R Sliker
D. A. Roberts

Clevite Corporation
Electronic Research Division
Cleveland, Ohio 44108

ABSTRACT

34206

A new type of miniature resonator for the 100-1000 MHz range has been developed which consists of a piezoelectric CdS transducer evaporated onto a single crystal quartz wafer. Energy trapping principles have been applied to localize the acoustic energy in the quartz wafer to the volume under and immediately surrounding the electrically driven CdS film. Resistances at resonance of 50 ohms and electrical Q's of 5000 typically have been realized with 279 MHz devices. Both shear and longitudinal mode resonators have been fabricated, but shear mode operation has the important advantage that devices with a zero frequency-temperature coefficient are possible.

FOREWARD

This report was prepared by Clevite Corporation, 540 East 105th Street, Cleveland, Ohio 44108, under NASA Contract No. NAS 9-4373. The work was administered under the direction of the Manned Spacecraft Center, Mr. S. Gaudiano, Contract Monitor.

This report covers research work conducted from May 28, 1965, to July 28, 1966, in the Electronic Research Division, Dr. Hans Jaffe, Director. Mr. Don A. Berlincourt is Head, Electromechanical Research Department. Dr. Todd R. Sliker is Head, Applied Physics Section, and served as Principal Investigator for this project. A. Guard and J. E. Tozier contributed significantly to the experimental work and assisted in writing this report. Other persons who contributed to this project are W. K. Bower, W. R. Cook, Jr., P. Rander, and C. Hora.

TABLE OF CONTENTS

LIST OF ILLUSTRATIONS

LIST OF ILLUSTRATIONS (Cont'd)

THIN FILM PIEZOELECTRIC RESONATING DEVICE

Final Report
May 28, 1965, through July 28, 1966
Contract No. NAS 9-4373

1. INTRODUCTION

This final report describes work done on a new type of high frequency piezoelectric resonator. The work has been sponsored by the Manned Spacecraft Center of the National Aeronautics and Space Administration under Contract No. NAS 9-4373. The contract, which was entered into as of May 28, 1965, called for the development and delivery of a total of twenty-four resonators. The contract specified that four resonators were to be in hermetically sealed packages and four resonators were not to be in hermetically sealed packages at each of the following three operating frequencies: 259.7, 279.0, and 296.8 MHz.

The objective of the contract has been "to fabricate functional piezoelectric resonating devices to useful specifications with vacuum techniques." The contract described these useful specifications in terms of performance goals and requirements as follows:

"1. TEMPERATURE: The resonator shall operate over a temperature range from 40 to 120 degrees Fahrenheit. (Performance Requirement).

2. VOLTAGE: The resonator shall have a minimum voltage breakdown of 30 V rms when measured at the maximum temperature. (Performance Requirement).

3. LOADED Q: The resonator shall exhibit a Q of 1000 minimum when operating into a resistive load equal to its output impedance. (Performance Requirement).

4. INSERTION LOSS: The insertion loss of the resonator shall be less than 1.0 db when measured at the design center frequency. (Performance Goal).

5. FREQUENCY SHIFT: The maximum frequency shift allowable shall be .005 from the design center frequencies under all conditions of voltage and temperature. (Performance Goal). (A maximum of no more than 1% is a performance requirement).

6. DESIGN CENTER FREQUENCIES: The resonators shall be fabricated to the following frequencies 259. 7, 279. 0 and 296. 8 MHz ± . 001%.(Performance Goal).

7. RESONANCE IMPEDANCE: The series impedance at resonance shall be 50 ohms nominal. (Performance Goal). "

Near the end of this final report we will compare the electrical characteristics of the resonators that have been fabricated with the contract performance goals and requirements.

The composite resonators that have been developed under this contract depend on the piezoelectric properties of vacuum deposited films of cadmium sulfide. The deposition and structural properties of vacuum deposited films of CdS have been under investigation for a number of years. In 1959, L. R. Shiozawa of these laboratories first observed that the growth rate of CdS along the c-axis is strongly connected with its polarity. He then demonstrated that as a result of the growth polarity, polycrystalline layers deposited from the vapor phase are strongly piezoelectric. Subsequently, Foster[1, 2] at Bell Laboratories and deKlerk[3, 4] at Westinghouse observed substantial piezoelectric effects in very thin vapor deposited CdS layers,and they showed that these layers may be used as transducers in the frequency range above 100 MHz. Foster has evaporated CdS transducers for longitudinal or shear mode generation with losses as low as 6 db per transducer at 300 MHz. He has studied the evaporation conditions required to produce such efficient transducers. He and others at Bell Laboratories have used this knowledge in the fabrication of high frequency acoustic delay lines. J. deKlerk and his co-workers have produced single and multiple layer CdS transducers operating in the microwave region. They have used these transducers in studies of the acoustic attenuation properties of various solids as a function of temperature.

The basic idea for the composite resonator to be described in this report was conceived by D. R. Curran while a section head in these laboratories. Since September 1965, Mr. Curran has been Filter Products Manager with Clevite's Piezoelectric Division.

The composite resonator is shown schematically in Fig. 1. The thickness of the CdS layer is chosen so that there is one-half standing acoustic wave in the CdS at the principal resonance. The thickness of the quartz is chosen so that there are an integral number of half-waves in the quartz at this principal resonance. Typically, we have chosen to have 9 $\lambda/2$ standing acoustic waves in the quartz. The metal electrodes are on the order of 1000 Å thick, which is much less than the thickness of either the quartz or the CdS layer. The quartz single crystal wafer is part of the resonant structure, but according to energy trapping theory[5-7] most of the acoustic energy is localized in the volume under and immediately surrounding the electroded area. The c-axis of the CdS can be oriented with respect to the substrate normal to produce primarily either longitudinal or shear waves. The potential advantage of generating shear waves is that a cut of quartz near to the AT-cut can be used to balance out the frequency-temperature dependence of the CdS layer. Hence, the frequency-temperature dependence of the complete composite resonator can in principle be made zero. If the c-axis of the CdS is normal to the substrate, longitudinal mode acoustic waves will be generated and there is no cut of crystal quartz that can then be used to produce a composite resonator with a zero frequency-temperature dependence. However, it is experimentally easier to produce longitudinal mode CdS films than shear mode films. The resonators may be accurately tuned by evaporating a layer of SiO_x.[8] Several resonators, which may all be on the same wafer, may then be combined in a filter network.

The most common way to fabricate a compact resonator whose frequency is independent of temperature (in the vicinity of room temperature) is to electrode an AT-cut wafer of crystal quartz on both faces. Because the fundamental resonance frequency of these conventional resonators is inversely proportional to the thickness of the quartz wafer, the wafers must be very thin at high frequencies. An AT-cut wafer would have to be 0.025 mm thick to have a fundamental frequency of about 65 MHz. A wafer this thin is on the border of present manufacturing capabilities. It is possible, of course, to operate at odd overtones (n = 3, 5, 7, . . .) of the fundamental frequency, but under idealized conditions the electromechanical coupling factor k is reduced accordingly (1/3, 1/5, 1/7, . . .). A great advantage of the

composite resonator over a conventional resonator operating at a high overtone is that the effective electromechanical coupling factor is significantly higher for the same frequency and wafer thickness. This means that the composite resonator has a substantially greater bandwidth than the corresponding conventional resonator. It is anticipated that the composite resonator will have its greatest utility for frequencies between 100 and 1000 MHz.

Section 2 of this report presents a mathematical analysis of the design considerations and expected performance of the composite resonator. A number of piezoelectric parameters are calculated as a function of the angle between the hexagonal c-axis of CdS and the applied electric field. Probably the most important of these parameters is the electromechanical coupling factor since it shows under what conditions it is possible to obtain pure shear or pure longitudinal mode generation. Starting with the basic piezoelectric equations, an equivalent circuit is derived for both shear and longitudinal mode composite resonators in terms of fundamental physical parameters. From this it is possible to derive an expression for the composite resonator impedance as a function of frequency. A computer solution of the impedance function is given. The problem of the exact quartz cut required for a temperature stable composite resonator is considered.

The techniques which have been developed for the successful fabrication of composite resonators are given in Section 3. This section describes the apparatus; cleaning and evaporation procedures; and the mounting, tuning, and sealing of completed resonators. Test procedures and experimental measurements are reported in Section 4. Transmission circuit data are given as a function of temperature. Impedance and half-lattice bridge measurements are presented. Capacity measurements at 1 MHz and resistance measurements at dc are also included. The experimentally determined electrical characteristics of the composite resonators are compared with the contract specifications in Section 5.

2. ANALYSIS

2.1 Piezoelectric Equations for CdS Transducers

In writing the piezoelectric equations for evaporated films of CdS it is convenient to consider strain S and electric displacement D as the independent variables and stress T and electric field E as the dependent variables. Then in matrix form

$$T = c^D S - hD$$
$$E = -hS + \beta^S D \tag{1}$$

where c^D is the elastic stiffness at constant electric displacement, h is a piezoelectric stress constant, and β^S is the dielectric impermeability at constant strain. The c^D constants are fourth order tensors, the h constants are third order tensors, and the β^S constants are second order tensors. Both S and T are second order symmetric tensors while E and D are vectors. Standard notation has been used in writing these equations.[9, 10]

Evaporated CdS is found to deposit in the hexagonal or class 6 mm form. Although the c^D, h, and β^S constants have not been determined experimentally for rotated cuts for CdS, they can be calculated from the known constants[11] for unrotated cuts. In each case it will be assumed that the rotation is taken around the Y-axis. The amount of rotation is given by the angle θ between the c-axis of the hexagonal CdS and the normal to the electroded surfaces. The transformation equations for the c^D constants can be obtained from Eq. (53) given by Cady[12]. These equations are actually derived for quartz, but they also apply to CdS if c^D_{14} is set equal to zero. The transformation equations for the h constants are the same as Eq. (196) given by Cady for the e constants. The β^S constants transform according to Eq (148) given by Cady. If θ is zero, the c^D, h, and β^S matrix has the form shown in Table I. However, for θ not equal to zero, the c^D, h, and β^S matrix has the form shown in Table II. The constants are marked with a prime because they apply to a rotated cut. An exact solution of the nine piezoelectric equations implied by Table II has not been attempted because of its complexity. However, approximations can be used to simplify the problem. For example, since

$$\beta'^S_{13} = \sin\theta \cos\theta \, (\beta^S_{11} - \beta^S_{33}) \tag{2}$$

Table I. Matrix of c^D, h, and β^S constants for hexagonal CdS when the c-axis is parallel to the applied electric field E.

c_{11}^D	c_{12}^D	c_{13}^D	0	0	0	0	0	h_{31}
c_{12}^D	c_{11}^D	c_{13}^D	0	0	0	0	0	h_{31}
c_{13}^D	c_{13}^D	c_{33}^D	0	0	0	0	0	h_{33}
0	0	0	c_{44}^D	0	0	0	h_{15}	0
0	0	0	0	c_{44}^D	0	h_{15}	0	0
0	0	0	0	0	$\frac{c_{11}^D - c_{12}^D}{2}$	0	0	0
0	0	0	0	h_{15}	0	β_{11}^S	0	0
0	0	0	h_{15}	0	0	0	β_{11}^S	0
h_{31}	h_{31}	h_{33}	0	0	0	0	0	β_{33}^S

Table II. Matrix of c^D, h, and β^S constants for hexagonal CdS rotated around the Y-axis.

c'^D_{11}	c'^D_{12}	c'^D_{13}	0	c'^D_{15}	0	h'_{11}	0	h'_{31}
c'^D_{12}	c'^D_{22}	c'^D_{23}	0	c'^D_{25}	0	h'_{12}	0	h'_{32}
c'^D_{13}	c'^D_{23}	c'^D_{33}	0	c'^D_{35}	0	h'_{13}	0	h'_{33}
0	0	0	c'^D_{44}	0	c'^D_{46}	0	h'_{24}	0
c'^D_{15}	c'^D_{25}	c'^D_{35}	0	c'^D_{55}	0	h'_{15}	0	h'_{35}
0	0	0	c'^D_{46}	0	c'^D_{66}	0	h'_{26}	0
h'_{11}	h'_{12}	h'_{13}	0	h'_{15}	0	β'^S_{11}	0	β'^S_{13}
0	0	0	h'_{24}	0	h'_{26}	0	β'^S_{22}	0
h'_{31}	h'_{32}	h'_{33}	0	h'_{35}	0	β'^S_{13}	0	β'^S_{33}

and β_{11}^S and β_{33}^S are the same within about 5%, then $\beta_{13}^{'S} << \beta_{33}^{'S}$. The cross term c_{35}^D is given by

$$c_{35}^{'D} = \cos\theta \sin\theta \left[\sin^2\theta\, c_{11}^D - \cos^2\theta\, c_{33}^D + (\cos^2\theta - \sin^2\theta)(2c_{44}^D + c_{13}^D) \right] \quad (3)$$

and the curve is plotted for CdS in Fig. 2. It turns out that the maximum value of $c_{35}^{'D}$ is about 0.4×10^{10} N/m^2, whereas the typical values of $c_{33}^{'D}$ and $c_{55}^{'D}$ are 9.0 and 1.7×10^{10} N/m^2, respectively. Hence to a good approximation the thickness shear and longitudinal modes are uncoupled. Then, for thickness longitudinal modes the piezoelectric equations are

$$\begin{aligned} T_3 &\cong c_{33}^{'D} S_3 - h_{33}^{'} D_3 \\ E_3 &\cong -h_{33}^{'} S_3 + \beta_{33}^{'S} D_3 \quad . \end{aligned} \quad (4)$$

The corresponding equations for thickness shear modes are

$$\begin{aligned} T_5 &\cong c_{55}^{'D} S_5 - h_{35}^{'} D_3 \\ E_3 &\cong -h_{35}^{'} S_5 + \beta_{33}^{'S} D_3 \quad . \end{aligned} \quad (5)$$

The transformation equation for $c_{33}^{'D}$ is

$$c_{33}^{'D} = \sin^4\theta\, c_{11}^D + \cos^4\theta\, c_{33}^D + 2\sin^2\theta \cos^2\theta\, (2c_{44}^D + c_{13}^D). \quad (6)$$

Figure 3 is obtained for CdS and Fig. 4 for CdSe when values for c_{11}^D, c_{33}^D, c_{44}^D, and c_{13}^D from the paper by Berlincourt et al[11] are used. The transformation equation for $h_{33}^{'}$ is

$$h_{33}^{'} = \cos^3\theta\, h_{33} + \cos\theta \sin^2\theta\, (h_{13} + 2h_{15}) \quad , \quad (7)$$

where $h_{33} = e_{33}/\epsilon_{33}^S$, $h_{31} = e_{31}/\epsilon_{33}^S$, and $h_{15} = e_{15}/\epsilon_{11}^S$. Values of the piezoelectric stress constant e and the dielectric constant ϵ are given by Berlincourt et al. The quantity $h_{33}^{'}$ is plotted for CdS and CdSe in Fig. 5. The transformation equation for $\beta_{33}^{'S}$ is

$$\beta_{33}^{'S} = \frac{\sin^2\theta}{\epsilon_{11}^S} + \frac{\cos^2\theta}{\epsilon_{33}^S} \quad (8)$$

and the results are shown in Fig. 6.

For c'^{D}_{55} the transformation equation is

$$c'^{D}_{55} = \sin^2\theta \cos^2\theta(c^{D}_{11}+c^{D}_{33}-2c^{D}_{13}) + (\cos^2\theta-\sin^2\theta)^2 c^{D}_{44} \qquad (9)$$

and the results are shown in Fig. 7 for both CdS and CdSe. For h'_{35} one has

$$h'_{35} = -\cos^2\theta \sin\theta (h_{33}-h_{31}) - \sin\theta (1-2\cos^2\theta)h_{15} \qquad (10)$$

and the results are given in Fig. 8.

One of the most striking features of Figs. 3 through 8 is that the c^{D} and β^{S} constants are relatively independent of θ whereas the h_{33} and h_{35} constants are highly dependent on θ and actually go through a change of sign.

The electromechanical coupling factor for the h set of piezoelectric equations may be defined as the ratio of the mutual elastic and dielectric energy density to the geometric mean of the elastic and dielectric self energy densities. This means that

$$k \equiv \frac{U_m}{\sqrt{U_e U_d}} \quad , \qquad (11)$$

where U_m is the mutual energy, U_e is the elastic energy, and U_d is the dielectric energy. The internal energy is given by

$$U = \frac{1}{2} S_i T_i + \frac{1}{2} D_m E_m \qquad (12)$$

where i goes from 1 to 6 and m goes from 1 to 3. Substitution of Eqs. (4) into Eq. (12) gives

$$U = \frac{1}{2} c'^{D}_{33} S_3^2 - h'_{33} S_3 D_3 + \frac{1}{2} \beta'^{S}_{33} D_3^2 \quad .$$

Thus, $U_m = h'_{33} S_3 D_3/2$, $U_e = c'^{D}_{33} S_3^2/2$, and $U_d = \beta'^{S}_{33} D_3^2/2$. The electromechanical coupling factor for the thickness longitudinal mode is

$$k_{long.} = \frac{h'_{33}}{\sqrt{c'^{D}_{33}\, \beta'^{S}_{33}}} \qquad (13)$$

Similarly, from Eqs. (5) it follows that the electromechanical coupling factor for the thickness shear mode is

$$k_{shear} = \frac{h'_{35}}{\sqrt{c'^{D}_{55}\, \beta'^{S}_{33}}} \qquad (14)$$

The quantities $k_{long.}$ and k_{shear} are plotted in Fig. 9 for CdS; the same quantities are plotted in Fig. 10 for CdSe. It is seen that the behavior of the electromechanical coupling factors is qualitatively the same for CdS and CdSe. In the case of CdS the analysis indicates that the generation of thickness longitudinal modes will be minimized when θ equals 39 or 90°. The generation of thickness shear modes will be minimized when θ equals 0 or 64°. In this report it will be understood that θ equals 0° for a longitudinal mode composite resonator and θ equals 39° for a shear mode composite resonator. It is fortuitous that k_{shear} is near a maximum when θ equals 39°; this fact greatly increases the practicality of shear mode composite resonators.

In fabricating longitudinal mode resonators, X-cut single crystal quartz wafers have been used and the c-axis of the CdS has been made parallel to the wafer normal.

In the case of shear mode resonators the substrates have been nearly AT-cut single crystal quartz wafers and the desired angle between the c-axis of the CdS film and the wafer normal has been 39°. However, it is also necessary to control the orientation of the projection of the c-axis of the CdS film in the plane of the wafer faces with respect to the X-axis of the quartz. This preferred orientation is illustrated in Fig. 11. The Y_c face of the electrically driven CdS film will shear, which means that there will be particle motion in the direction perpendicular to the Y_c Z_c' plane. This will produce particle motion in the X_q direction in the quartz wafer. Thus, the shear mode excited in the quartz will be the one necessary for fabrication of a device with a zero frequency-temperature coefficient.

2.2 Equivalent Circuit

The derivation of the equivalent circuit of a composite resonator operating in the longitudinal mode begins with Eq. (4) The appropriate form of Newton's equation is

$$\rho_c \frac{\partial^2 \xi_3}{\partial t^2} = \frac{\partial T_3}{\partial z} \tag{15}$$

where ρ_c is the density of CdS, ξ_3 is the longitudinal displacement, t is the time, and T_3 is the stress in the z direction. But, from Eq. (15) we obtain

$$\rho_c \frac{\partial^2 \xi_3}{\partial t^2} = c_{33}^{'D} \frac{\partial^2 \xi_3}{\partial z^2} \tag{16}$$

since $S_3 = \frac{\partial \xi_3}{\partial z}$ and $\nabla \cdot D = 0$ for an insulating material like CdS. Equation (16) is the so-called wave equation, and its solution has the following form:

$$\xi_3 = \left(A \sin \frac{\omega z}{v^D} + B \cos \frac{\omega z}{v^D}\right) e^{j\omega t} , \tag{17}$$

where ω is the frequency in radians/sec and $v^D = \sqrt{c_{33}^{'D}/\rho_c}$ is the velocity for elastic wave propagation. The physical situation for the CdS film may be represented as follows:

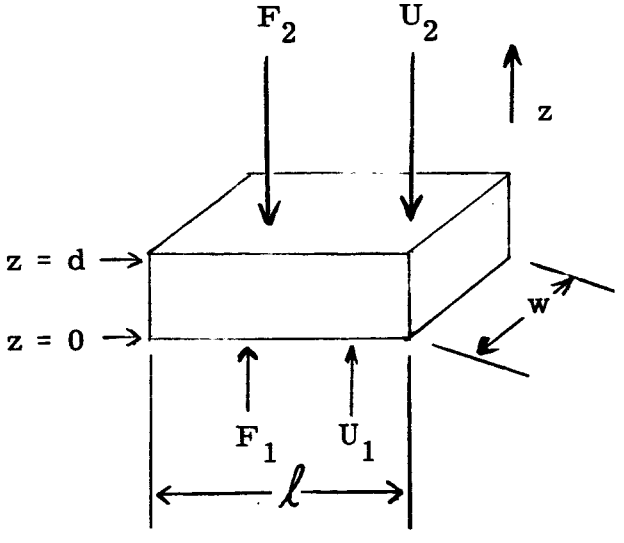

where F_1 and F_2 are forces acting on the electroded surfaces,and U_1 and U_2 are particle velocities at these surfaces. The boundary conditions for U_1 and U_2 are

$$\frac{\partial \xi_3}{\partial t}\Big|_{z=0} = +U_1 \quad \text{and} \quad \frac{\partial \xi_3}{\partial t}\Big|_{z=d} = -U_2 \ . \tag{18}$$

If Eq. (17) is differentiated with respect to time and evaluated at z=0, we obtain $B = U_1/j\omega e^{j\omega t}$. If the evaluation is at z=d we obtain

$$A = \frac{-1}{j\omega}\left[\frac{U_2 e^{-j\omega t}}{\sin\frac{\omega d}{v^D}} + \frac{U_1 e^{-j\omega t}}{\tan\frac{\omega d}{v^D}}\right] \ . \tag{19}$$

At z=0, we see from the drawing that $F_1 = -w\ell T_3$. Since $I = w\ell \frac{\partial D_3}{\partial t}$ and $D_3 = D_o e^{j\omega t}$, we have $D_3 = I/j\omega w\ell$ where I is the current. Combining these equations with Eqs. (17) and (19) we obtain

$$F_1 = \frac{h'_{33} I}{j\omega} + \frac{w\ell\, c'^D_{33}}{jv^D}\left[\frac{U_2}{\sin\frac{\omega d}{v^D}} + \frac{U_1}{\tan\frac{\omega d}{v^D}}\right] \ . \tag{20}$$

The mechanical impedance of the CdS film is

$$Z_o^D = w\ell\rho_c v^D = w\ell\sqrt{\rho_c c'^D_{33}} \ . \tag{21}$$

The force on the z=d surface is given by $F_2 = -w\ell T_3|_{z=d}$. Combining this with Eqs. (17), (19), and (21) we obtain

$$F_2 = \frac{h'_{33} I}{j\omega} + \frac{Z_o^D}{j}\left[\frac{U_2}{\tan\frac{\omega d}{v^D}} + \frac{U_1}{\sin\frac{\omega d}{v^D}}\right] \ . \tag{22}$$

The voltage across the film is obtained from Eq. (4) by integration as follows:

$$V = \int_o^d E_3 dz = -h'_{33}\left[\xi_3\right]\Big|_o^d + \beta'^S_{33} D_3 d \ . \tag{23}$$

After substituting in Eq. (17) and using Eq. (19) this becomes

$$V = \frac{h'_{33}}{j\omega}(U_1 + U_2) + \frac{I}{j\omega C_o} \ , \tag{24}$$

where $C_o = w\ell / \beta_{33}^{'S} d$. Under clamped conditions, S_3 is zero which means that both U_1 and U_2 are constrained to be zero. Then, we obtain

$$N \equiv \frac{\text{Force}}{\text{Voltage}} = h_{33}^{'} C_o \quad . \tag{25}$$

Consider the following equivalent circuit:

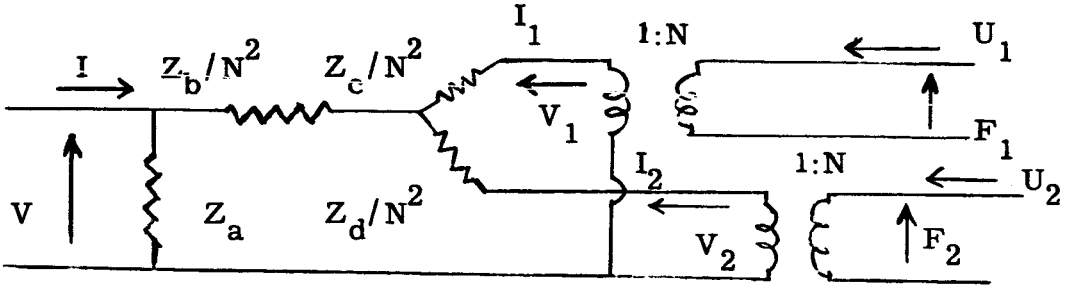

From this we obtain

$$V_1 = I_1 \left(Z_a + \frac{Z_b}{N^2} + \frac{Z_c}{N^2}\right) + I_2 \left(Z_a + \frac{Z_b}{N^2}\right) + IZ_a \quad ,$$

$$V_2 = I_1 \left(Z_a + \frac{Z_b}{N^2}\right) + I_2 \left(Z_a + \frac{Z_b}{N^2} + \frac{Z_d}{N^2}\right) + IZ_a \quad ,$$

and

$$V = Z_a (I_1 + I_2 + I) \quad .$$

Since

$$V_1 = F_1/N, \; V_2 = F_2/N, \; I_1 = NU_1, \text{ and } I_2 = NU_2,$$

we obtain

$$F_1 = U_1(N^2 Z_a + Z_b + Z_c) + U_2(N^2 Z_a + Z_b) + NIZ_a$$

and

$$F_2 = U_1(N^2 Z_a + Z_b) + U_2(N^2 Z_a + Z_b + Z_d) + NIZ_a \quad . \tag{26}$$

Comparing the NIZ_a terms in these equations with the leading terms in Eqs. (20) and (22) we obtain

$$Z_a = 1/j\omega C_o \quad . \tag{27}$$

Similar comparisons give

$$N^2 Z_a + Z_b + Z_c = \frac{Z_o^D}{j \tan \frac{\omega d}{v D}} \quad \text{and} \quad N^2 Z_a + Z_b = \frac{Z_o^D}{j \sin \frac{\omega d}{v D}}$$

Subtraction gives

$$Z_c = j Z_o^D \tan \frac{\omega d}{2v D} \quad , \tag{28}$$

if use is made of the trigonometric identity, $\tan \theta/2 = (1-\cos\theta)/\sin\theta$. The equivalent circuit then becomes:

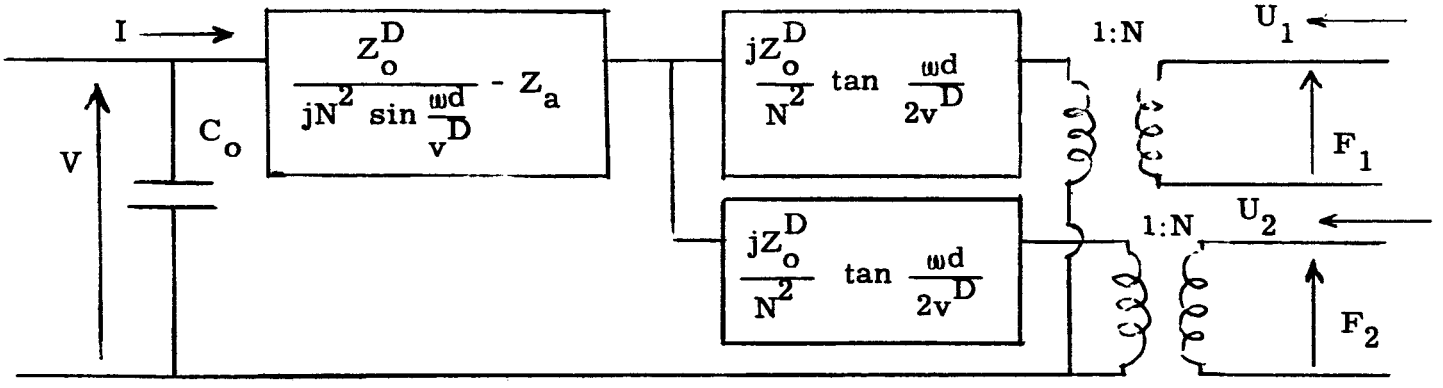

If the z=0 surface is free, $F_1 = 0$ and the equivalent circuit after further simplification becomes

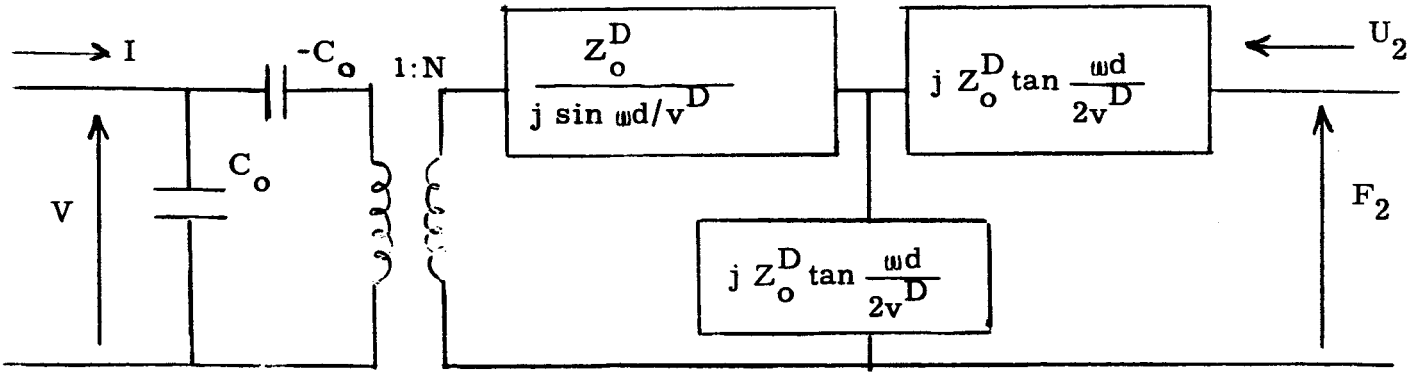

Now, it can be shown that

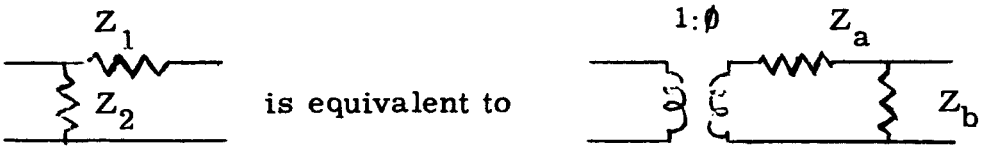

if $Z_a = Z_1(Z_1+Z_2)/Z_2$, $Z_b = Z_1+Z_2$, and $\phi = \frac{Z_1 + Z_2}{Z_2}$. Using this transformation and $\frac{1 + \cos\theta}{\sin\theta} = \text{ctn}\frac{\theta}{2}$, the equivalent circuit for the CdS film becomes:

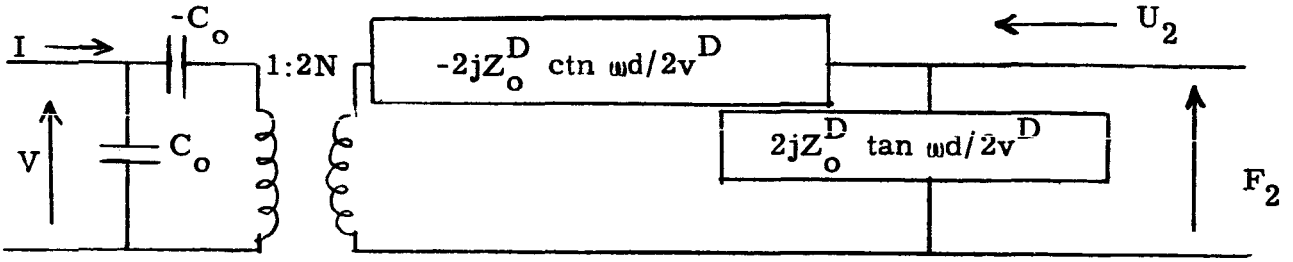

In the derivation of this equivalent circuit the effect of the electrodes has been neglected. This is a reasonable assumption as long as the electrodes are thin compared to the CdS film. Reference(10)provides useful background information on the derivation of equivalent circuits.

The same equivalent circuit is obtained for shear mode generation in CdS films. However, for the shear mode case we have

$$N = h'_{35}C_o,\quad Z_o^D = w\ell\sqrt{\rho_c\, c'^D_{55}}\ ,\quad \text{and}\quad v^D = \sqrt{c'^D_{55}/\rho_c}\ .$$

The equivalent circuit for the CdS film can be used in deriving the equivalent circuit of a quartz wafer which is driven mechanically. The equivalent circuit for a simple AT-cut quartz resonator operating in the shear mode would be

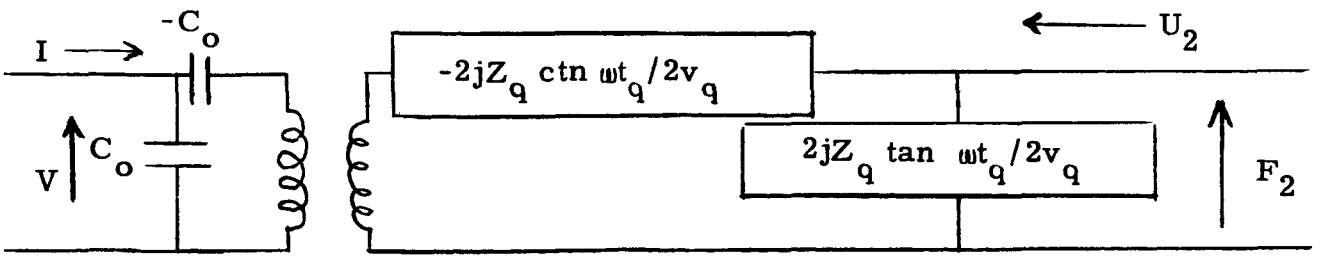

where $Z_q = A\rho_q v_q$, $v_q = \sqrt{c'^D_{66}/\rho_q}$, and t_q is the thickness of the quartz wafer. Here A is the area, ρ_q is the density of quartz, v_q is the velocity of shear mode propagation, and c'^D_{66} is the appropriate elastic stiffness constant for quartz. Since the quartz is driven mechanically rather than

electrically, the electrical terminals on the left are open circuited. Because of this, the equivalent circuit becomes

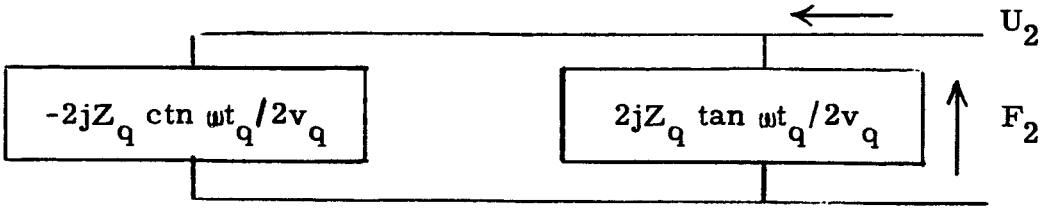

Combining these parallel impedances gives

$$Z = \frac{Z_1 Z_2}{Z_1 + Z_2} = \frac{4Z_q^2}{2jZ_q \left[\tan(\omega t_q/2v_q) - \operatorname{ctn}(\omega t_q/2v_q) \right]}$$

However, this may be simplified as follows:

$$1/\left[\tan(\alpha/2) - \operatorname{ctn}(\alpha/2)\right] = \frac{1}{\frac{1-\cos\alpha}{\sin\alpha} - \frac{1+\cos\alpha}{\sin\alpha}} = \frac{-\sin\alpha}{2\cos\alpha} = \frac{-\tan\alpha}{2}$$

Thus, the equivalent circuit for a mechanically-driven quartz wafer becomes:

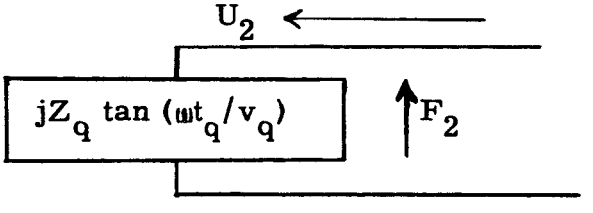

This may then be combined with the equivalent circuit for a CdS film as follows:

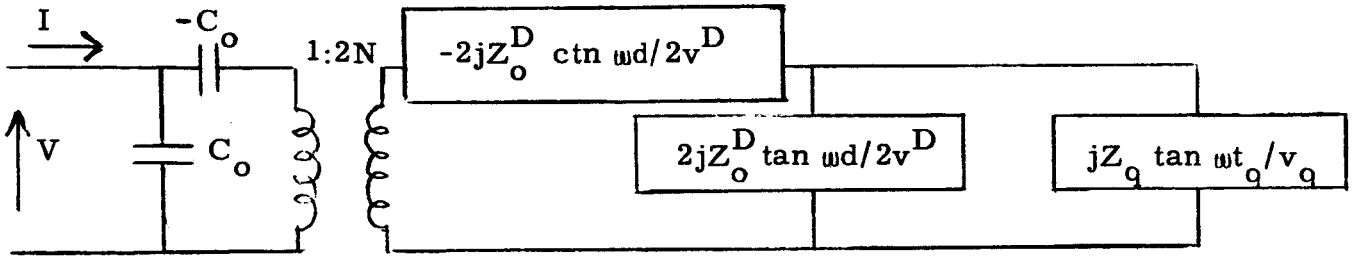

This is the equivalent circuit for a CdS-quartz resonator operating in the shear mode without any losses.

It can be shown that if losses are included, the equivalent circuit for a shear mode composite resonator is as shown in Fig. 12. The symbols used in this figure are defined as follows: A is the active area of the CdS transducer; t_c and t_q are the thicknesses of the CdS film and quartz substrate, respectively; ρ_c and ρ_q are the densities of CdS and quartz; $c_{55}^{'D}$ and $c_{66}^{'D}$ are the appropriate elastic stiffness constants for CdS and quartz, respectively; and Q_c^o and Q_q^o are the mechanical quality factors of CdS and quartz at the principal electrical antiresonance frequency, $f_A = \omega_A/2\pi$. As usual, MKS units are used except as otherwise noted. A $(1/\omega)$ dependence is assumed for the two mechanical quality factors. This relationship has been verified experimentally[13] above 50 MHz for AT-cut quartz plates in air.

The theoretical impedance function for a shear mode resonator with nine half-waves in the quartz at the principal response frequency has been computer programmed over a frequency range ± 40% of the principal response frequency. The results are shown in Figs. 13-16. In this computation Q_c^o and Q_q^o were taken to be 1000 and 20,000, respectively. Figure 13 is a plot of the relative impedance characteristic $|Z(f)/Z(f_{R10})|$ over a broad frequency range. The so-called "principal" resonator response (frequency $\cong f_{R10}$) is indicated as that mode in which there are nine half waves in the quartz substrate and one half-wave in the CdS evaporated layer. Figure 14 shows the computer result for the principal resonance in more detail, along with a simplified shear mode electrical equivalent circuit representation for the principal resonance. The circuit parameters are given as a function of the area (in square millimeters) of the top electrode (i. e., the active transducer area). Table III tabulates the computer results for the resonance and antiresonance frequencies (f_R, f_A) along with corresponding impedances (Z_R, Z_A); the effective electromechanical coupling coefficient k_{eff}; and the electrical Q value as a function of m, the number of half-waves in a resonator of 10 half-waves thickness at the principal resonance f_{R10} = 278.4 MHz. The resonance and antiresonance impedances are given in terms of the active transducer area A. The effective

electromechanical coupling coefficient k_{eff} is defined in the usual way[14] as

$$k_{eff}^2 = \frac{f_p^2 - f_s^2}{f_p^2} \cong \frac{2(f_A - f_R)}{f_A} , \qquad (29)$$

where f_s is the motional (series) resonance frequency and f_p is the parallel resonance frequency.

The electrical Q of a resonance response (in this case equal to the mechanical quality factor Q_M for the composite resonator) is defined as

$$Q_M = \frac{f_R}{2\,\delta f} , \qquad (30)$$

where $f_{hp} = f_R + \delta f$ is the frequency at which the impedance is $\sqrt{2}\, Z_R$.[15]

Table III. Computer results for a typical CdS-quartz resonator.

m	f_R	f_A	$Z_R \times A$	$Z_A \times A$	k_{eff}	Q_M
6	167.4 MHz	167.8 MHz	0.86 Ω-mm^2	2076 Ω-mm^2	6.4%	12,000
7	195.5	195.9	0.79	1684	6.8	9,500
8	223.3	223.9	0.79	1318	7.1	7,900
9	250.9	251.5	0.85	982	7.0	6,800
10	278.4	279.0	1.00	688	6.5	6,000
11	306.0	306.5	1.30	447	5.6	5,600
12	333.8	334.1	1.84	267	4.6	5,200
13	361.8	362.1	2.86	147	3.6	4,700
14	390.1	390.2	4.79	76	2.8	3,800

An interesting feature of the response characteristics is that the maximum effective electromechanical coupling occurs near the harmonic modes m=8 and 9. This might suggest an alternative definition of a "principal" response as that mode for which the electromechanical coupling is a maximum. Such a mode would contain, for instance, between 0.9 and 0.8 half-waves in the CdS layer and 9.1 to 9.2 half-waves in the quartz substrate. It is not expected, however, that obtaining an extra 1/2% in k_{eff} will be an important design consideration. It is significant, in view of naturally-arising fabrication problems, that the parameters Q_M and k_{eff} are not particularly sensitive to a slight departure from an integer ratio between

the number of half-waves in the quartz and CdS, respectively. In particular, this phenomenon suggests that it is probably sufficient if the thickness of the evaporated CdS layer is controlled to 10%.

It is interesting that according to Fig. 13 the harmonic responses near the principal response are strong. Were this feature, in fact, undesirable, one possible method of overcoming it would be to put two resonators in series, both having the same CdS layer thickness, but having a difference in thickness of the two respective quartz substrates equal to one half-wave. Their principal resonances would then coincide and the other harmonic responses would not. Likewise, if the device were to operate on the antiresonance portion of the response, then two such resonators could be connected in parallel.

2.3 Frequency-Temperature Coefficient

The determination of the quartz crystal cut required for a shear mode composite resonator with a zero frequency-temperature coefficient at room temperature depends on assumed values for the frequency-temperature coefficients of thin film CdS. The currently available information on the frequency-temperature dependence of the elastic constants of bulk CdS is given by Berlincourt et al.[11] For the longitudinal mode resonator, the interpretation of their data is straightforward. The temperature coefficient of c_{33}^D at 25°C is given as -216×10^{-6}/°C, with no correction for thermal expansion. As $f \propto \sqrt{c_{33}^D/\rho_c}$, it follows that since no correction was made for thermal expansion $\frac{1}{c_{33}^D}\frac{dc_{33}^D}{dT}$ was equated with $\frac{2}{f}\frac{df}{dT}$, where T is temperature. Hence, $(1/f)(df/dT) = -108 \times 10^{-6}$/°C for the longitudinal mode, first order frequency-temperature coefficient in bulk CdS. Because no additional information to the contrary was available, this same value of the coefficient was assumed for thin film CdS. Measurements on longitudinal mode resonators discussed in Section 4.1 showed that this assumption was valid.

For the shear mode resonator, the available information on temperature coefficients is incomplete. There is not enough information to calculate $(1/c_{55}^{'D})(dc_{55}^{'D}/dT)$ for the rotated CdS cut corresponding to pure shear mode generation. The only shear constant information available is contained in the temperature coefficient for s_{44}^{D}. This factor is $(1/s_{44}^{D})(ds_{44}^{D}/dT) = +96 \times 10^{-6}/°C$. Again, this value was not corrected for thermal expansion. Assuming that the temperature coefficients for s_{44}^{D} and $c_{55}^{'D}$ are approximately equal, the same reasoning used previously leads to a value of $-48 \times 10^{-6}/°C$ for the first order frequency-temperature coefficient for a shear mode CdS film. Admittedly, the assumption in this case is rather speculative. The weakness of this supposition is reflected in the non-zero frequency-temperature dependence observed for shear mode resonator 035R-C (see Fig. 23).

In order to calculate the quartz cut needed for the shear mode resonator, one requires that the amount of time for the acoustic wave to propagate through the CdS plus the quartz be independent of temperature. Given this constraint, we obtain

$$a_1 + n(\theta - \theta_o)\frac{\partial b_1}{\partial \theta} = 0 \quad , \tag{31}$$

where a_1 is the temperature coefficient for CdS, n is the number of half-waves in the quartz wafer, θ is the angle between the thickness direction of the quartz wafer and the crystallographic Y-axis. (The rotation is taken around the X-axis.) θ_o is this angle for the AT zero-temperature coefficient cut in quartz, and b_1 is the first order frequency-temperature coefficient for quartz. For a synthetic Y-bar seed-type quartz plate (with a diameter-to-thickness ratio of about 40) operated at the 5th harmonic overtone, Bechmann[16] gives $\partial b_1/\partial\theta = -5.05 \times 10^{-6}/°C/°\theta$ and $\theta_o = 35° 22'$. Using a value for a_1 of $-48 \times 10^{-6}/°C$, we find that θ should be 34° 18' for a shear mode resonator with a zero first order frequency-temperature coefficient at room temperature.

There is no similar way of achieving a zero first order frequency-temperature coefficient for the longitudinal mode resonator. Both CdS and

quartz possess negative first order frequency-temperature coefficients for all quartz cuts close to the X-cut and the Z-cut. The X-cut of quartz has $b_1 = -21 \times 10^{-6}/°C$ and the Z-cut has $b_1 = -70 \times 10^{-6}/°C$.

The frequency-temperature dependence of a simple quartz resonator is given by $f(T) = f_o(1 + b_1(T-T_o) + b_2(T-T_o)^2 + \ldots)$, where f_o is the resonance frequency at room temperature T_o. Since $b_1(T-T_o) << 1$, one obtains

$$1/f(T) = P_q(T) \cong P_{qo}(1-b_1(T-T_o)) , \tag{32}$$

where $P_q(T)$ is the period at a given temperature and P_{qo} is the period at room temperature. However, the period is just the time required for acoustic energy to travel both ways through the quartz. A similar expression applies to the time required for acoustic energy to travel both ways through CdS:

$$P_c(T) \cong P_{co}(1-a_1(T-T_o)) \quad . \tag{33}$$

For the composite resonator we write

$$P_r(T) \cong P_{ro}(1-c_1(T-T_o)) \quad . \tag{34}$$

In the composite resonator at room temperature there are exactly n half-waves in the quartz and one half-wave in the CdS at the principal response. Hence, we have

$$P_{ro} = P_{co} + P_{qo} = P_{co} + nP_{co} \quad . \tag{35}$$

But, at any temperature we have

$$P_r(T) = P_c(T) + P_q(T) \quad . \tag{36}$$

Substituting Eqs. (32)-(35) into Eq. (36) gives $(n+1)P_{co}(1-c_1(T-T_o)) = P_{co}(1-a_1(T-T_o)) + nP_{co}(1-b_1(T-T_o))$. Solving this for c_1 gives

$$c_1 = \frac{a_1 + nb_1}{1+n} \quad . \tag{37}$$

For the longitudinal mode composite resonator we take $a_1 = -108 \times 10^{-6}/°C$, $b_1 = -21 \times 10^{-6}/°C$, and $n = 9$. Substituting these values into Eq. (37) gives $c_1 = -29.7 \times 10^{-6}/°C$. This is in good agreement with the experimental frequency-temperature coefficient of $-30.5 \pm 0.6 \times 10^{-6}/°C$ discussed in Section 4.1.

3. FABRICATION TECHNIQUES

3.1 Apparatus

A schematic of the bell jar apparatus used in the fabrication of composite resonators is shown in Fig. 17. The pumping system consisted of a standard forepump and oil diffusion pump combination. A liquid nitrogen trap was used between the diffusion pump and the bell jar to prevent back-streaming of oil vapors. The sulfur and cadmium sulfide crucibles were made of quartz and fabricated to our specifications by Quartz Scientific, 34602 Lakeland Blvd., Eastlake, Ohio. The heater coils for these crucibles were made with tantalum wire. The mask changer-substrate holder combination was designed to hold three quartz wafers simultaneously. The mask changer plate held nine masks and could be rotated to any of three positions. Thus, in principle, as many as three different masks could be placed over a given wafer substrate without breaking the vacuum. A total of four No. C1-418 chromalox cartridge heaters (manufactured by Edwin L. Wiegand Company, Pittsburgh, Pennsylvania) were sufficient to heat the substrate holders to 350°C. These heaters were firmly clamped to the heated plate with aluminum blocks to provide good heat conduction. A chromel-alumel thermocouple was used to continuously monitor the temperature of the heated plate. The heated plate, mask changer plate, and shutter were all made of aluminum which was not attacked by sulfur vapors when heated to high temperatures. The heated base plate had mounting holes for the crystal holder assembly of a Westinghouse Model 701 Quartz Crystal Microbalance. This microbalance head was rated for temperatures up to 400°C. Because the coin silver contacts provided with the microbalance head would be quickly attacked by sulfur vapors, they were replaced with aluminum contacts. The sensitivity of the microbalance was deliberately reduced by placing a perforated aluminum foil in front of the exposed microbalance crystal to cut down on the amount of material which was allowed to deposit onto the crystal. It was then possible to monitor the deposition of CdS films as thick as 30 μ .

The entire substrate holder-mask changer unit could be rotated about a horizontal axis so that the quartz wafers could be tilted with respect to the vapor stream from the CdS crucible. This feature was used in the evaporation of shear mode CdS films. It was also possible to raise or lower the entire substrate holder-mask changer unit on two threaded support rods.

The substrate holders are shown in more detail in Fig. 18. These were made of aluminum, and the heated plate was designed to accommodate three of them. Two steel springs were used to hold down each quartz wafer. Two No. 69 holes were drilled close to the intersecting scribe markings on the bottom of each substrate holder. These were located to match holes in the stainless steel masks and were used for mask alignment.

3.2 Mask Preparation

The masks were made from stainless steel shim stock 0.001 inches thick by means of a standard photo etching technique. The mask designs were first drawn ten times actual size. These drawings were then reduced to actual size by photographic means. The positives were then used in the making of the masks. Full size photographic positives of the three kinds of masks used in the fabrication of composite resonators are reproduced in Fig. 19. The small holes in each mask were used for aligning the masks with respect to the substrate holders. The two wide rectangular slots in each mask were required to prevent interference between the mask and the steel springs used to hold the quartz wafers in place. The active area of the CdS film was defined by that part of the top electrode which overlapped the bottom electrode. About 1 mm^2 of the CdS was electrically driven. The area of the bottom electrode and the area of the CdS film were made about ten times larger than this to promote energy trapping of acoustic energy in the quartz to the volume under and immediately surrounding the 1 mm^2 active area. Once away from the active area, the top electrode was made to fan out to give greater conductivity. High conductivity leads and electrodes are required for devices with a low resistance at resonance.

The procedure used in making the stainless steel masks is as follows:

The stainless steel shim stock (Code L-1, Precision Steel Warehouse, Inc., Downers Grove, Ill.) is dipped in Kodak Photo-Resist and allowed to dry for at least one hour. The positive of the mask is placed on the stainless steel and they are exposed to ultraviolet light for a period of 15 minutes. The stainless steel piece is then developed in Kodak Photo-Resist Developer for five minutes and then dyed with Kodak Photo-Resist Dye, after which it is placed in a drying oven for about 15 minutes. Then the piece is taken and etched in Hunt's Rapid Circuit Etch Solution. It was observed that the best results were obtained with the etchant at about 65°C. The stainless steel piece is etched for 2-3 minutes or until the entire pattern is etched out sharp and clear. Care must be taken to keep from over etching or the pattern becomes blurred and not well defined.

3.3 Substrate Cleaning Procedure

The quartz wafers were chemically cleaned according to the following procedures:

1. Boil in methyl alcohol five (5) minutes.
2. Boil in dilute alconox solution fifteen (15) minutes. (Alconox, Inc., New York 3, N. Y.).
3. Boil in distilled H_2O fifteen (15) minutes.
4. Boil in concentrated HNO_3 fifteen (15) minutes; rinse in distilled H_2O.
5. Boil in 25% NaOH solution fifteen (15) minutes; rinse in distilled H_2O.
6. Boil in distilled H_2O five (5) minutes.
7. Boil in methyl alcohol five (5) minutes.
8. Blow dry in jet of prepurified nitrogen gas; hold over methyl alcohol vapors to observe visible contamination, as evidenced by the appearance of fringes. Repeat steps 7 and 8 if necessary.

During steps 1-7 the fragile wafers were held in a glass basket made to our specifications by Adria Scientific Glass Works, 1500 Coit Avenue, Cleveland, Ohio 44112.

Immediately prior to evaporation, the masks, substrate holders, and quartz wafers were subjected to further cleaning by glow discharge. The glow discharge power supply circuit is shown in Fig. 20. The negative voltage (HV-) was connected to a 2-1/2 x 6 inch aluminum electrode in the bell jar. The glow discharge voltage was gradually increased as the pressure in the bell jar was reduced to approximately 100 μ Hg. The current in the primary of the high voltage transformer was monitored and kept between 6 and 9 A rms.

3.4 Specifications for Quartz Wafers

The X-cut and nearly AT-cut quartz wafers were obtained from two suppliers. These were Valpey-Fisher Corporation, 1016 First Street, Holliston, Massachusetts, and Piezo Crystal, Inc., Carlisle, Pennsylvania. The specifications given to Valpey-Fisher Corporation for X-cut quartz wafers were as follows:

1. Starting material: Sawyer Research Products Y-bar seed type cultured quartz, slow grown.
2. Quartz cut: X-cut wafers ± 15'.
3. Fundamental frequencies: 28.80 MHz ± 0.1%, 31.03 MHz ± 0.1%, and 32.92 MHz ± 0.1% for thickness compressional mode.
4. Diameter: 0.312 ± 0.001 inches.
5. Polish: optical.
6. Flatness: less than 1/10th wavelength of sodium light.
7. Parallelism: less than one wavelength of sodium light over a 4 mm diameter region in the center of the wafer.

The specifications for the nearly AT-cut wafers ordered from Valpey-Fisher Corporation were the same except as follows:

1. Quartz cut: Y-cut angle of 34° 18' ± 5'.
2. Fundamental frequencies: 28.84 MHz ± 0.1%, 31.06 MHz ± 0.1%, and 32.96 MHz ± 0.1% for thickness shear mode.

The thickness of an X-cut quartz wafer with a fundamental frequency of 31.03 MHz is 92.65 μ. For a nearly AT-cut quartz crystal with a fundamental frequency of 31.06 MHz, the thickness is 53.54 μ.

3.5 Evaporation Procedures

A quartz crystal microbalance, Westinghouse Model 701, was used to monitor the thickness of the metals and CdS films. The bottom electrode, CdS, and top electrode were deposited in three separate evaporations, because the masks had to be changed outside the system.

With the mask holder in position and the large shutter directly below the substrates closed, the system was pumped down to a pressure less than 6×10^{-5} mm Hg. The shutter was opened and 100 Å of Cr was deposited from a W basket. The shutter was then closed while the Au, premelted onto its W filament, was remelted. The shutter was opened and 1000 Å of Au was deposited. The shutter was closed, and then reopened for deposition of an additional 100 Å of Cr.

The 100 Å of Cr evaporated directly on the quartz wafer was for good adhesion. The 1000 Å of Au was for high conductivity of the bottom electrode. The 100 Å of Cr between the Au layer and the CdS had two purposes: to increase the crystallinity of the CdS film and to improve adhesion.

The system was then opened so the mask holder could be rotated into position for the CdS evaporation. The W filaments for Cr and Au were replaced by quartz crucibles (see Fig. 17) giving a source to substrate distance of 4-1/2". A single crucible of CdS was placed directly beneath the substrates. The CdS was obtained from General Electric Company in powdered form. To increase the resistivity of the evaporated CdS films, 0.3% by weight of Cu_2S (obtained from Fisher Scientific Company) was added to the CdS charge. A 0.030" thick fiberfax plug (The Carborundum Company, Perth Amboy, New Jersey) was placed on top of the CdS charge to prevent splatter on the substrates.

Two supplementary crucibles of S were positioned on each side of the CdS crucible, and a small secondary shutter was added just above the sources. The sulfur was obtained from American Smelting and Refining Company, South Plainfield, New Jersey, and had a purity of 99.999+%. The separate S sources were used to produce higher resistivity CdS films. For the deposition of longitudinal mode CdS films the quartz wafers were horizontal. However, when shear mode CdS films were desired, the wafers were tilted about 50° from the horizontal.

With the bell jar cleaned, the system was reassembled and the pump down begun. When the pressure was less than 3×10^{-4} mm Hg, the shutter directly below the substrates was opened and the chromalox heaters were operated at a power of 450 W. When the substrate temperature reached 250°C, the power was turned off; when the temperature dropped to 225°C, the power was turned on again to a value sufficient to stabilize the temperature and hold it at 200°C, the preferred evaporation temperature. Heating the quartz wafers to 250°C was intended as a bake-out procedure to drive off adsorbed gases.

With the heaters back on, the large shutter was closed and pre-heating of the crucibles started. The S crucibles were heated at 6 A, then turned down to 2.2 A when the S melted. The CdS crucible was heated at 8 A for 10 minutes, then turned up to 11 A for 5 minutes, and finally set at 9.5 A, the desired setting for evaporation. The CdS was held at the 9.5 A setting at least 5 minutes before opening the shutter in order to stabilize the deposition rate, typically 0.3 μ/min. Two minutes before opening the shutters, the S crucibles were turned up to 4.1A.

Both shutters were opened and the microbalance calibrated by visually observing the fringes that formed on the masks. A continual record of thickness was maintained throughout the evaporation to detect any change in rate. When the desired thickness was reached, the CdS crucible was turned off, the small shutter over the sources was closed, and the heaters were turned off. After 2 minutes, the small shutter was reopened. The S crucibles were held at 4.1 A until the substrate temperature dropped to 130°C after the CdS evaporation was completed. Then the S crucibles were turned off and both shutters closed.

When the substrate temperature dropped below 60°C, the system was opened to change masks. At this point the system was given a general cleaning to remove all CdS and S from the base plate, filament supports, shutters, and bell jar.

The system was reassembled and pumped down to a pressure less than 6×10^{-5} mm Hg. Then 3000 Å of Al, premelted onto two W filaments, was evaporated from two directions at a 13 cm source to substrate distance.

The system was then opened and the resonators removed for mounting.

3.6 Mounting

After the composite resonators were removed from the substrate holders, leads were attached to the bottom and top evaporated electrodes using DuPont air dry silver paint. These leads were 2 x 4 mm pieces of gold on silver foil. It was found advisable to keep the silver paint off the CdS film in order to prevent spalling, i. e., peeling of the CdS from the substrate. The resonator was mounted on a transistor header as shown in Fig. 21 by soft soldering the two foil leads to two of the header wires. A third header wire was bent over to make contact with the header rim. The resonator was mounted with its unelectroded side up to facilitate tuning. The cans for the headers were obtained from Hudson Tool and Die Company, Inc., 18-38 Malvern Street, Newark 5, New Jersey.

3.7 Tuning

The frequencies of the principal response and the other overtones are determined by the thickness of the quartz wafer substrate plus all the evaporated layers. Although the thicknesses of the CdS and metal layers were monitored with a quartz crystal microbalance during the evaporations, this procedure was not sufficiently accurate to properly set the principal response frequency. Fine tuning was done by evaporating a layer of SiO_x after the composite resonator had been mounted. Of course, samples selected for fine tuning had to have their principal response frequency above the target frequency.

A given sample was connected into the transmission circuit shown in Fig. 22. As the generator was manually tuned through the principal response, the antiresonance appeared as a sharp dip in the voltage monitored by the RF voltmeter. It was necessary to make a small correction since the target frequency was for resonance rather than antiresonance. As the SiO_x deposited, the amount of frequency lowering could be monitored with an electronic counter connected to the VHF signal generator. A computer Measurements Company counter was used which consisted of a Model

800A solid state counter together with a Model 802A frequency range module and a Model 834B 600 MHz heterodyne converter.

Prior to pump down, the unelectroded side of the quartz wafer was wiped clean with a Q-tip moistened in reagent grade acetone. The SiO_x was obtained from Union Carbide in lump form. The evaporation source was fabricated from tantalum sheet stock and was heated by a tungsten coil. Deposition rates between 60 and 80 Å of SiO_x per second were used, and the pressure inside the bell jar was kept less than 3×10^{-5} mm Hg. The diameter of the evaporated SiO_x layer was made relatively large (about 6 mm) in order to preserve the energy trapping criteria. To prevent the composite resonator from being heated by the SiO_x source, the shutter was not opened for more than 30 seconds at a time. A cooling period followed during which the antiresonance frequency of the principal response was determined by means of the transmission circuit.

3.8 Sealing

Hermetically sealed packages were made by sealing the cans and headers together with epoxy cement in a dry atmosphere. Prior to sealing, the separate parts were placed in a dry box for a period of not less than 12 hours. The dry box provided a continuously circulated water-free atmosphere. The units were sealed in a dry atmosphere because residual moisture could condense on the quartz wafers at low temperatures and degrade the electrical Q's of the devices. After the cans and headers were sealed together, the epoxy cement was allowed to cure at room temperature for 24 hours. A faster cure at elevated temperatures was avoided because of the possible formation of blow holes in the epoxy seal. A sealed unit is shown in Fig. 21.

4. TEST PROCEDURES AND MEASUREMENTS

4.1 Transmission Circuit Measurements

The transmission circuit apparatus is shown in Fig. 22. Its operation in conjunction with an electronic counter has already been explained in Section 3.7. Initial measurements on a given composite resonator were generally made with the transmission circuit because it provided

a convenient method of locating the principal response and other overtone resonances.

When the resonance frequencies of longitudinal mode devices were determined with the transmission circuit, only the series of overtone frequencies corresponding to the compressional mode was observed. But in principle it should be possible to excite the compressional mode as well as two shear modes in a given device. For example, this could happen if the c-axis of the CdS film were tilted at 20° from the substrate normal. In fact, the excitation of all three modes was observed in only one sample, 035R-C. This sample had a nearly AT-cut wafer as the substrate. It was found that the resonances could be grouped into three harmonic series as shown in Table IV.

Table IV. Resonance frequencies observed for sample 035R-C

Series A	B	C
53.9 MHz	60.8 MHz	114.0 MHz
80.9	90.2	171.5
107.8	119.7	229.7
134.8	149.2	287.8
161.7	179.8	345.6
188.8	210.0	
215.6		
242.8		
269.4		
296.6		
323.5		
350.6		

The average difference between harmonic resonances is 27.0 MHz in Series A, 29.8 MHz in Series B, and 58.3 MHz in Series C. Starting with values of the stiffness coefficient q given by Cady[17] for AT-cut quartz, it can be shown that Series A, B, and C correspond to the slow shear, fast shear, and longitudinal modes, respectively. The mode of excitation intended for this particular sample was the slow shear (Series A), and in

fact this was the strongest of the three series. The fast shear mode series (Series B) was the weakest of the three series observed with sample 035R-C.

The transmission circuit was also the preferred means of determining the frequency vs. temperature characteristic. These temperature runs were made after the resonator packages were sealed. The results for the principal response of the desired slow shear mode for sample 035R-C are shown in Fig. 23. This was the only determination of the frequency-temperature characteristic of a shear mode resonator. It was found that the frequency decreased 10 ppm/°C as the temperature increased. In theory, it should be possible to make a shear mode composite resonator with a stability of 0 ppm/°C at room temperature. We believe that Fig. 23 represents a reasonable first approximation to this theoretical limit. With a better understanding of the frequency-temperature characteristics of CdS itself and with better control over the CdS film thickness and the tilt of the c-axis, it should be possible to come much closer to a room temperature stability of 0 ppm/°C.

The frequency-temperature characteristic of the principal response of longitudinal mode composite resonator 037R-B is shown in Fig. 24. In this case it was found that the frequency decreased 31 ppm/°C as the temperature increased. This figure agrees closely with the predicted value of 29.7 ppm/°C. A group of 11 other longitudinal mode resonators was measured from approximately -45 to +100°C. For this group the frequency of the principal response was found to decrease 30.5 ± 0.6 ppm/°C as the temperature increased.

4.2 Impedance Bridge Measurements

Although the transmission circuit was good for initially locating resonances, it was not useful for quantitative impedance measurements. Instead, the impedance bridge apparatus shown in Fig. 25 was used for point-by-point measurements of impedance as a function of frequency.

The equivalent circuit representation around the principal response frequency has already been shown in Fig. 14. If the shunt capacity C_o is tuned out with an external inductor, then a symmetrical response is

obtained which is characteristic of the motional branch composed of L_1, R_1, and C_1. The tuning out of C_o was accomplished with the variable inductor L shown in Fig. 25. Components L and C were part of a special adapter. The variable inductor L consisted of a 2-inch piece of straight wire. Connection was made to one end of the wire with an alligator clip. This clip could be slid back and forth along the wire to vary the inductance. Capacitor C shown in Fig. 25 could be varied from 2.4 to 30.6 pF. The Triplett multimeter which was used to monitor the output of the VHF detector was kept on the 2.5 V ac scale.

The procedure used to adjust L and C resulted in C_o being tuned out. After the VHF generator was adjusted to the principal response frequency (as previously determined with the transmission circuit), a resonator package with no quartz wafer in it was inserted into the adapter. With this open-circuited sample it was possible to tune out the assorted distributed capacitances in the circuit with the variable inductor L. The inductor was adjusted to give a measured impedance on the order of 2000 Ω with the phase angle capacitive at 90°. Bridge limitations prevented measurement above 2000 Ω. Next, a short-circuited resonator package was inserted into the adapter. The leads of the header for this sample were short circuited with a piece of gold on silver foil of the same type normally used to mount the quartz wafer. Without changing the frequency of the VHF generator, the distributed inductances were tuned out by adjusting the variable capacitor C to give a minimum measured impedance (less than 3 Ω) with a phase angle of zero degrees. At this point the preliminary tuning was completed, and experiments showed that it was not necessary to repeat the tuning of C. The shunt capacity C_o of a given resonator was next tuned out. For this purpose, frequencies far from resonance (typically f_R + 1 MHz and f_R - 1 MHz) were chosen. The resonator to be measured was inserted into the adapter and the frequency set at f_R - 1 MHz. The variable inductor L was adjusted to give a maximum impedance Z_M with a capacitive phase angle. The frequency was then changed to f_R + 1 MHz and L was adjusted to give a high measured impedance with an inductive phase angle. Further adjustments were made in L until the magnitude of the impedance was the

same at f_R + 1 MHz and f_R - 1 MHz. At the higher frequency the impedance had an inductive phase angle, while at the lower frequency the impedance had a capacitive phase angle. With L and C properly adjusted, it was possible to make point-by-point measurements of the magnitude and phase angle of the resonator impedance as a function of frequency. Final impedance measurements were made after the resonator packages had been sealed and frequency vs. temperature measurements had been completed.

Plots of the magnitude of the impedance vs. frequency are given in Figs. 26-31 for six of the 24 contract samples. Figure 26 shows distinct spurious mode responses on the high side of the resonance frequency. Spurious modes are much less distinct in Figs. 27-31.

The electrical Q of a given resonator is given by $f_R/\Delta f$, where f_R is the resonance frequency of the principal response. If the magnitude of the impedance at resonance is Z_R, then the magnitude of the impedance at the half-power points is $\sqrt{2}\, Z_R$. The quantity Δf is the frequency difference between the half-power points. At the half-power point frequencies the resistive part of the impedance is equal to the reactive part.

Of the 24 composite resonators shipped to NASA-Houston only 5 had Q's less than 2000. There were 9 samples with Q's between 2000 and 4000. Another 9 samples had Q's between 4000 and 6000. Only one sample (047R-B) had a Q above 6000; the Q of this sample was about 9000.

The impedance bridge apparatus was also used to determine precisely the resonance frequency f_R. An analysis of data on all 24 of the contract samples shows that 14 had their resonance frequency within 0.02% of the target frequency. Another 7 had their resonance frequency between 0.02% and 0.1% of the target frequency. Our ability to tune resonators with SiO_x should continue to improve with more practice.

One parameter that should be brought under better control is the impedance at resonance. Although 14 of the 24 contract samples had impedances at resonance between 20 and 80 Ω , the remaining 10 samples had impedances at resonance above 80 Ω . We speculate that the higher values of impedance at resonance are due primarily to a poor bond between the quartz wafer substrate and the evaporated layers. Probably this problem could be cleared up by giving more attention to cleanliness.

4.3 Half-Lattice Bridge Measurements

The half-lattice bridge is shown in Fig. 32. This circuit provides a relatively fast means of obtaining information on bridge isolation as a function of frequency. Because of the logarithmic amplifier, the circuit could only be used below 220 MHz. Even so, the circuit was useful in examining the fundamental frequency (somewhat below 30 MHz) and some of the lower overtones. It was particularly good at showing spurious responses which might be missed in the point-by-point impedance measurement described in the previous section.

To balance the bridge, the variable capacitor and resistor were adjusted until the bridge isolation at f_R + 2 MHz and f_R - 2 MHz was equally high. This procedure had the effect of balancing out the shunt capacity C_o of the resonator. The value of R_T was chosen to be approximately $1/(4\pi f_R C_o)$

The frequency of the VHF source was varied continuously by a motor drive which simultaneously drove a potentiometer. The latter was then used to supply the X-axis sweep for the X-Y recorder.

The fundamental and second through sixth harmonic overtone responses of sample 026R-A which are shown in Figs. 33-35 were obtained with the half-lattice bridge. This particular sample was a shear mode resonator. These figures illustrate the type of information obtained with the half-lattice bridge. In addition, they show that although the fundamental resonance has inharmonic overtones between 27.7 and 28.2 MHz, the second through sixth harmonic overtones appear to become progressively freer of spurious responses. This same observation was made on all resonators measured on the half-lattice bridge. We do not know of a sound explanation for this phenomenon. In fact, when an AT-cut quartz wafer is electroded on both sides, it is found that the spurious responses become progressively worse as one goes to higher harmonic overtones.

4.4 Measurements of dc Resistivity and Shunt Capacity

In making composite resonators it was desirable that the dc resistivity be as high as possible. The dc resistance of almost all the samples was checked with a Simpson multimeter. Values in excess of 10^7 Ω were fairly common. Since the active area was 1 mm^2 and the film

thickness for longitudinal mode resonators was about 8 μ , we see that the dc resistivity was often more than 10^8 Ω-cm.

Capacity and dissipation-factor measurements were made at 1 MHz on almost all composite resonators with a General Radio Type 716-C bridge using a substitution method. For longitudinal mode resonators with an active area of 1 mm^2 and a CdS film thickness of about 8 μ , the calculated value of the shunt capacity C_o was approximately 10 pF. Good resonators commonly had measured values of C_o between 10 and 20 pF and dissipation factors of less than 1%. During one period of the program a number of nonresonant samples were made that were characterized by C_o values in excess of 100 pF. These anomalously high values were attributed to CdS films containing layers of nonuniform resistivity. This difficulty was overcome by adding Cu_2S to the CdS charge and maintaining a higher sulfur pressure during the evaporations.

5. COMPARISON WITH CONTRACT SPECIFICATIONS

The contract goals and requirements have already been listed in the Introduction. These terms will now be compared with the experimental results.

1. The contract required that the resonators operate over a temperature range from 40 to 120°F. This corresponds to a range from 4 to 49°C on the Centigrade scale. This requirement was exceeded since samples were regularly tested from -45 to +100°C, and all samples that were tested were operative over this extended range. The temperature limits at which the resonators become inoperative were not determined.

2. It was a contract requirement that the resonators have a minimum voltage breakdown of 30 V rms when measured at 49°C. This requirement is probably not consistent with the contract goal of a series impedance of 50 Ω at resonance. Since the impedance of a resonator at resonance is purely resistive, we see that the device would have to dissipate 18 W at resonance. This seems unreasonably high for so small a device as the composite resonator described in this report. In fact, the composite resonators were regularly tested with voltages of 1 V rms at room temperature, and none were damaged by this treatment. No samples were tested to destruction.

3. The contract required that the resonators exhibit a Q of at least 1000 when operating into a resistive load equal to their output impedances. The method of Q measurement described in Section 4. 2 did not employ a resistive load, but measured the intrinsic electrical Q of the device itself. There were 9 contract samples with Q's between 2000 and 4000. Another 9 samples had Q's between 4000 and 6000. Only one sample had a Q above 6000; the Q of this sample was about 9000. To us, the achievement of these high Q values is the major accomplishment of the program.

4. The performance goal on insertion loss was not tested.

5. The contract stated as a performance goal that the maximum frequency shift allowable should be 0. 005 from the design center frequencies under all conditions of voltage and temperature. A maximum of no more than 1% was set down as a performance requirement. By referring to Fig. 24 it can be seen that between 4 and 49°C the total frequency shift from the design center frequency (measured at room temperature) was less than 0. 08% for the typical longitudinal mode resonator. For the one shear mode resonator that was checked as a function of temperature, it can be seen from Fig. 23 that the corresponding frequency shift was only 0. 03%. Thus, the contract requirement of a frequency shift less than 1% was met, but the contract goal was not attained.

6. The contract stated that as a performance goal the resonators should be fabricated to the following design center frequencies within ± 0. 001%: 259. 7, 279. 0, and 296. 8 MHz. As stated in Section 4. 2 there were 14 of the 24 contract samples that had their resonance frequency within 0. 02% of the target frequency. Another 7 had their resonance frequency between 0. 02 and 0. 1% of the target frequency. Thus, a good approach was made to the performance goal, and our ability to tune resonators should further improve with more practice.

However, it should be realized that if a resonator has an electrical Q of 5000, the frequency difference between the half-power points is about 0. 056 MHz. But 0. 001% of the design center frequency is roughly 0. 0028 MHz. Therefore, it is necessary to tune the resonator with an accuracy of 1/20th of the frequency difference between the half-power points. Such an accuracy is difficult to achieve.

7. It was stated in the contract as a performance goal that the series impedance at resonance should be 50 Ω nominal. Although 14 of the 24 contract samples had impedances at resonance between 20 and 80 Ω, the remaining 10 samples had impedances at resonance above 80 Ω. Better control of the fabrication process is required to produce composite resonators with more uniform values of impedance at resonance.

6. SUMMARY AND CONCLUSIONS

In this report we have described a new type of miniature resonator for the 100-1000 MHz range. A mathematical analysis of the design considerations and expected performance of the device has been given. Fabrication techniques were described in detail. Experimental measurements were reported and compared with the contract specifications. It was seen that contract requirements 1, 3, and 5 on temperature, electrical Q, and frequency shift were exceeded. If the phrase "50 Ω nominal" is broadly construed, then performance goal 7 on resonance impedance was met by a majority of the contract samples. Considering the Q values that were attained, a reasonable approach was made to performance goal 6 on design center frequencies.

In conclusion, we may say that a new and useful device has been successfully reduced to practice. Both the feasibility and the practicality of these resonators have been demonstrated. Because of their high frequency capability, small size, good electrical Q, and other desirable properties, these composite resonators deserve the serious consideration of circuit designers.

7. LITERATURE CITED

1. N. F. Foster, IEEE Trans. on Sonics and Ultrasonics SU-11, 63 (1964).

2. N. F. Foster, Proc. IEEE 53, 1400 (1965).

3. J. deKlerk and E. F. Kelley, Rev. Sci. Instr. 36, 506 (1965).

4. J. deKlerk, P. G. Klemens, and E. F. Kelly, Appl. Phys. Letters 7, 264 (1965).

5. W. Shockley, D. R. Curran, and D. J. Koneval, "Energy Trapping and Related Studies of Multiple Electrode Filter Crystals," Proc. 17th Annual Frequency Control Symposium, pp. 88-126, 27 May 1963.

6. D. R. Curran and D. J. Koneval, "Energy Trapping and the Design of Single and Multi-Electrode Filter Crystals," Proc. 18th Annual Frequency Control Symposium, pp. 93-119, 4 May 1964.

7. D. R. Curran and D. J. Koneval, "Factors in the Design of VHF Filter Crystals," Proc. 19th Annual Frequency Control Symposium, 20 April 1965.

8. D. J. Koneval, W. J. Gerber, and D. R. Curran, "Improved VHF Filter Crystals Using Insulating Film Techniques," Proc. 20th Annual Frequency Control Symposium, 19 April 1966.

9. "IRE Standards on Piezoelectric Crystals," Proc. IRE 46, 765 (1958).

10. D. A. Berlincourt, D. R. Curran, and H. Jaffe, in Physical Acoustics, edited by W. P. Mason (Academic Press, Inc., New York, 1964), Vol. I, Part A.

11. D. A. Berlincourt, H. Jaffe, and L. R. Shiozawa, Phys. Rev. 129, 1009 (1963).

12. Walter G. Cady, Piezoelectricity (Dover Publications, Inc., New York, 1964).

13. H. E. Bommel, W. P. Mason, and A. W. Warner, Jr., Phys. Rev. 99, 1894 (1955).

14. H. Jaffe and D. A. Berlincourt, Proc. IEEE 53, 1372 (1965).

15. E. A. Guillemin, Introductory Circuit Theory, (John Wiley & Sons, Inc., New York, 1953), pp. 300 and 356.

16. R. Bechmann, Proc. IRE 44, 1600 (1956).

17. Ref. 12, p. 145.

8. INITIAL DISTRIBUTION

Copy No.

Electronic Research Division
1. H. Jaffe
2. Project Administrator

3. Patent Department

4-6. Library

Electronic Research Division
7. D. A. Berlincourt
8. W. R. Cook
9. W. J. Gerber
10. D. J. Koneval
11. H. Leo
12. K. A. Pim
13. D. A. Roberts
14. F. A. Shirland
15. T. R. Sliker
16. J. E. Tozier

17. Piezoelectric Division - D. R. Curran

18-23. NASA Manned Spacecraft Center
2101 Webster Road
Houston, Texas 77058
Attn: EE2/Saverio Gaudiano, Contract NAS 9-4373
(plus one reproducible copy)

24-27. NASA Manned Spacecraft Center
Management Services
Technical Information Dissemination Branch/BM6
2101 Webster Road
Houston, Texas 77058
Attn: Retha Shirkey, Contract NAS 9-4373

28. NASA Manned Spacecraft Center
2101 Webster Road
Houston, Texas 77058
Attn: John T. Wheeler, Technology Utilization Officer

29. NASA Manned Spacecraft Center
General Research Procurement Branch/BG751
2101 Webster Road
Houston, Texas 77058
Attn: John J. Daunt, Contract NAS 9-4373

30-32. U. S. Army Electronic Command
Electronic Parts and Materials Division
Fort Monmouth, New Jersey 07703
Attn: A. Rand
Dr. G. K. Guttwein
Dr. R. Bechmann

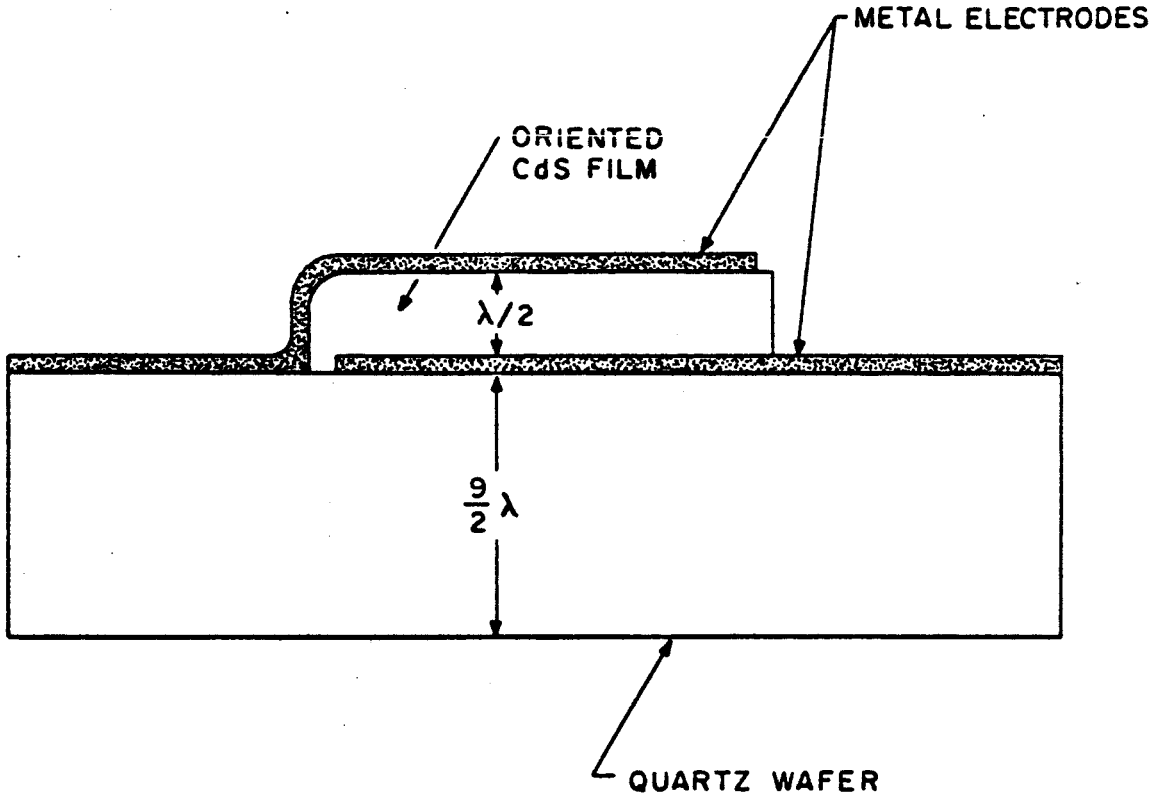

FIG. 1. SCHEMATIC OF COMPOSITE RESONATOR

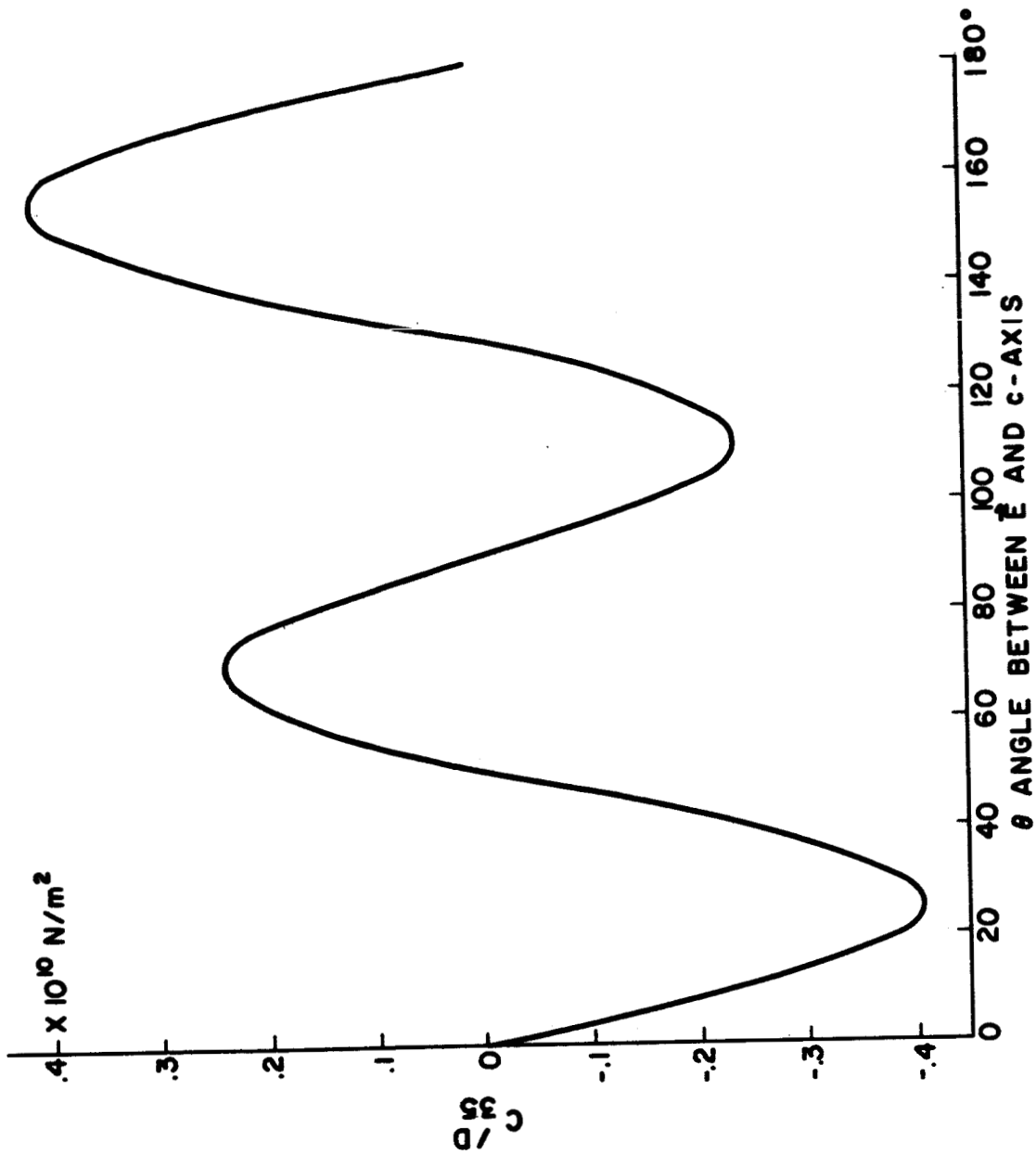

Fig 2. $^{1D}c_{35}$ vs. θ for CdS.

ERD 7102

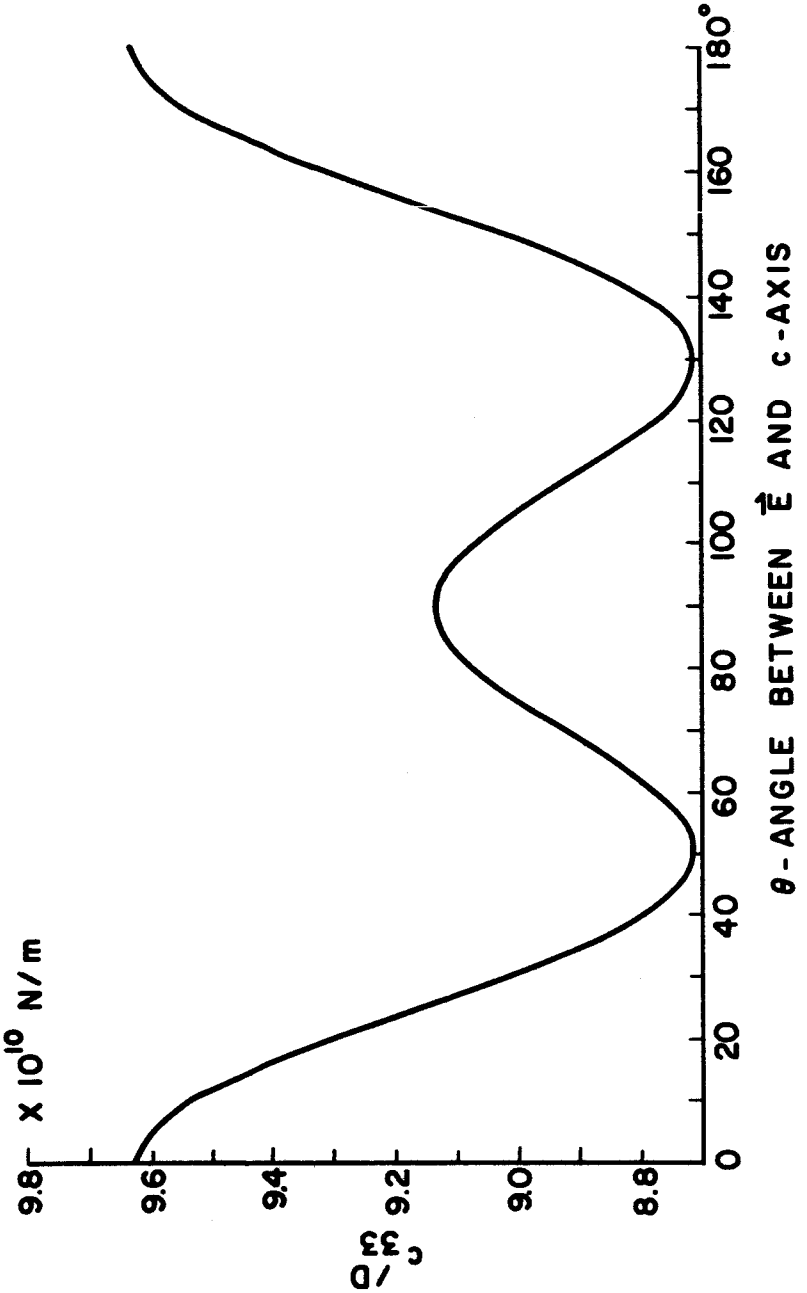

Fig. 3 c'^{D}_{33} vs. θ for CdS.

ERD 7096

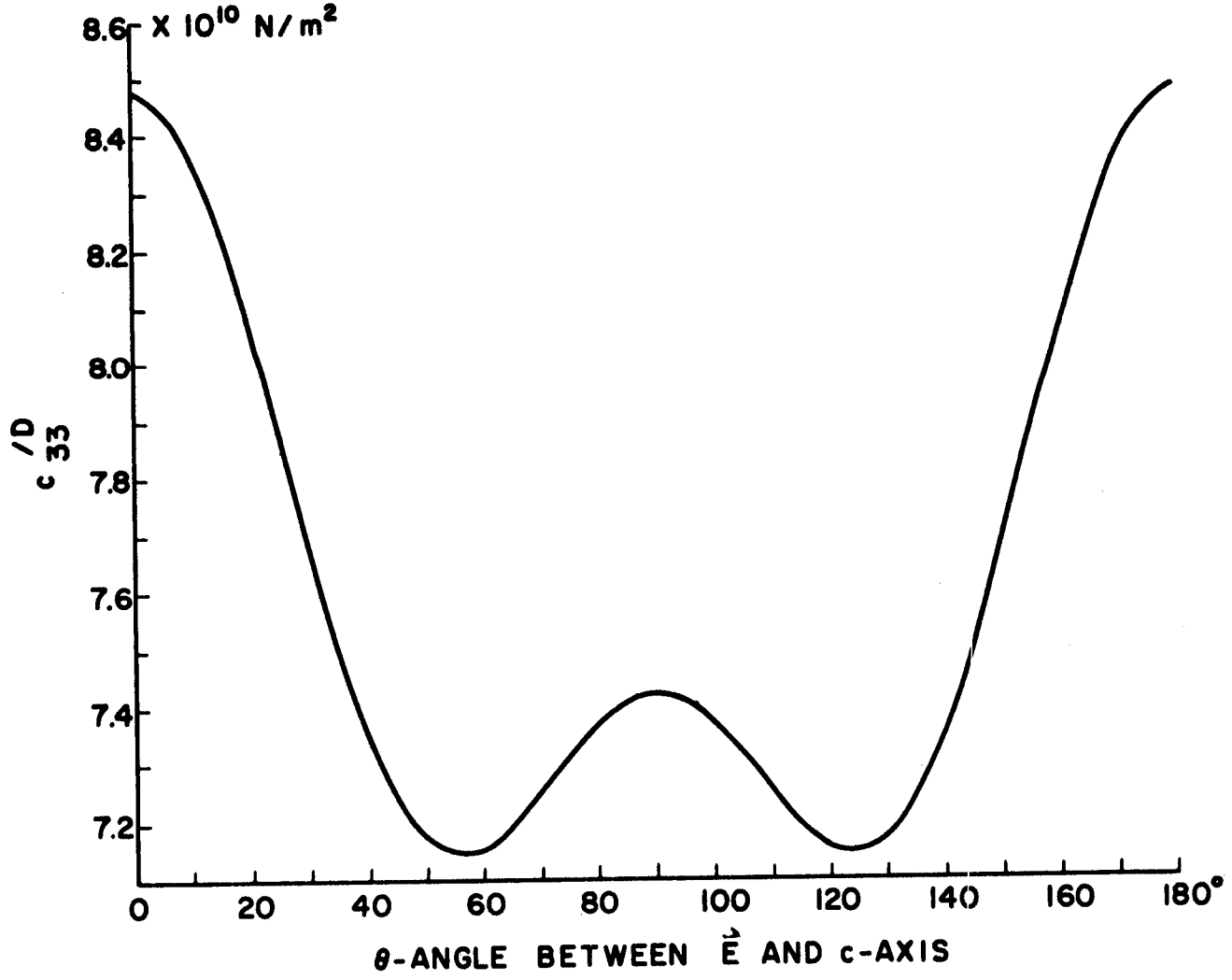

Fig. 4 $c'_{33}D$ vs. θ for CdSe.

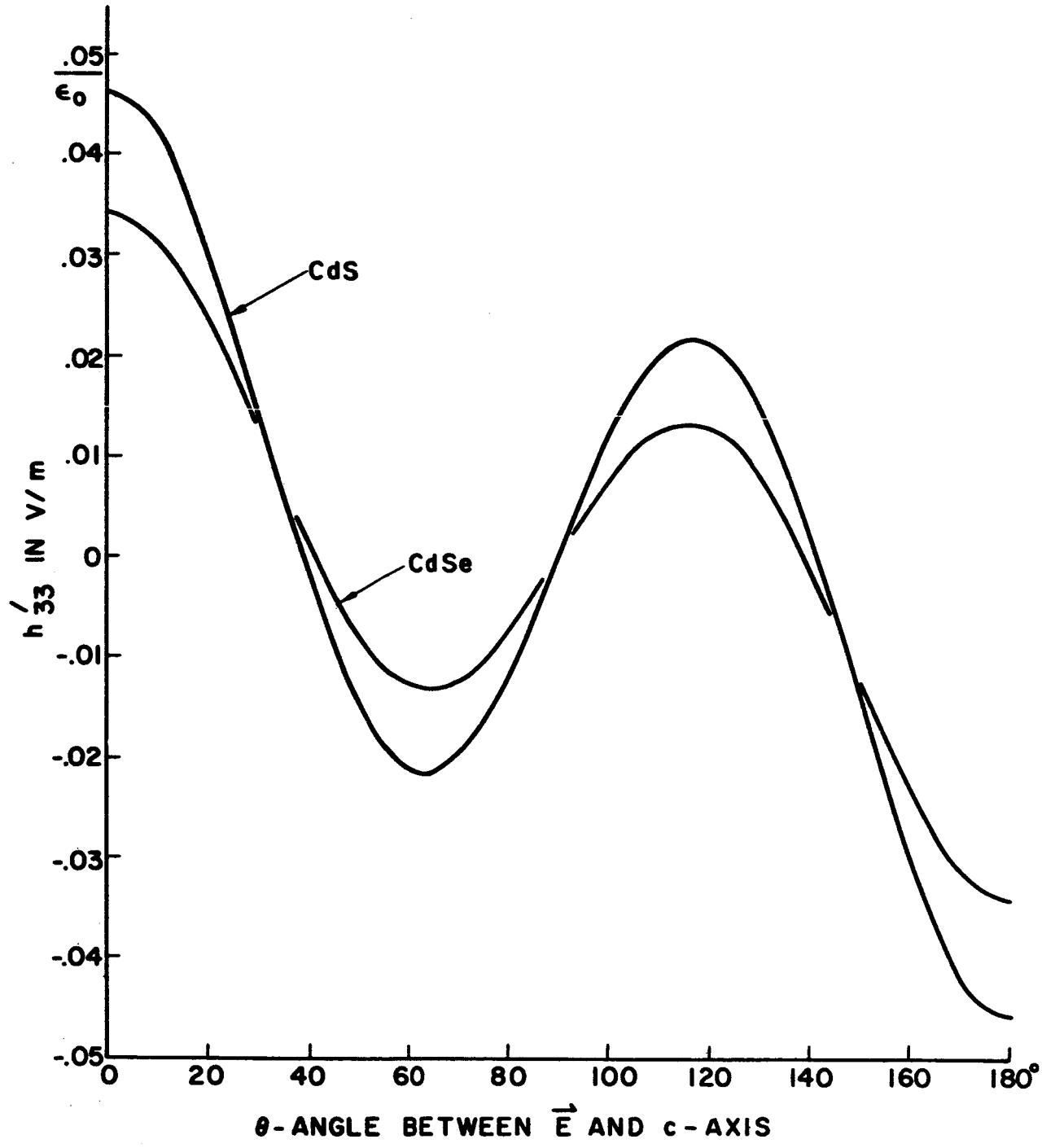

Fig. 5 h'_{33} vs. θ for CdS and CdSe.

ERD 7071

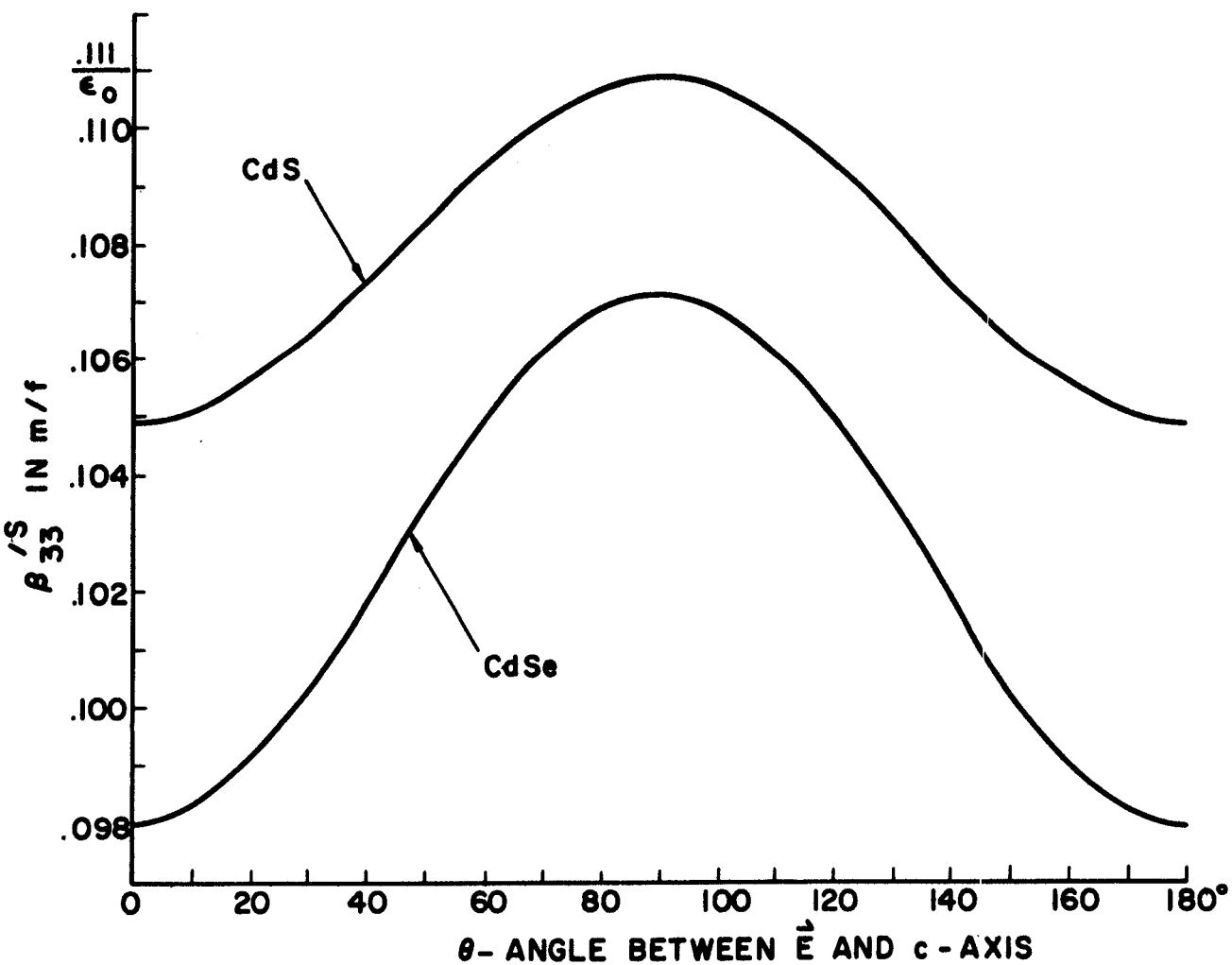

Fig. 6 β'^{S}_{33} vs. θ for CdS and CdSe.

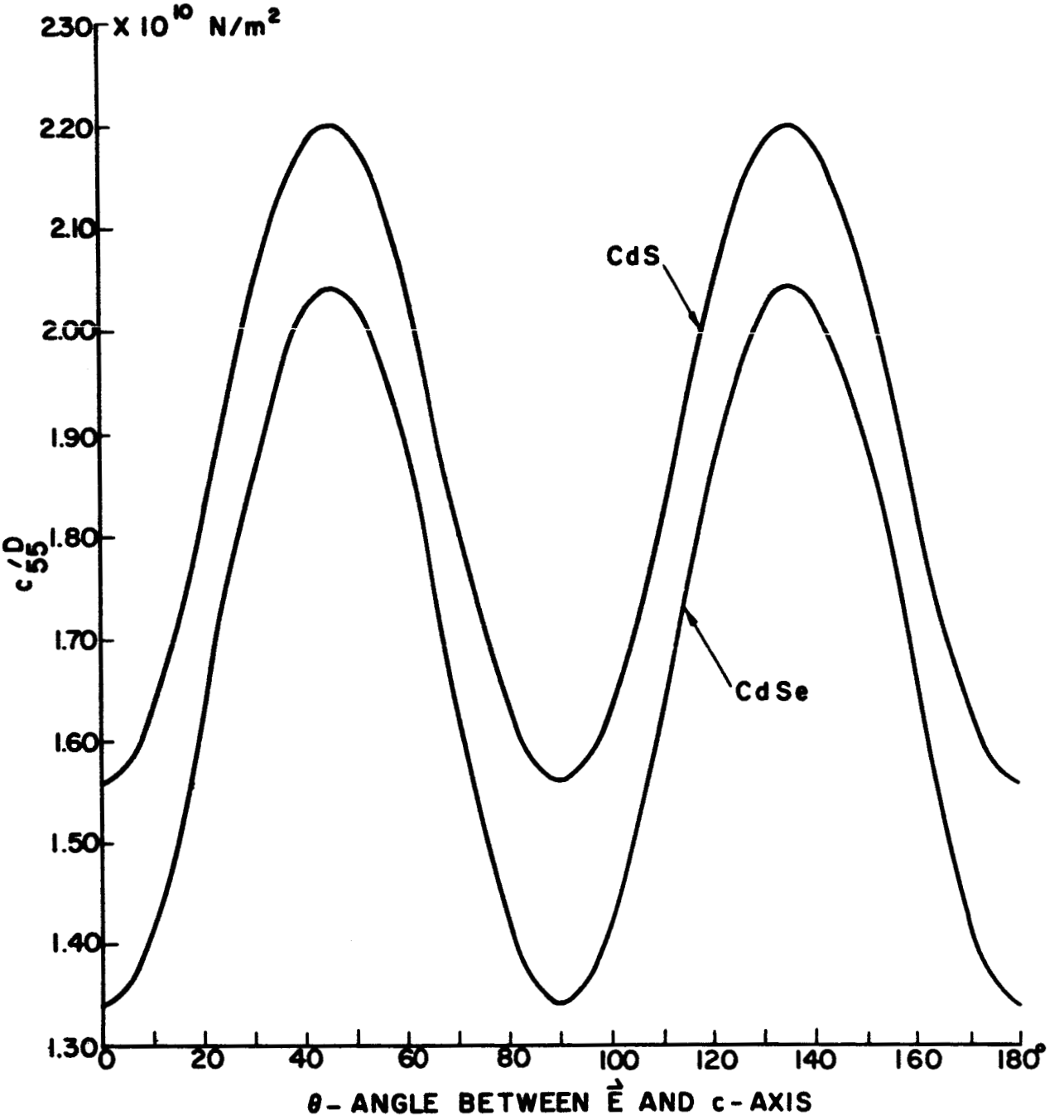

Fig. 7. $c_{55}^{'D}$ vs. θ for CdS and CdSe.

ERD 7099

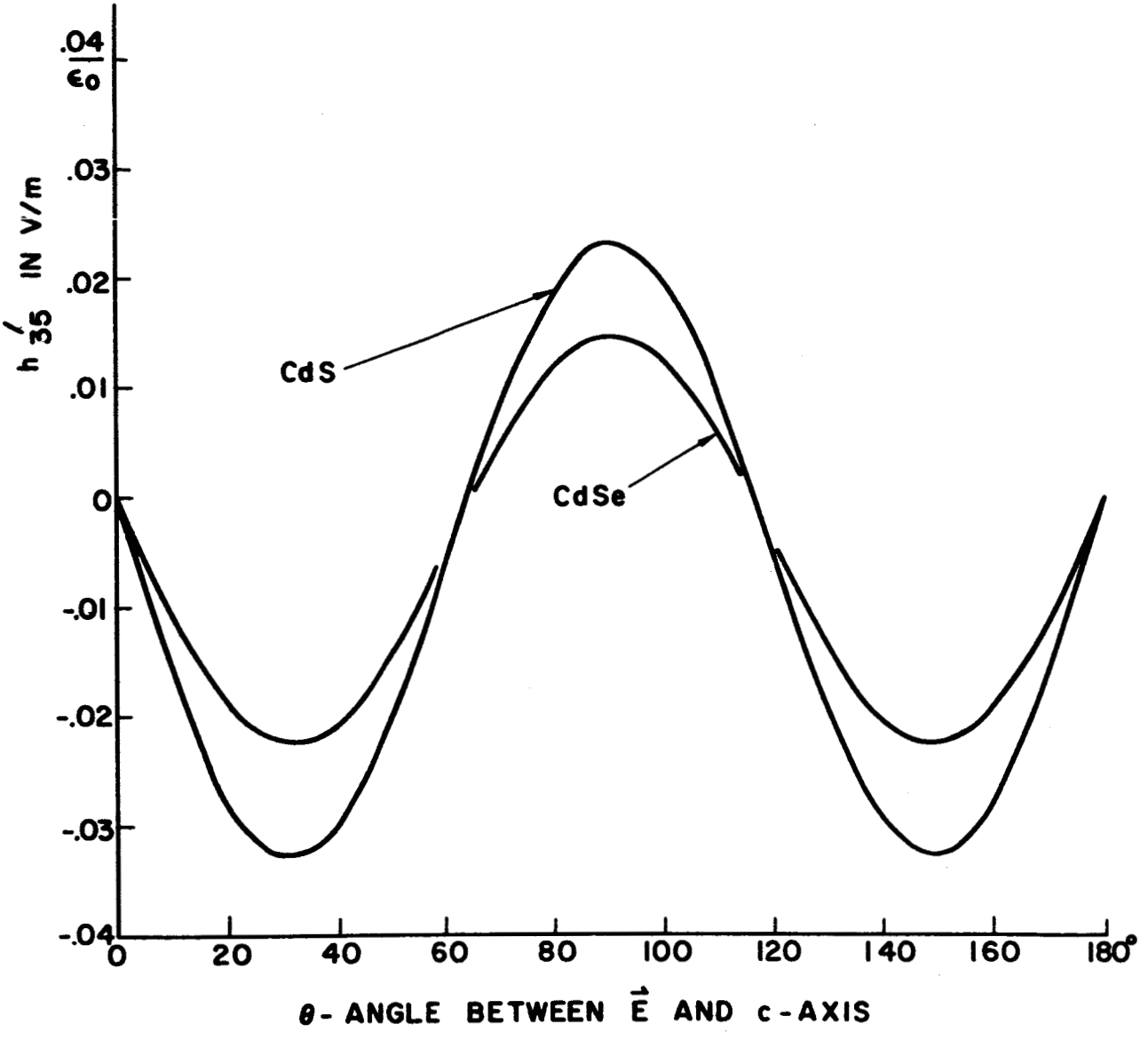

Fig. 8. h'_{35} vs. θ for CdS and CdSe.

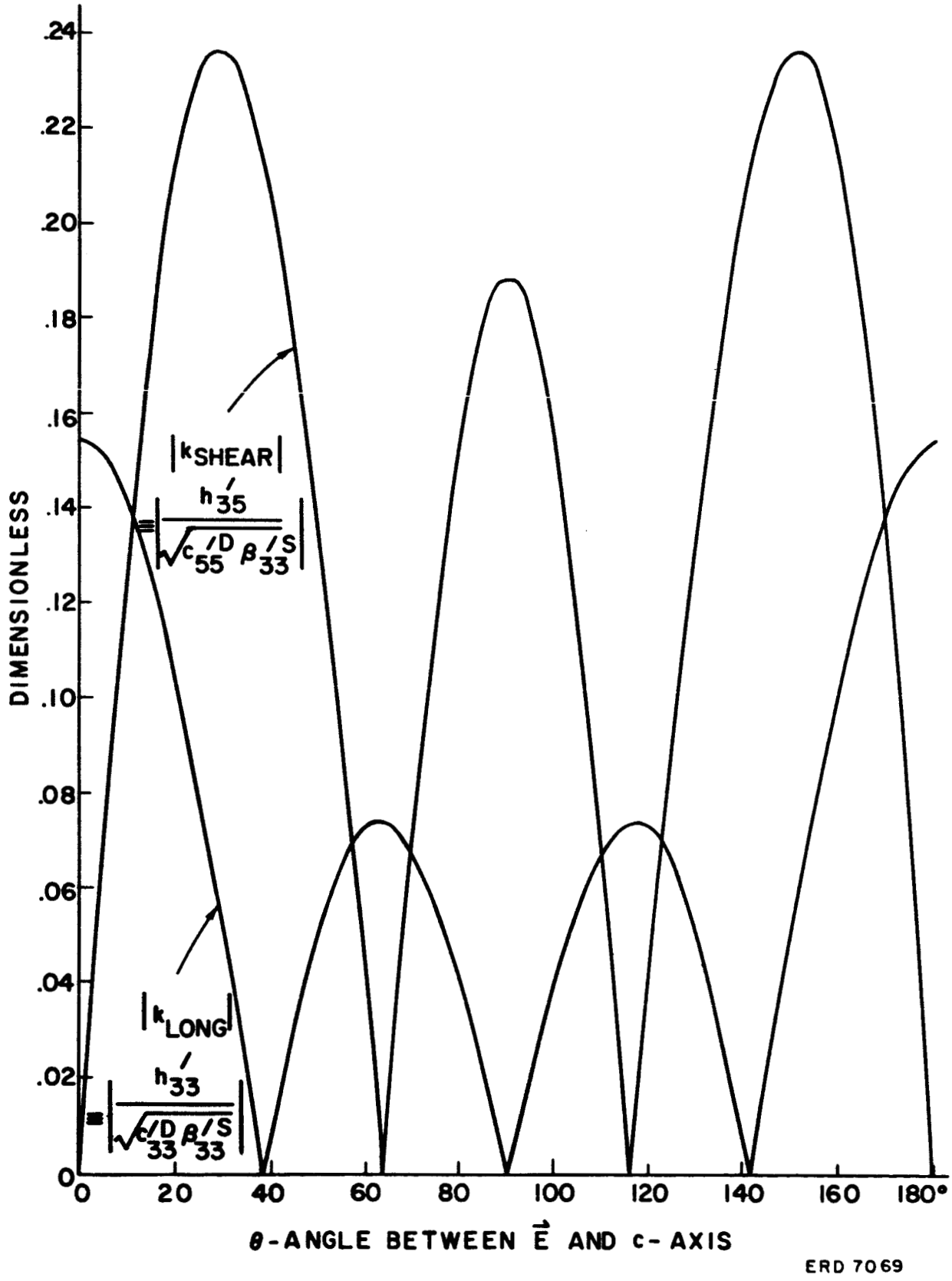

Fig. 9. LONGITUDINAL AND SHEAR ELECTROMECHANICAL COUPLING FACTORS AS A FUNCTION OF θ FOR CdS.

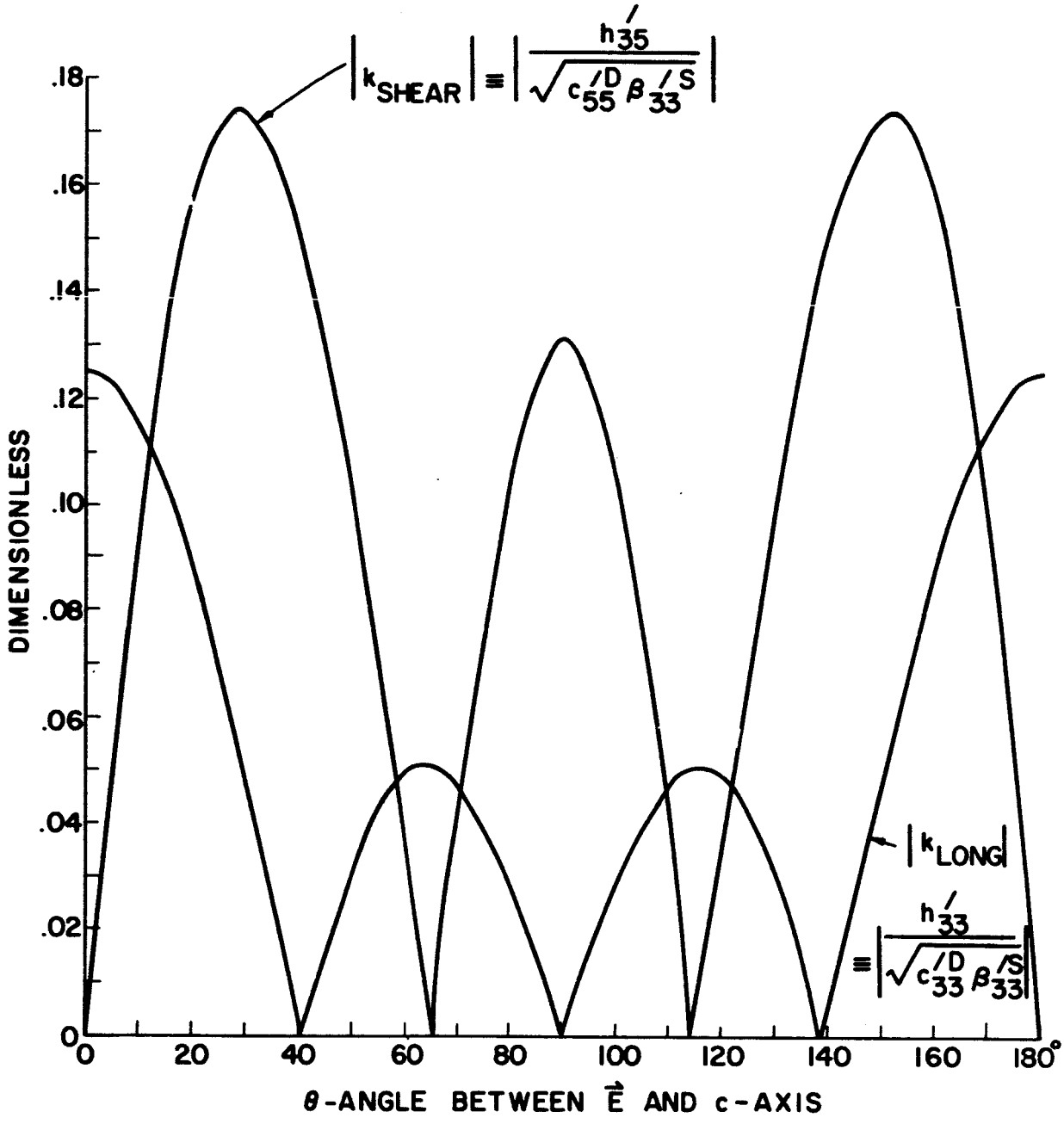

Fig. 10. LONGITUDINAL AND SHEAR ELECTROMECHANICAL COUPLING FACTORS AS A FUNCTION OF θ FOR CdSe.

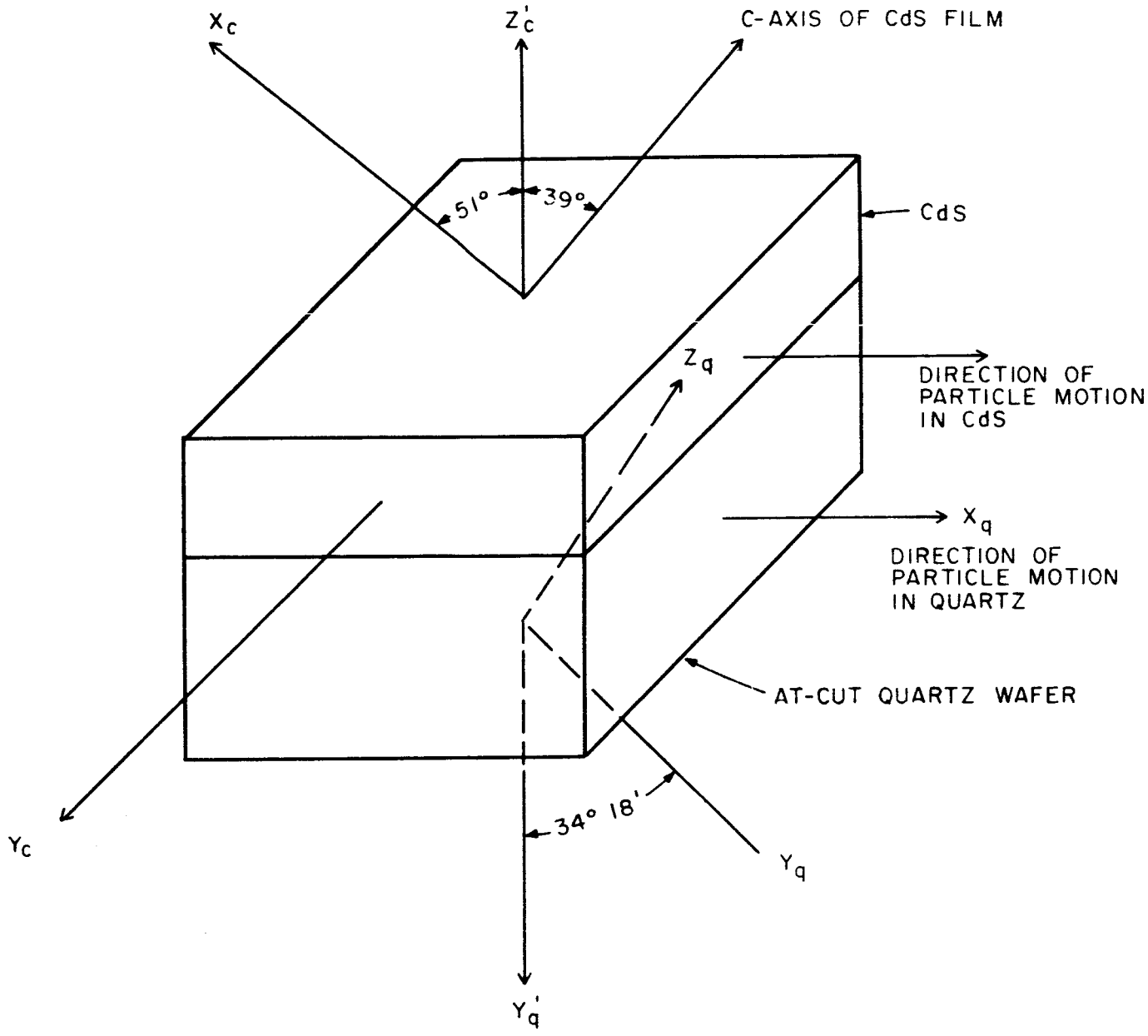

FIG. 11. PREFERRED ORIENTATION OF C-AXIS OF CdS FILM WITH RESPECT TO AT-CUT QUARTZ WAFER.

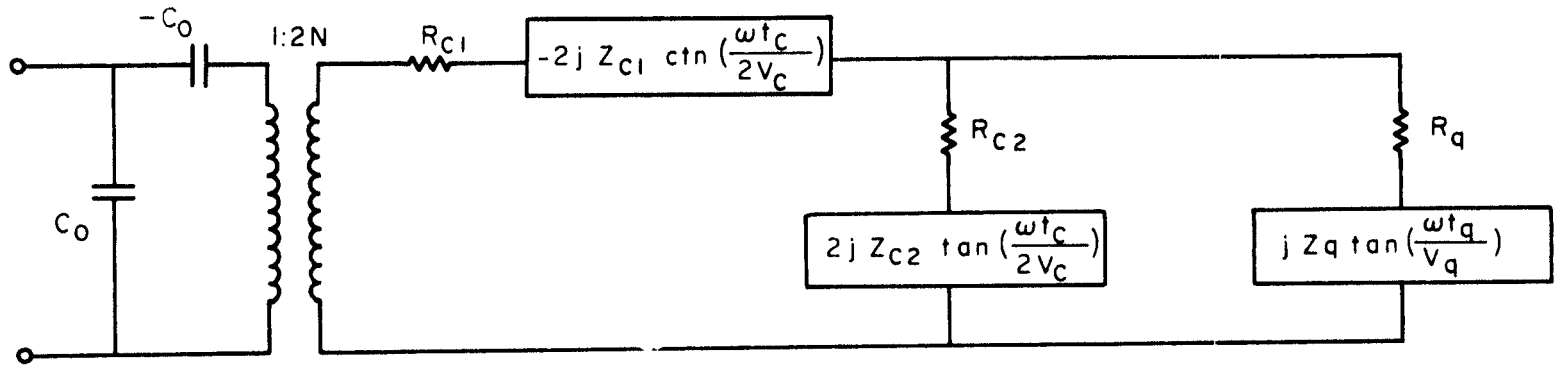

$$C_o = A/\beta_{33}^{'S}\, t_c$$

$$N = h_{35}^{'} C_o$$

$$Z_{c1} = A\rho_c v_c \left[1 + (\frac{\omega t_c}{2v_c})^2 / 4Q_c^2 \sin^2(\frac{\omega t_c}{2v_c})\right]^{-1}$$

$$Z_{c2} = A\rho_c v_c \left[1 + (\frac{\omega t_c}{2v_c})^2 / 4Q_c^2 \cos^2(\frac{\omega t_c}{2v_c})\right]^{-1}$$

$$v_c = \sqrt{c_{55}^{'D}/\rho_c}$$

$$Z_q = A\rho_q v_q \left[1 + (\frac{\omega t_q}{v_q})^2 / 4Q_q^2 \cos^2(\frac{\omega t_q}{v_q})\right]^{-1}$$

$$v_q = \sqrt{c_{66}^{'D}/\rho_c}$$

$$R_{c1} = \frac{\pi Z_{c1}}{4Q_c} (\frac{\omega}{\omega_A}) \frac{1}{\sin^2(\frac{\omega t_c}{2v_c})}$$

$$R_{c2} = \frac{\pi Z_{c1}}{4Q_c} (\frac{\omega}{\omega_A}) \frac{1}{\cos^2(\frac{\omega t_c}{2v_c})}$$

$$Q_c = Q_c^o(\omega_A/\omega)$$

$$R_q = \frac{n\pi Z_q}{2Q_q} (\frac{\omega}{\omega_A}) \frac{1}{\cos^2(\frac{\omega t_q}{v_q})}$$

$$Q_q = Q_q^o(\omega_A/\omega)$$

FIG. 12 CdS-QUARTZ RESONATOR EQUIVALENT CIRCUIT. THIS REPRESENTATION IS VALID OVER A BROAD FREQUENCY RANGE.

ERD 7108

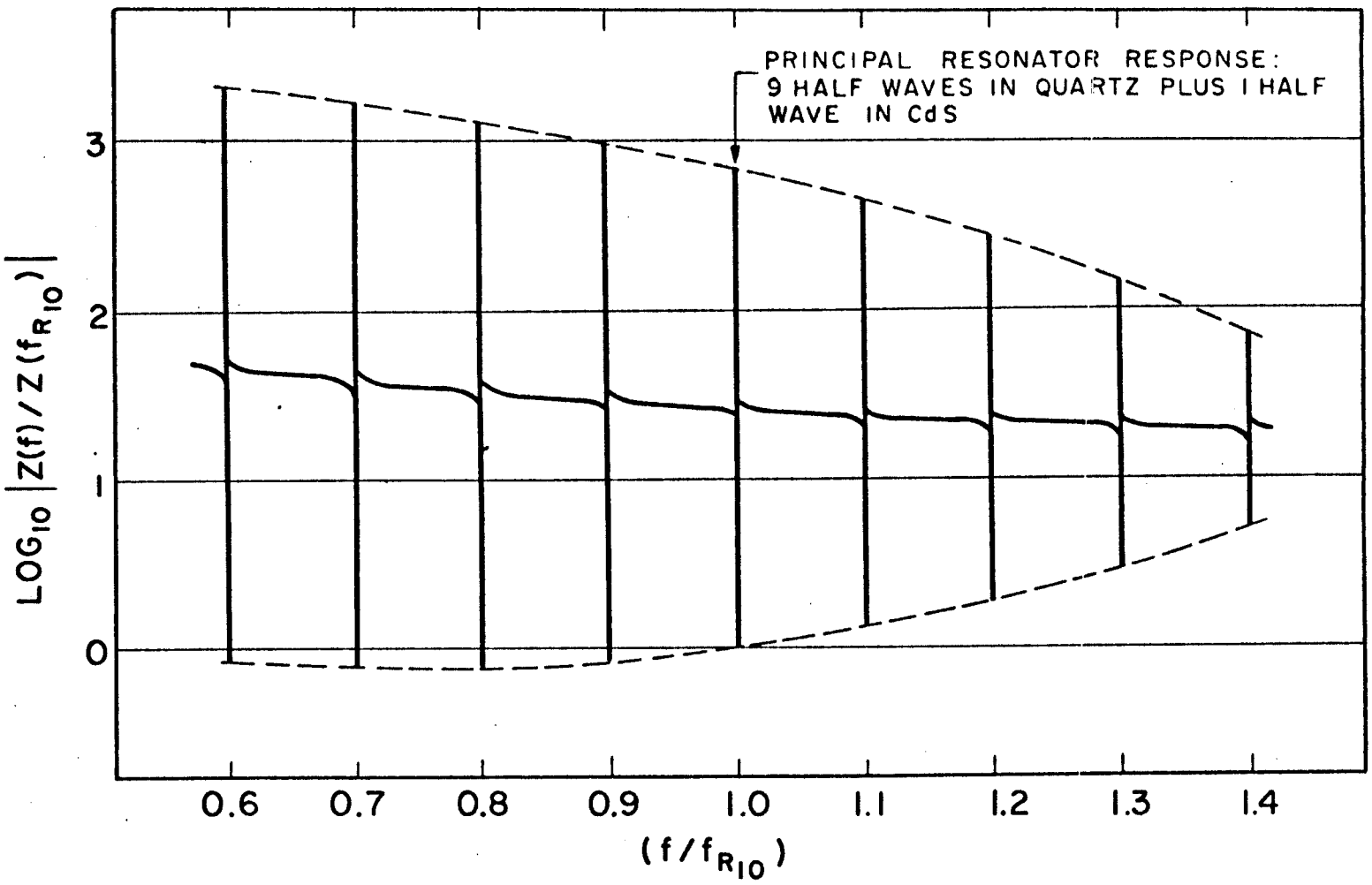

FIG. 13. THEORETICAL IMPEDANCE CHARACTERISTIC OF COMPOSITE CdS-QUARTZ RESONATOR. FREQUENCY RANGE SHOWN INCLUDES 4 HARMONIC RESPONSES ABOVE AND BELOW THE PRINCIPAL RESONANCE RESPONSE FREQUENCY $f_{R_{10}}$.

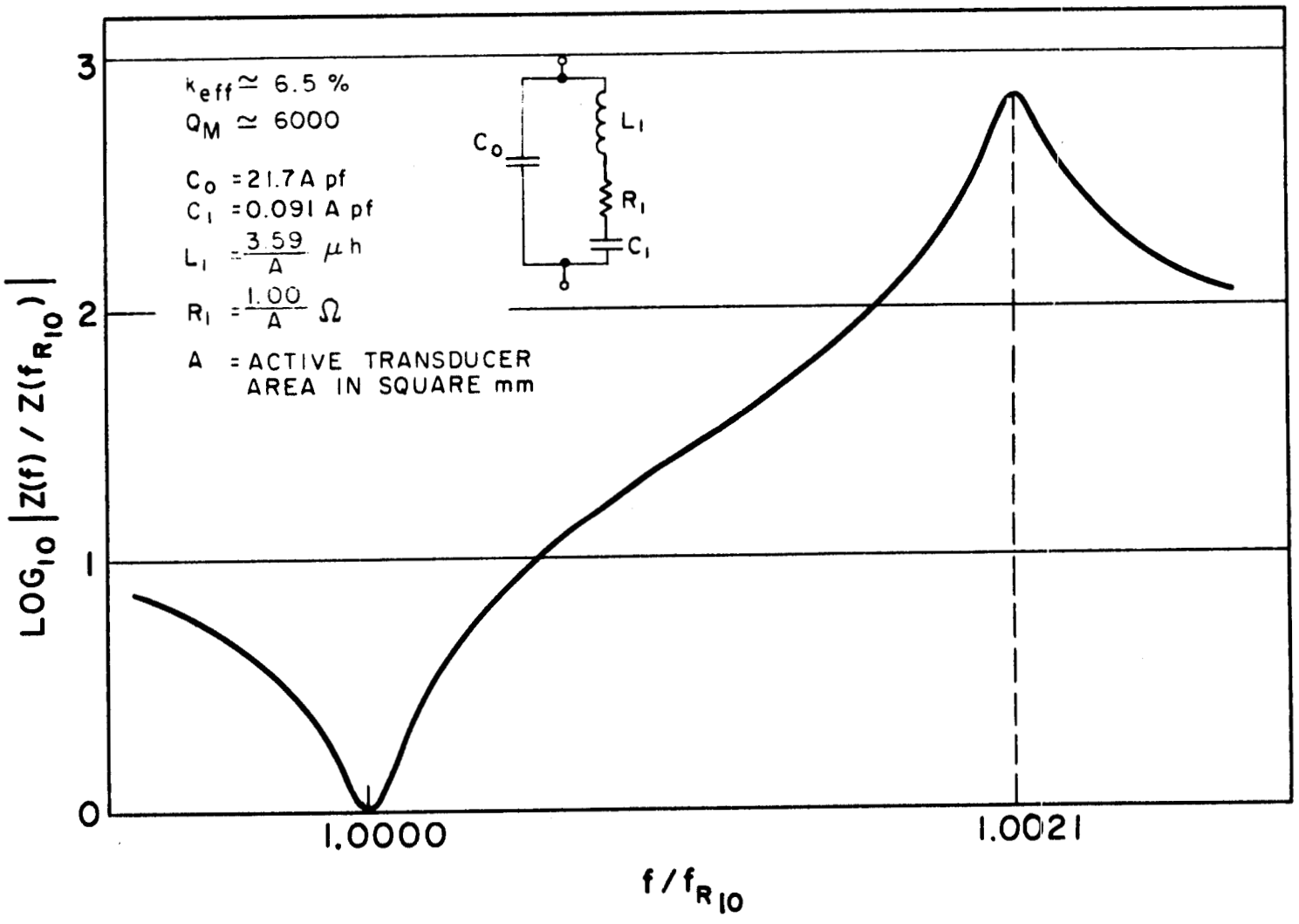

FIG. 14. THEORETICAL PRINCIPAL RESPONSE OF FIG. 13. ON EXPANDED FREQUENCY SCALE. ALSO INDICATED ARE PARAMETERS FOR THE ELECTRICAL EQUIVALENT CIRCUIT REPRESENTATION AROUND RESONANCE AND ANTI-RESONANCE FOR A RESONATOR WITH $f_{R_{10}} = 278.4$ Mc

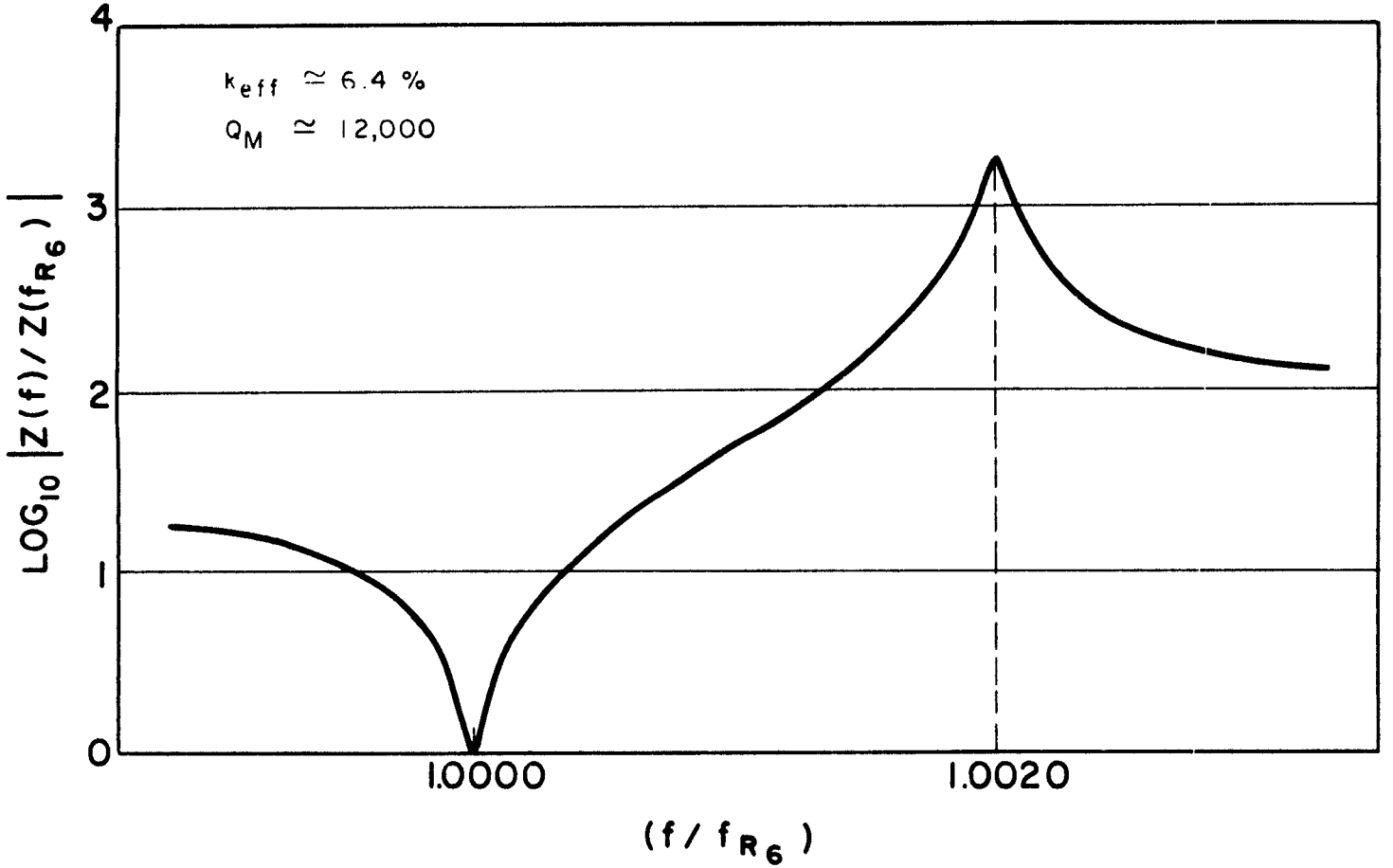

FIG 15 THEORETICAL IMPEDANCE CHARACTERISTIC NEAR 4TH RESONANCE BELOW PRINCIPAL RESONANCE RESPONSE IN CdS-QUARTZ RESONATOR.

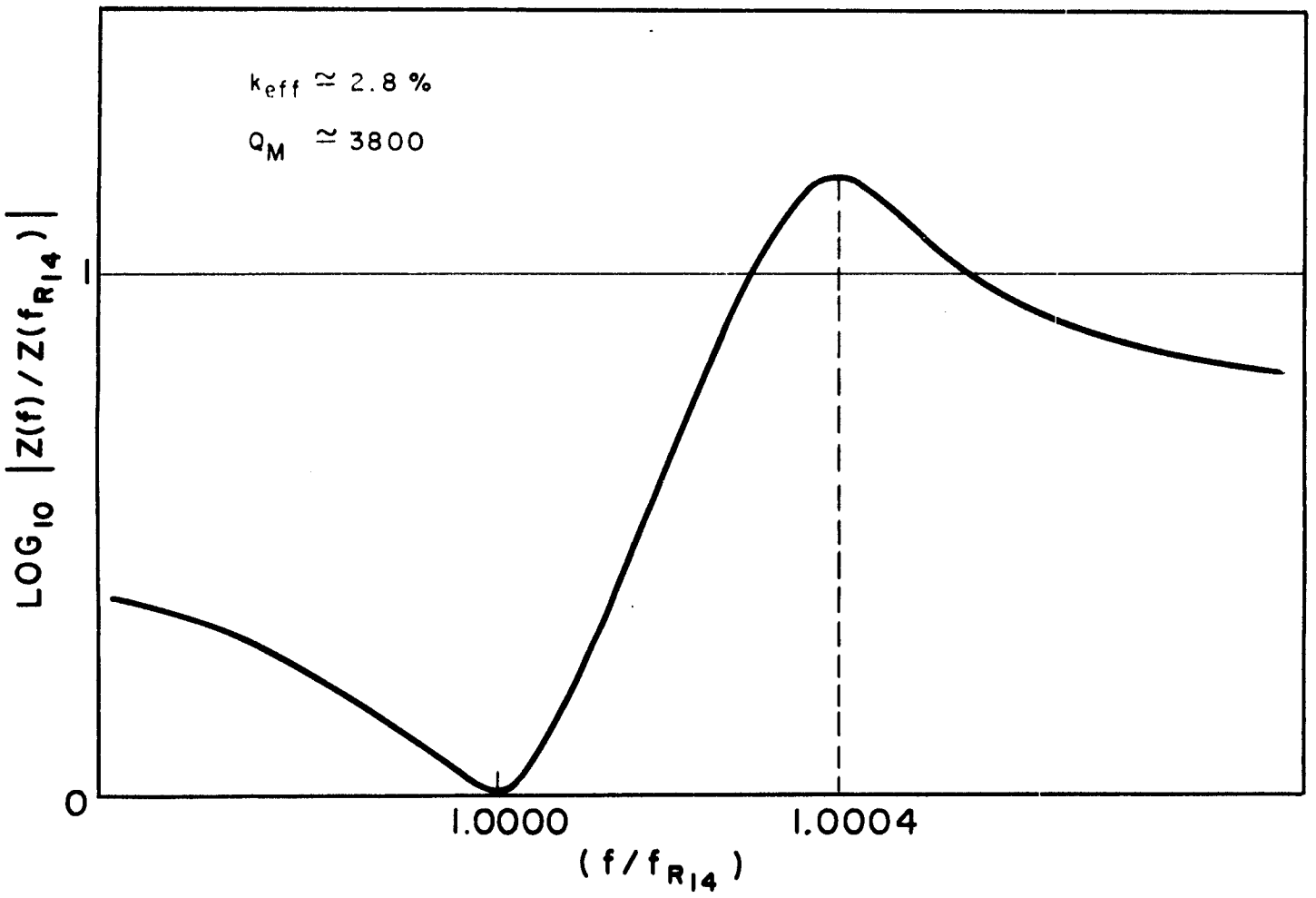

FIG. 16. THEORETICAL IMPEDANCE CHARACTERISTIC NEAR 4TH RESONANCE ABOVE PRINCIPAL RESONANCE RESPONSE IN CdS-QUARTZ RESONATOR.

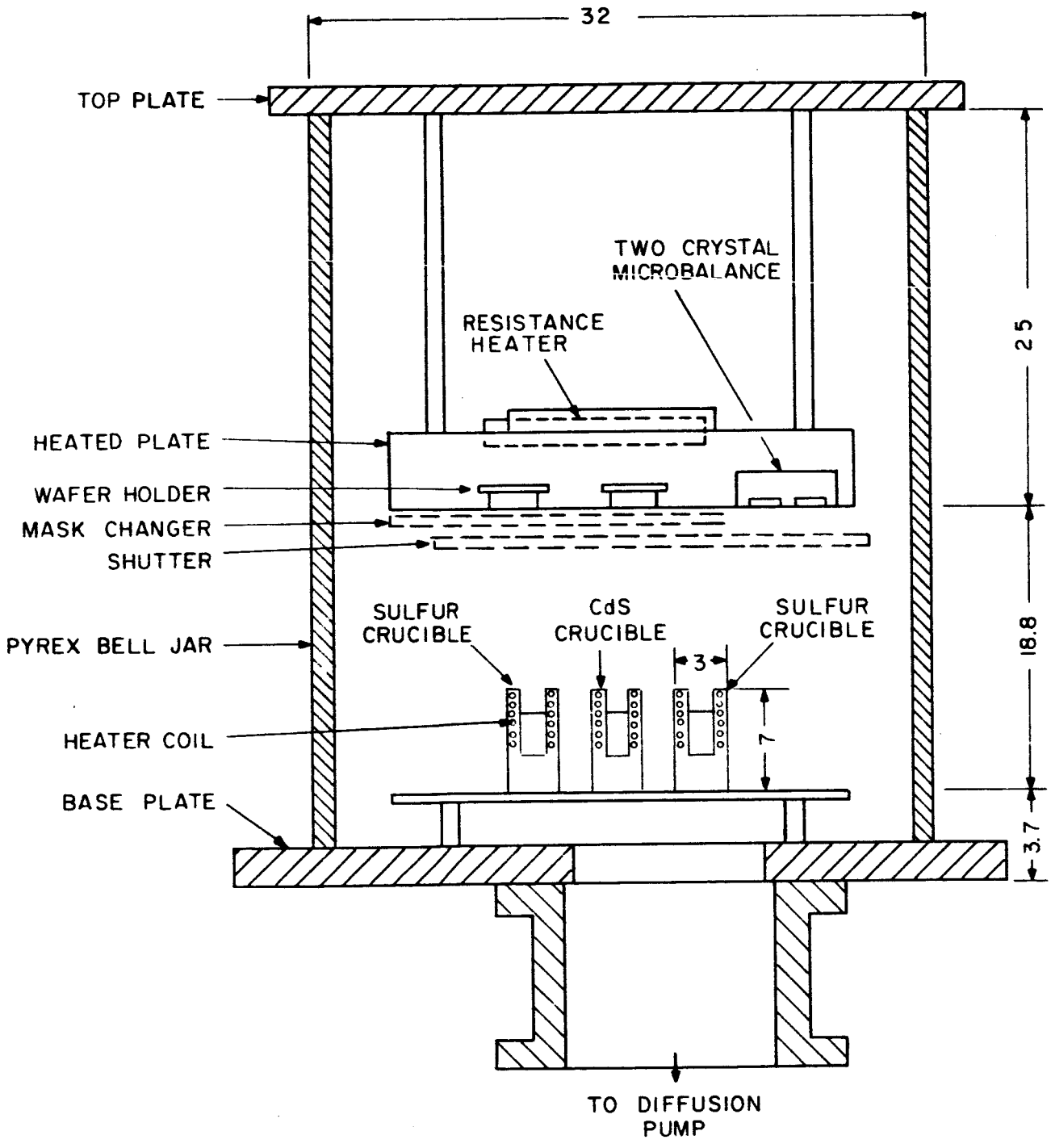

FIG. 17. SCHEMATIC OF BELL JAR APPARATUS.

ERD 7229

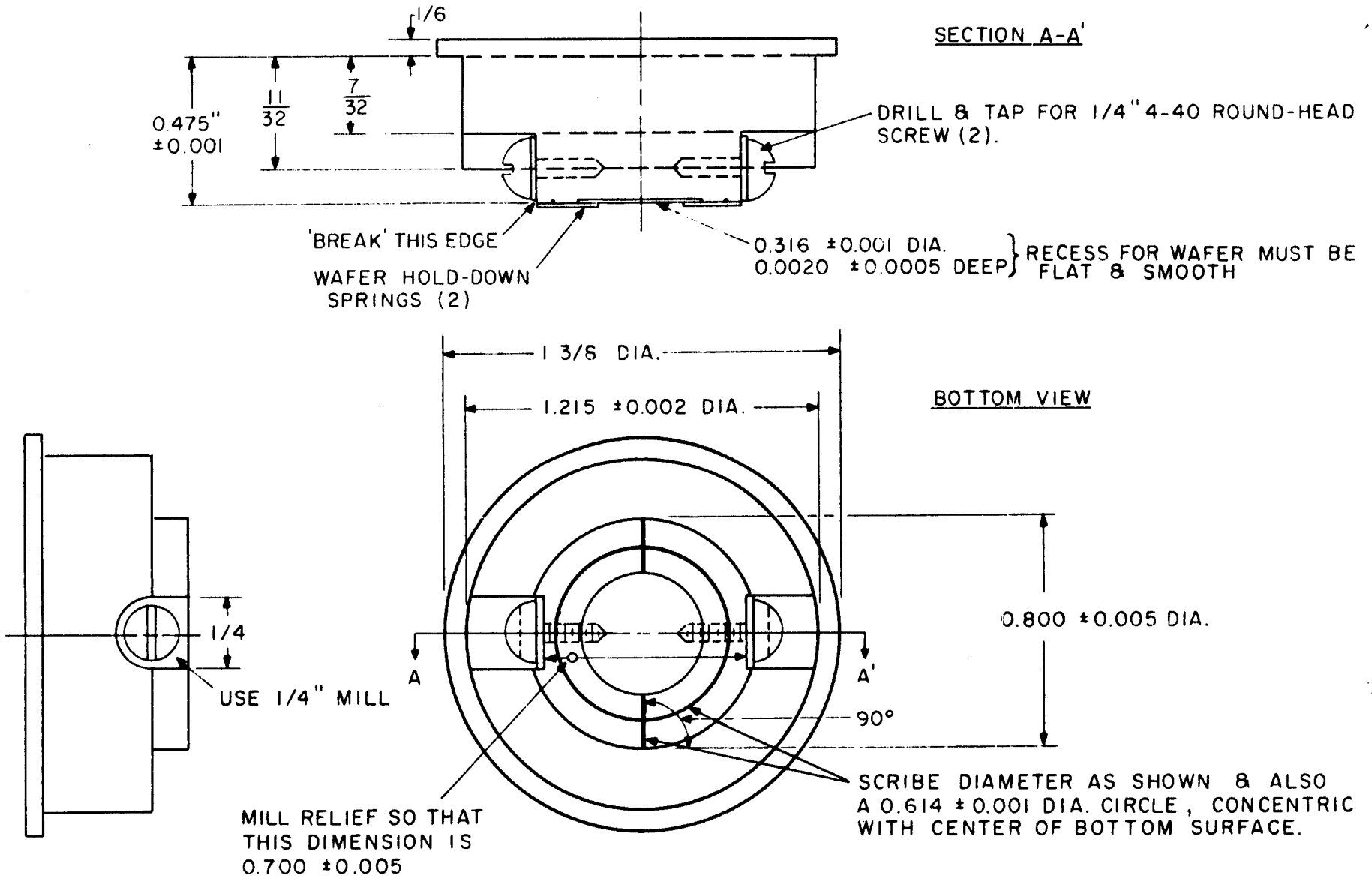

ERD 7231

FIG. 18. SUBSTRATE HOLDER

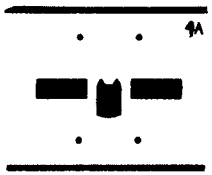

MASK FOR BOTTOM METAL ELECTRODE

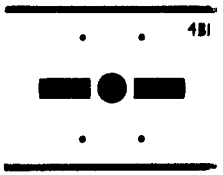

MASK FOR CdS LAYER

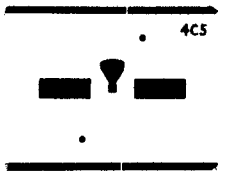

MASK FOR TOP METAL ELECTRODE

FIG. 19. MASKS USED FOR COMPOSITE RESONATOR EVAPORATIONS.

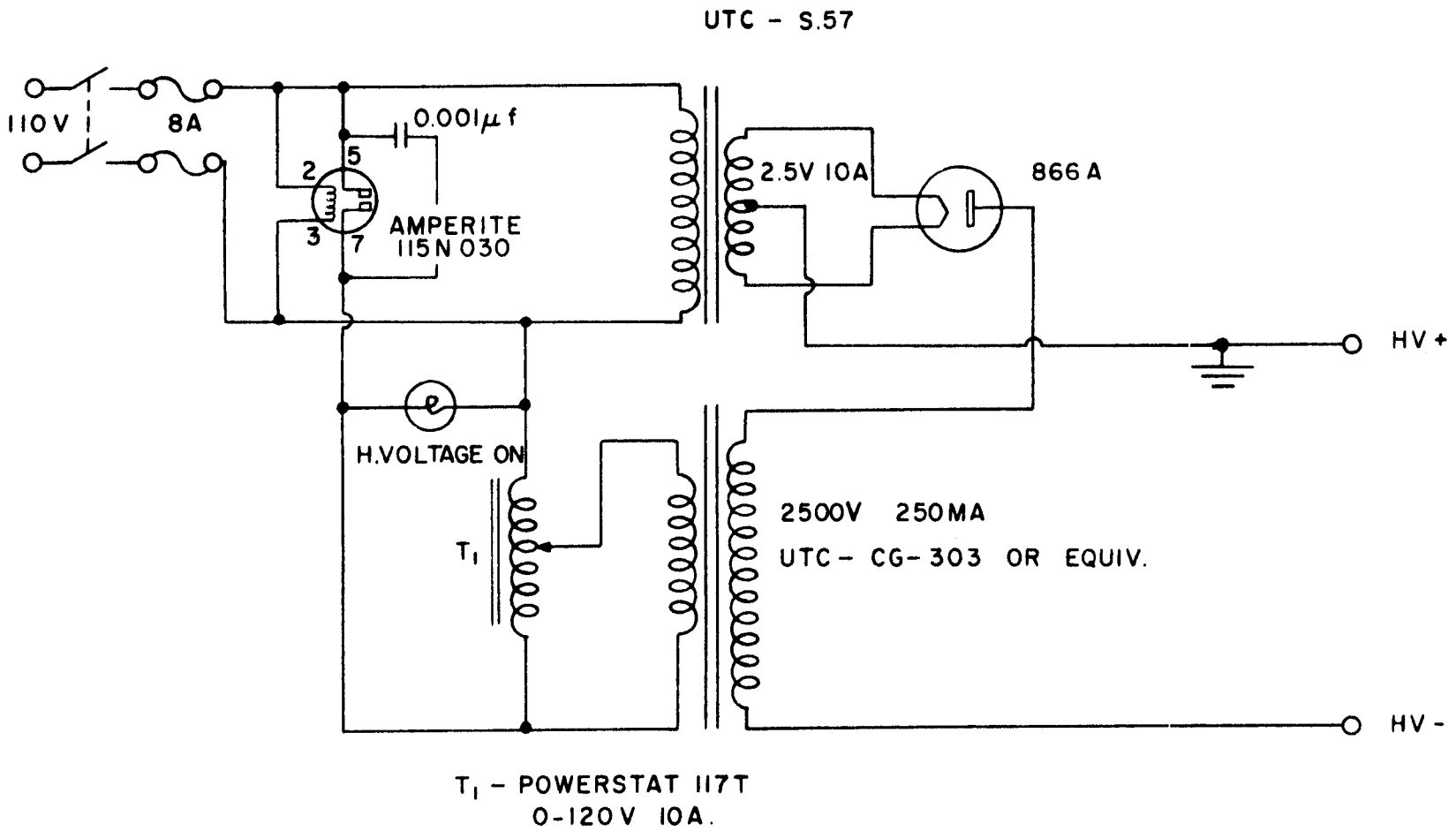

ERD 7228

FIG. 20. GLOW DISCHARGE POWER SUPPLY

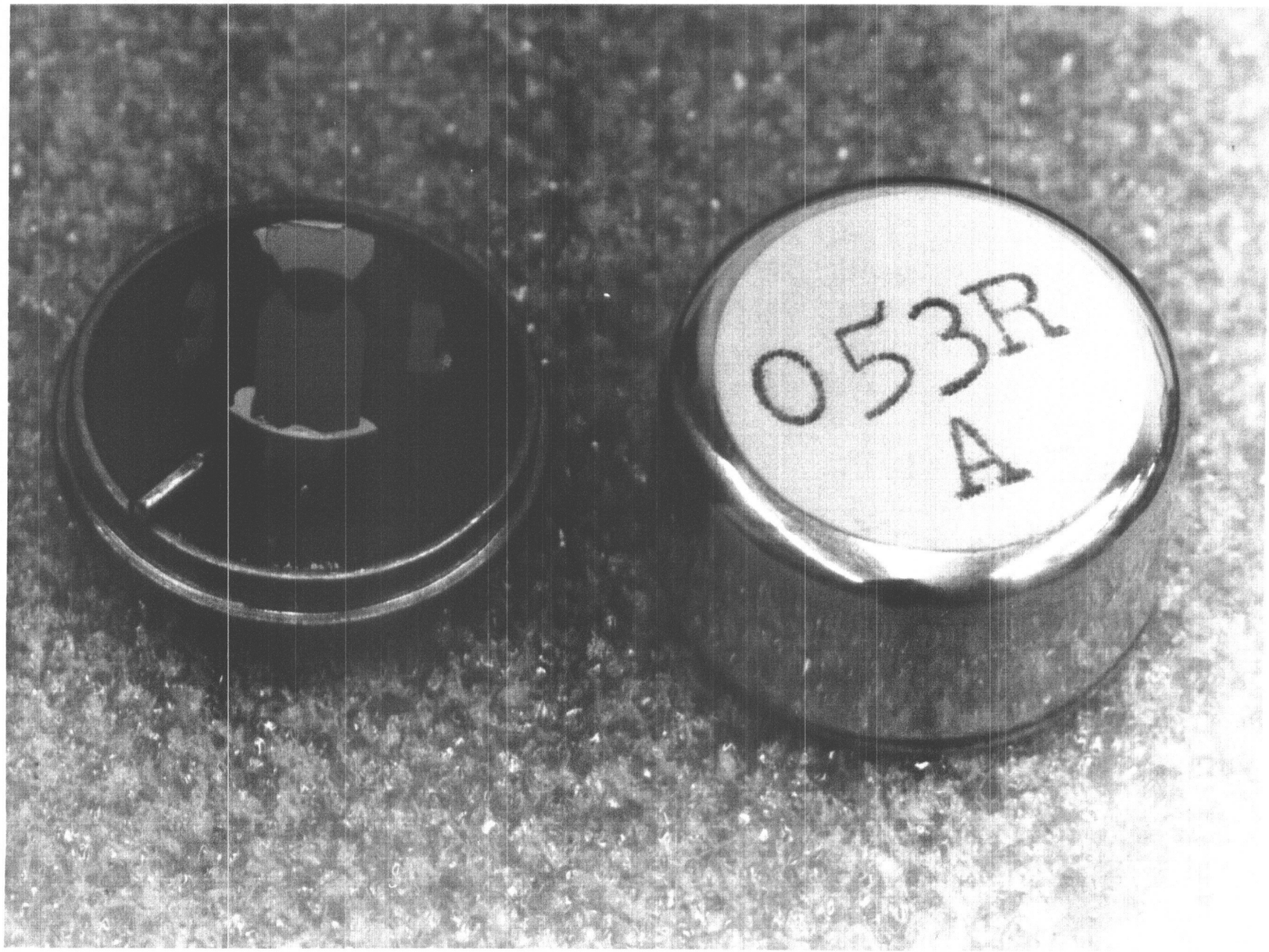

Fig. 21. Mounted composite resonator - unsealed and sealed.

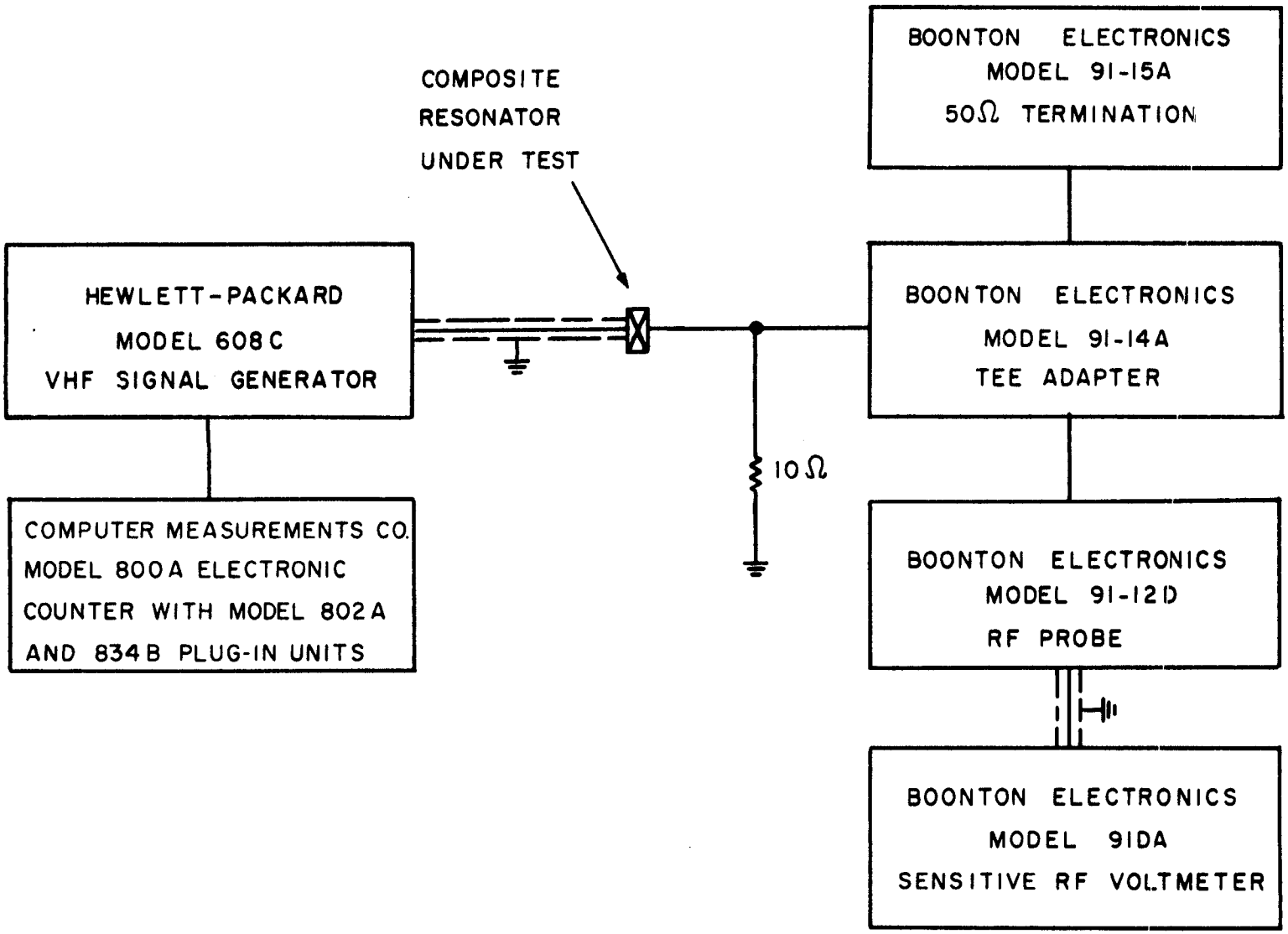

FIG. 22. TRANSMISSION CIRCUIT MEASUREMENT APPARATUS.

ERD 7217

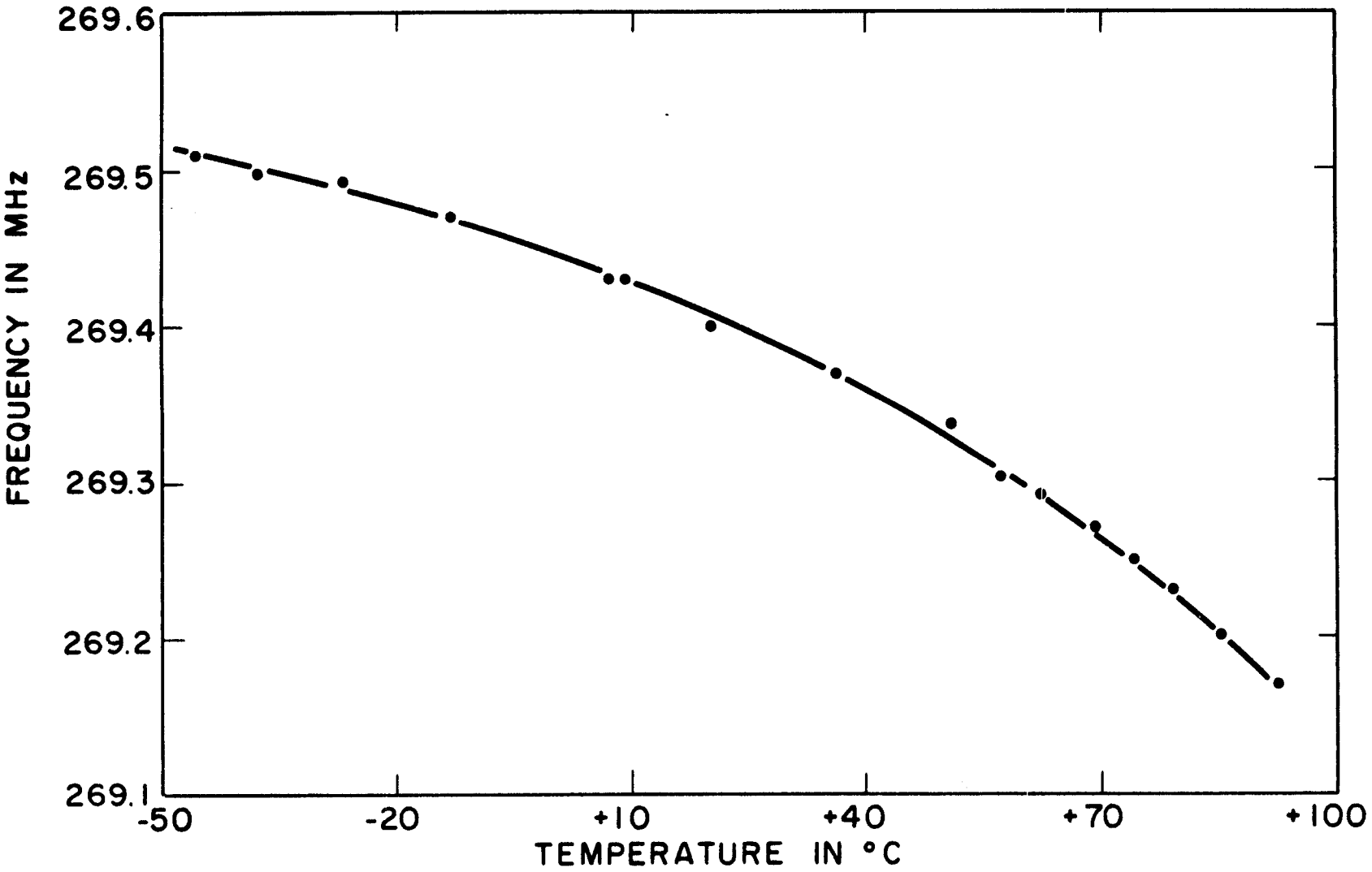

ERD 7197

FIG. 23. PRINCIPAL RESPONSE FREQUENCY vs. TEMPERATURE FOR SHEAR MODE COMPOSITE RESONATOR 035R-C.

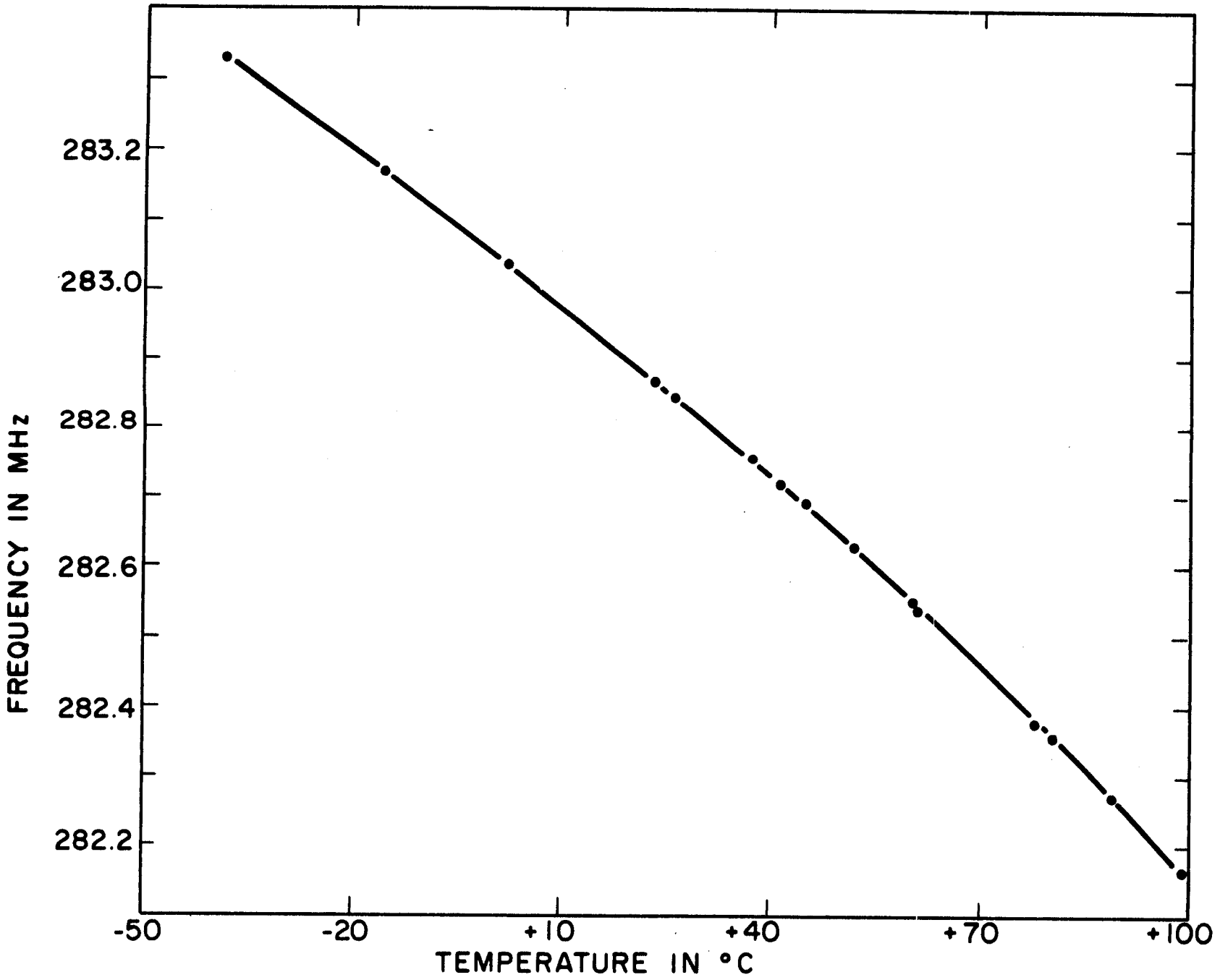

FIG. 24 PRINCIPAL RESPONSE FREQUENCY vs. TEMPERATURE FOR LONGITUDINAL MODE COMPOSITE RESONATOR 037R-B.

ERD 7198

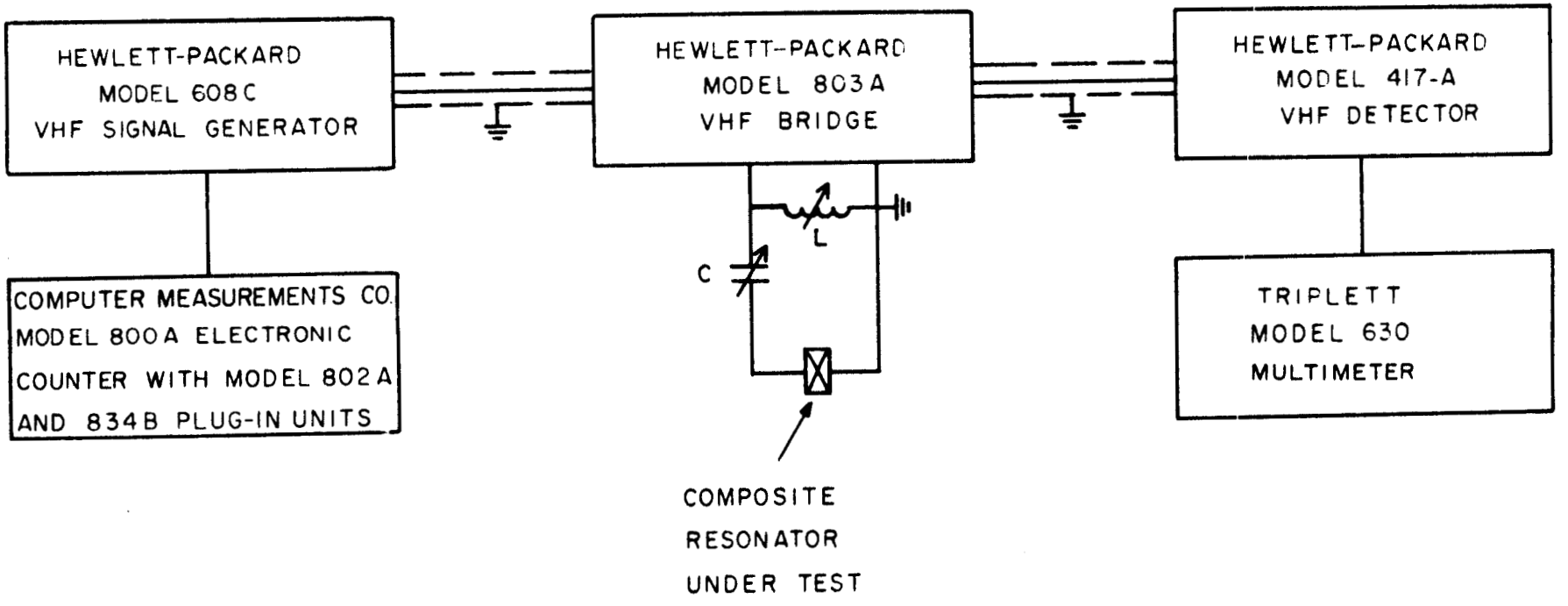

ERD 7218

FIG. 25. IMPEDANCE BRIDGE APPARATUS.

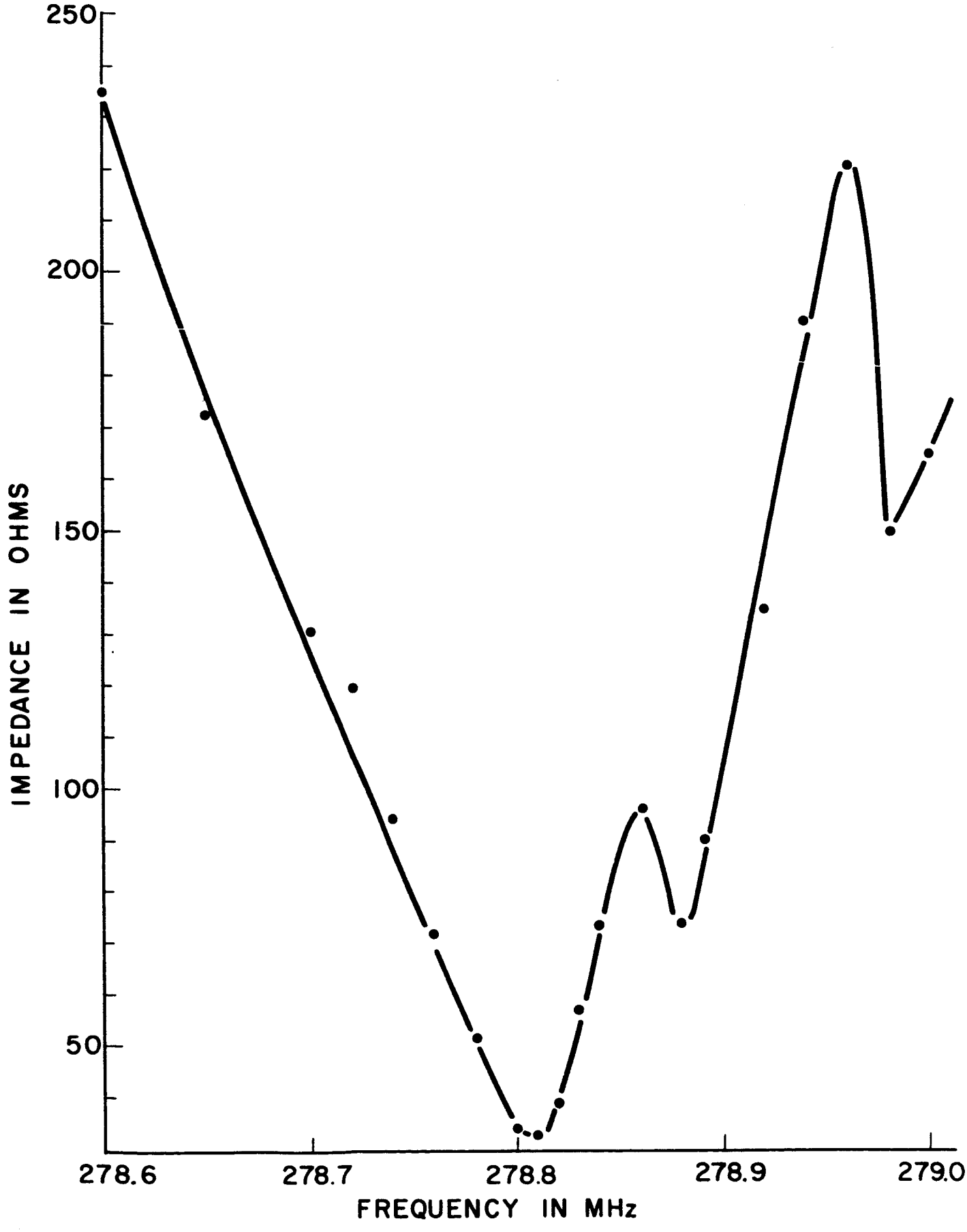

FIG. 26. IMPEDANCE vs. FREQUENCY CURVE FOR SAMPLE 047R-B.

ERD 7219

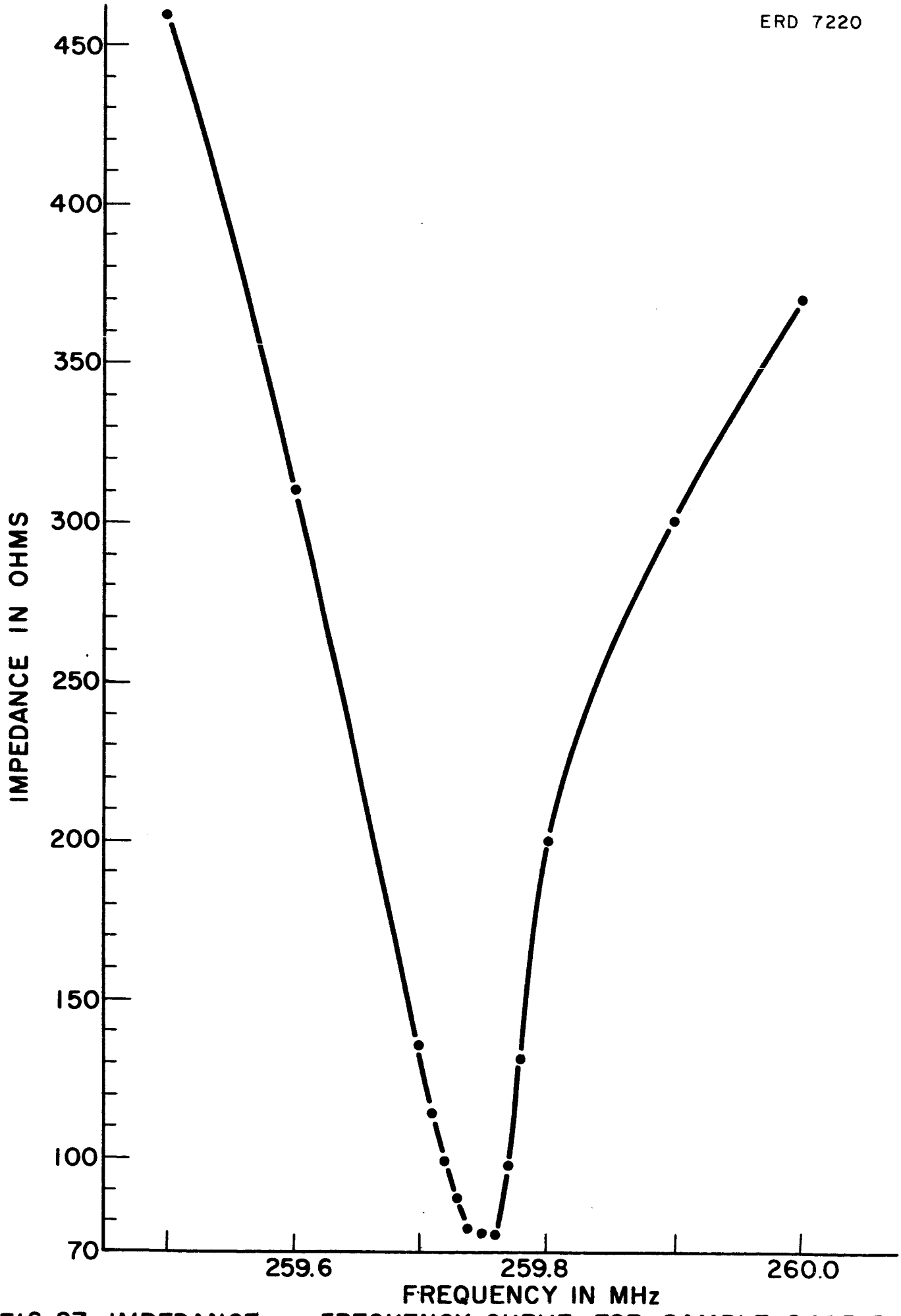

FIG. 27. IMPEDANCE vs. FREQUENCY CURVE FOR SAMPLE 049R-B.

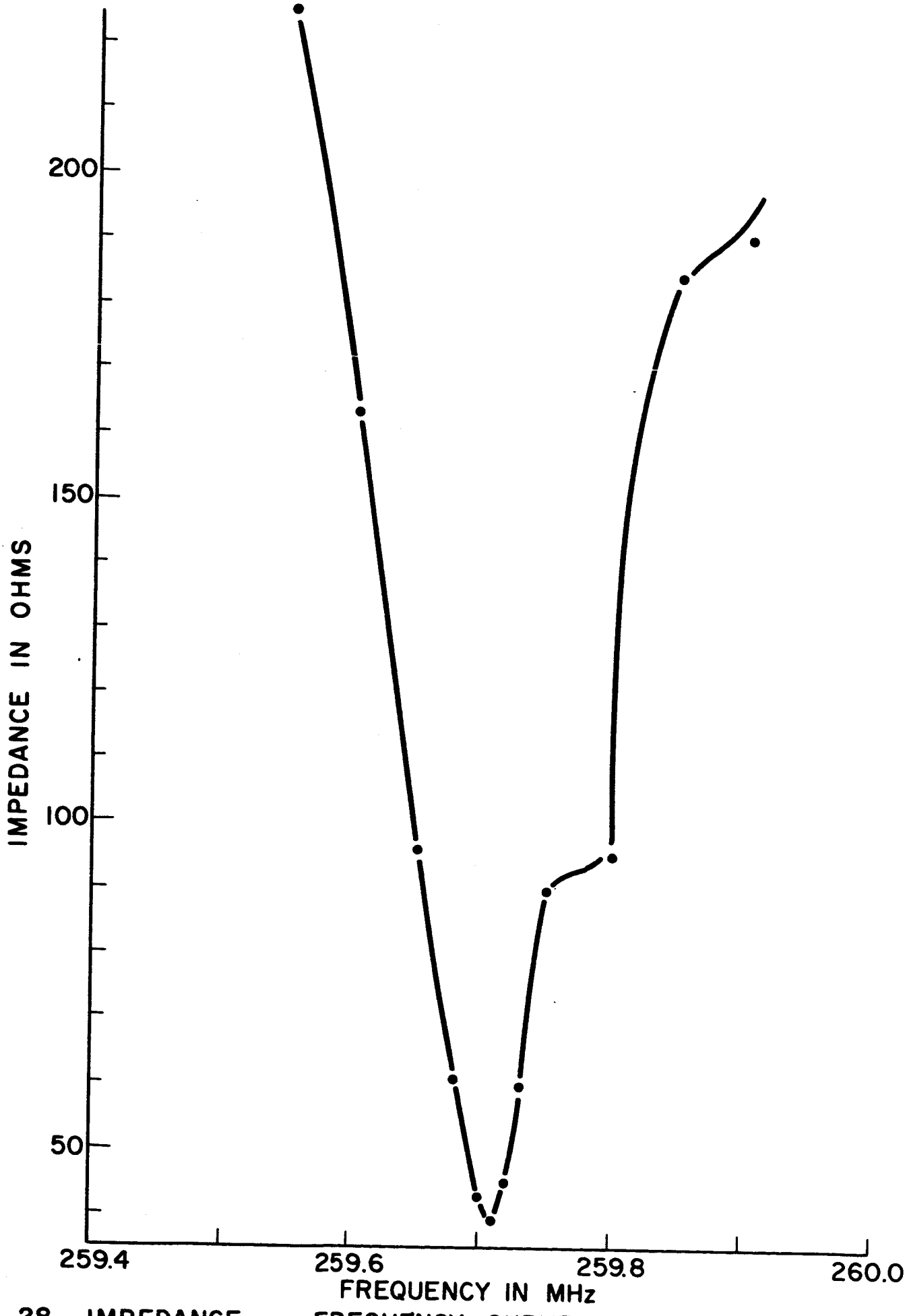

FIG. 28. IMPEDANCE vs. FREQUENCY CURVE FOR SAMPLE 053R-B.

ERD 7221

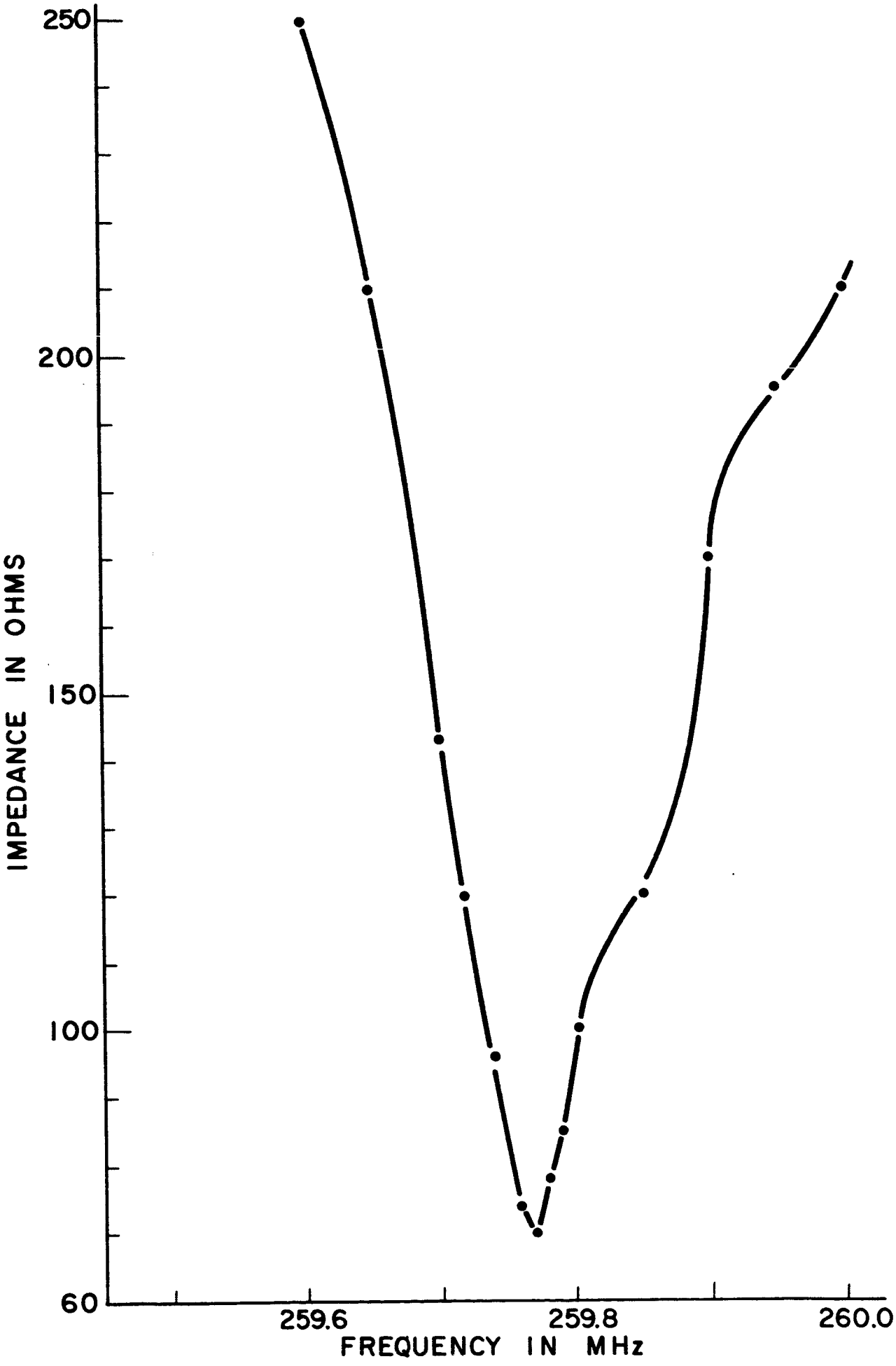

FIG.29. IMPEDANCE vs. FREQUENCY CURVE FOR SAMPLE 053R-C.

ERD 7222

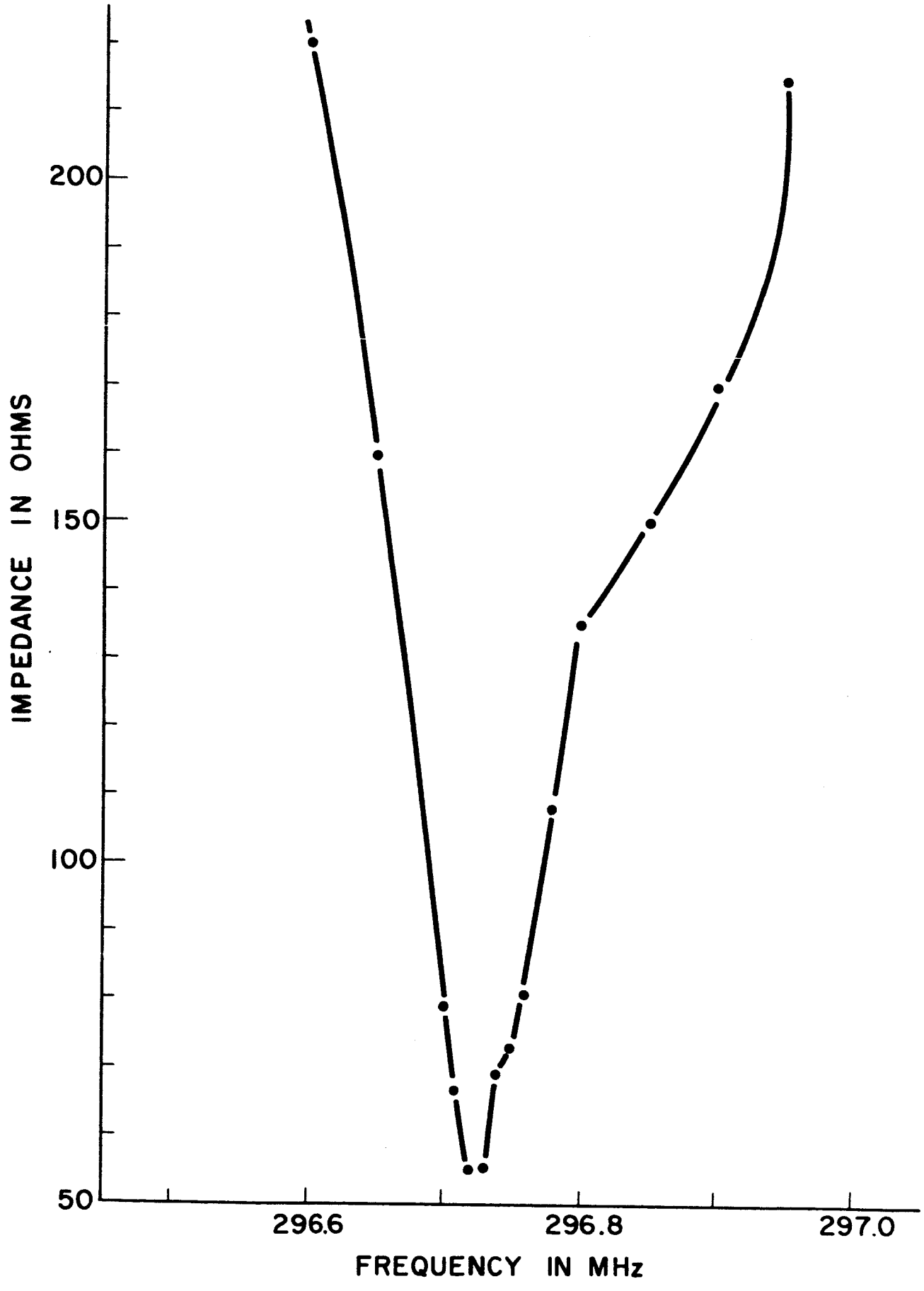

FIG. 30. IMPEDANCE vs. FREQUENCY CURVE FOR SAMPLE 054R-C.

ERD 7223

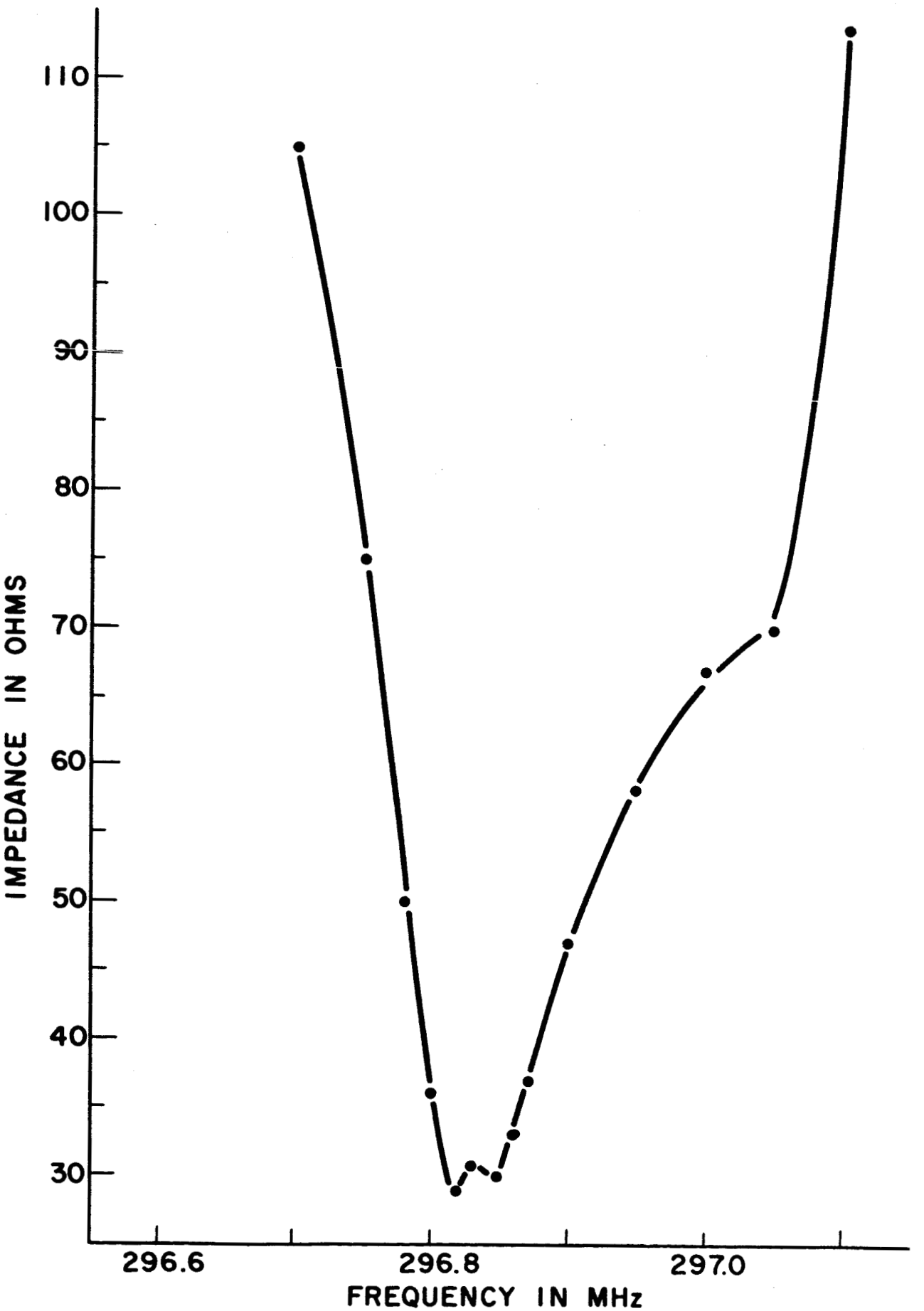

FIG. 31. IMPEDANCE vs. FREQUENCY CURVE FOR SAMPLE 056R-B

ERD 7224

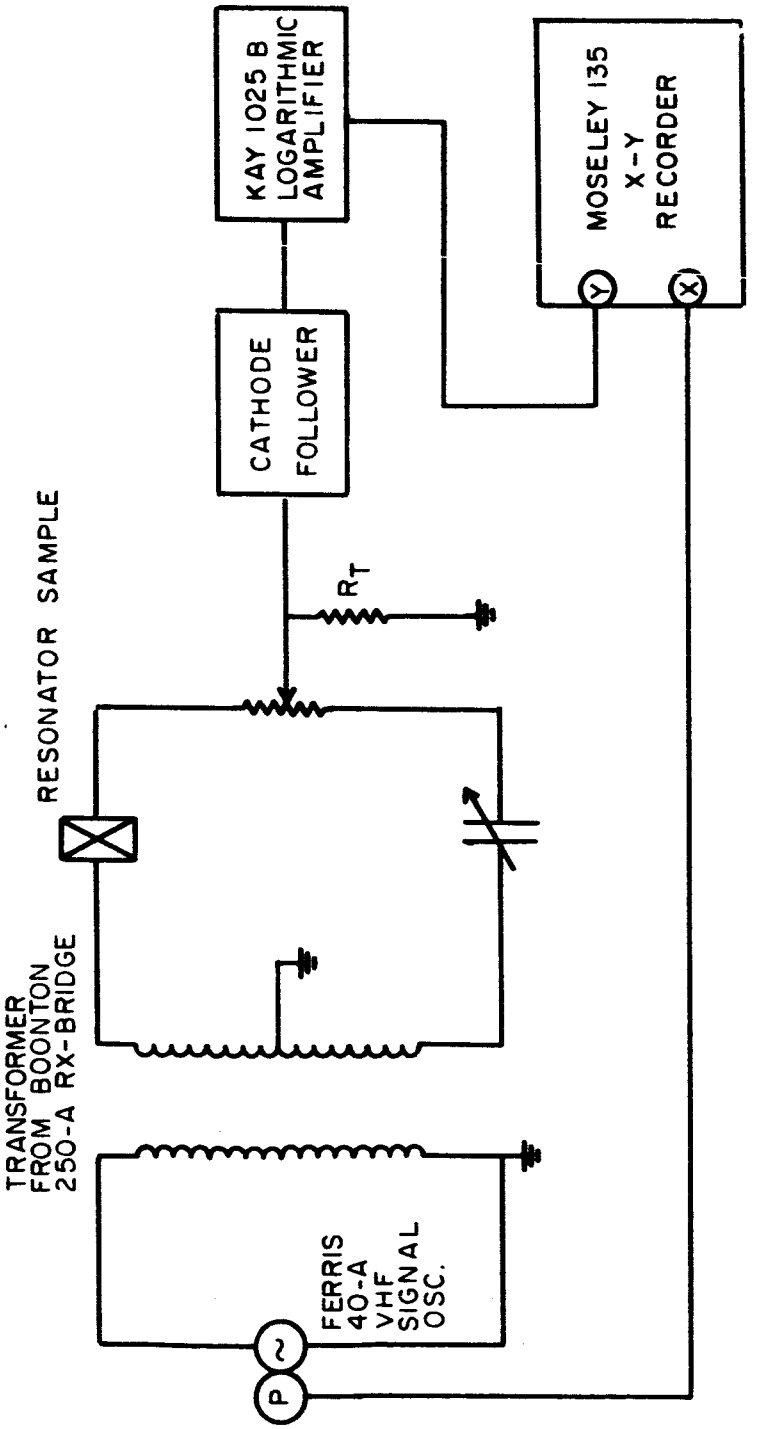

FIG 32. THE HALF-LATTICE BRIDGE WITH AUTOMATIC RECORDING OF BRIDGE ISOLATION IN DECIBELS.

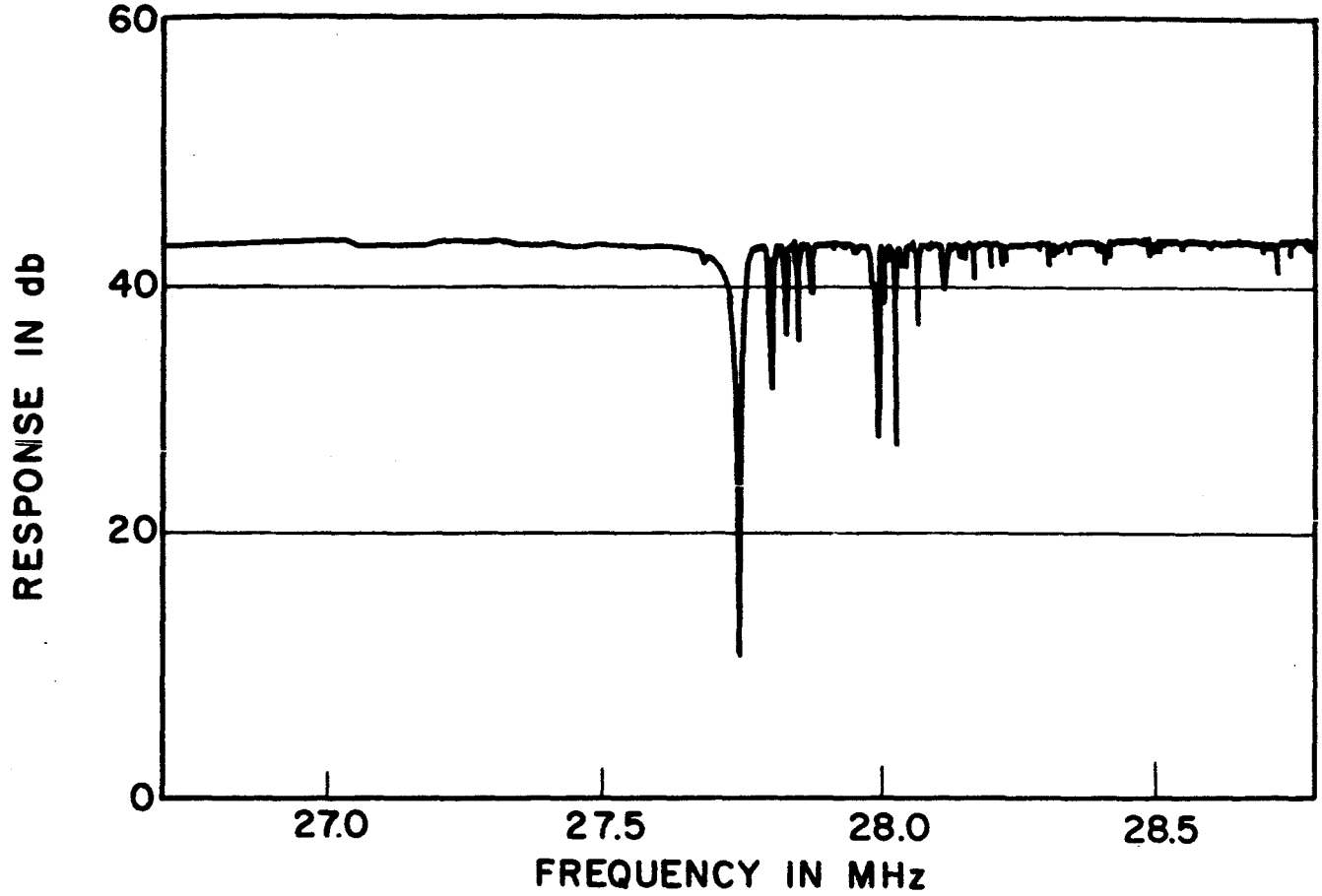

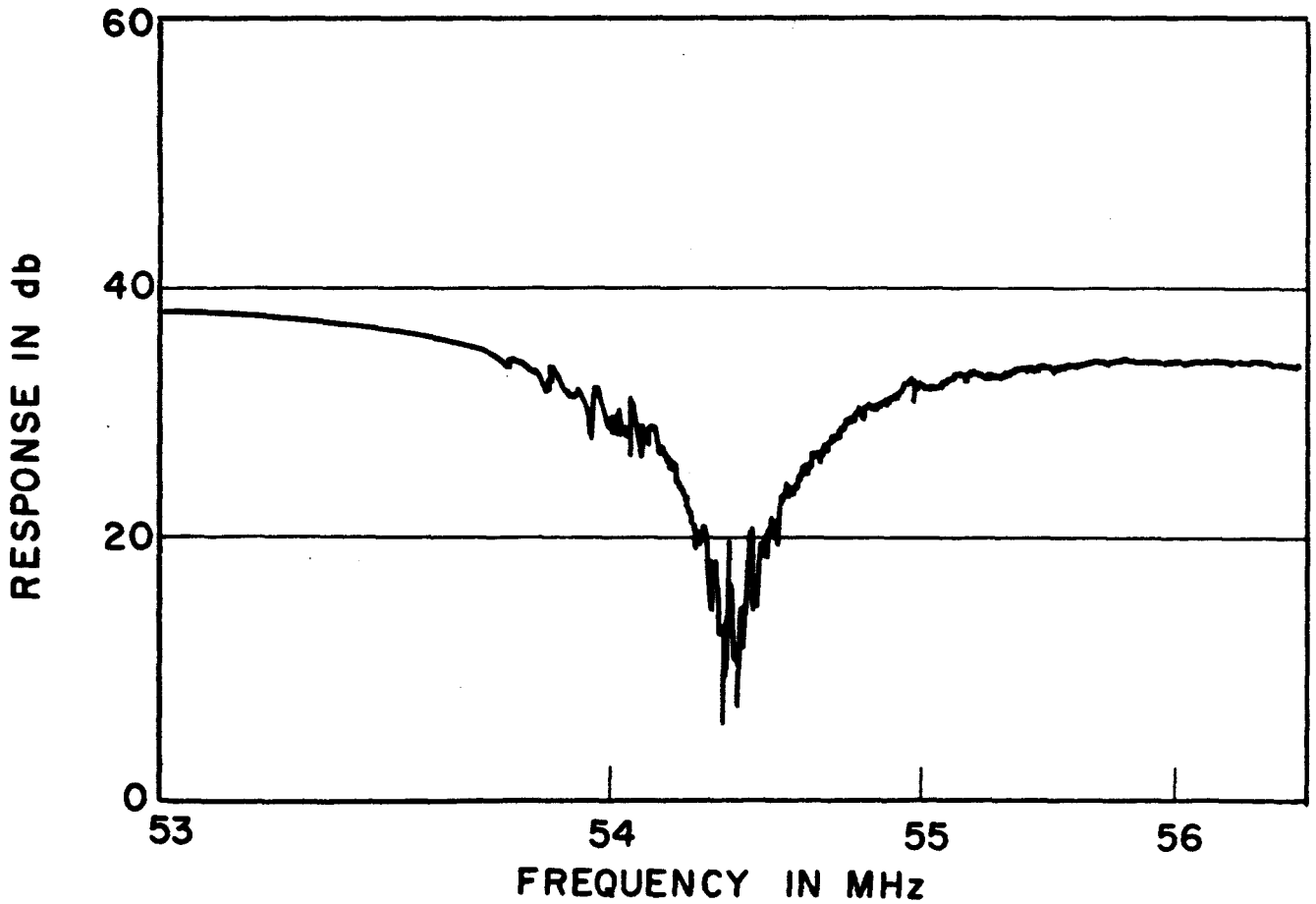

FIG. 33. FUNDAMENTAL AND SECOND OVERTONE RESPONSES OF SAMPLE 026R-A.

ERD 7227

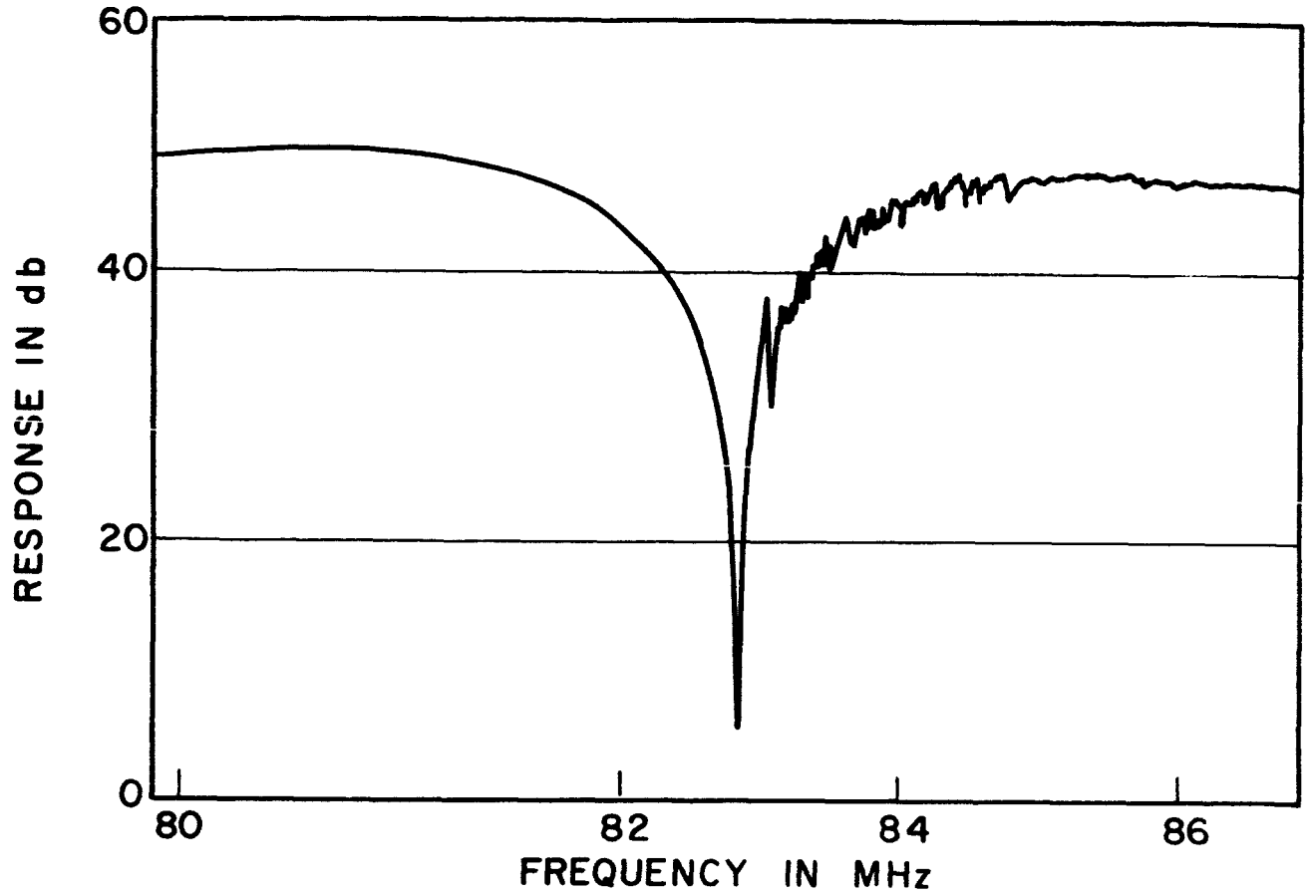

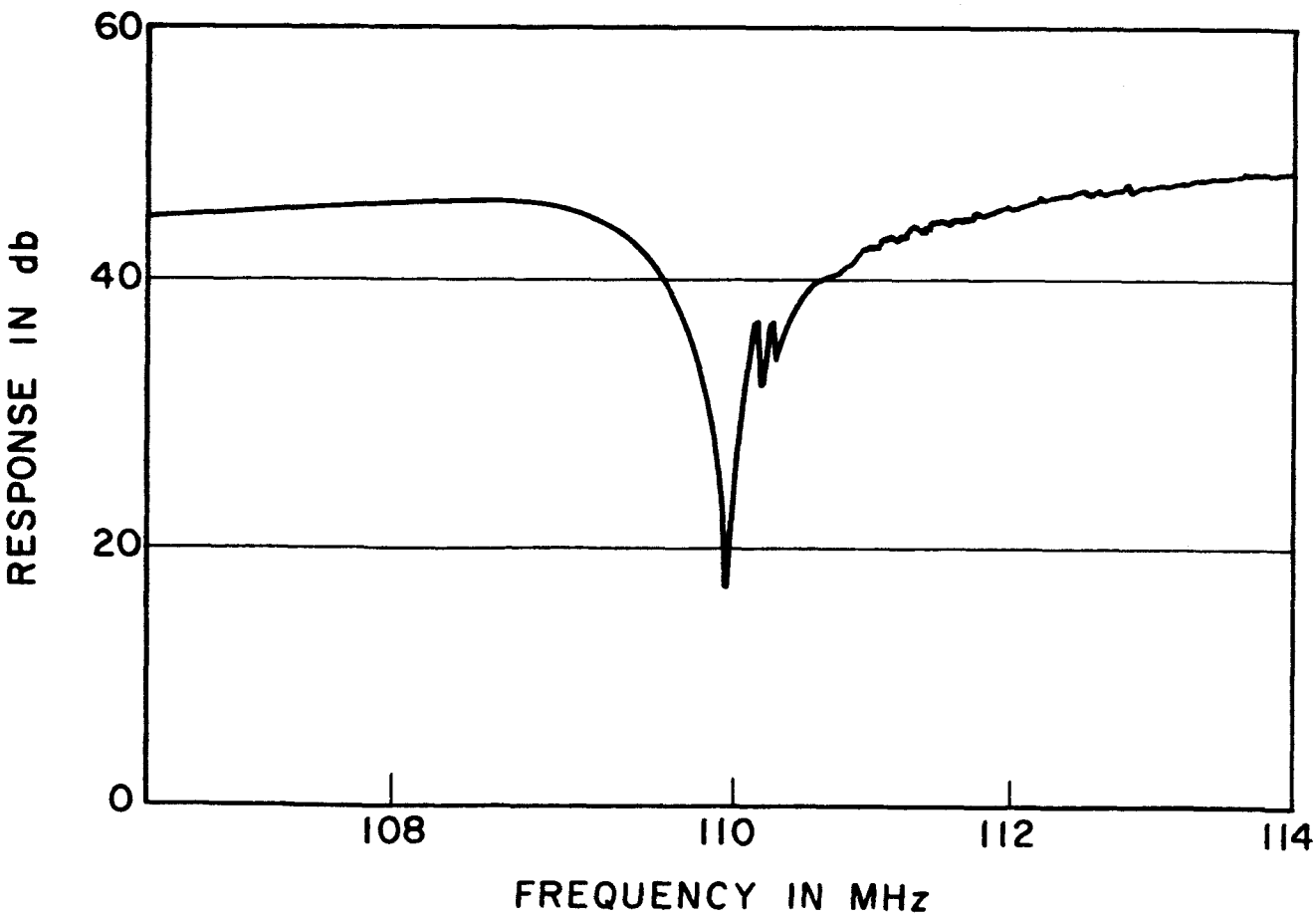

FIG. 34. THIRD AND FOURTH OVERTONE RESPONSES OF SAMPLE 026R-A.

ERD 7226

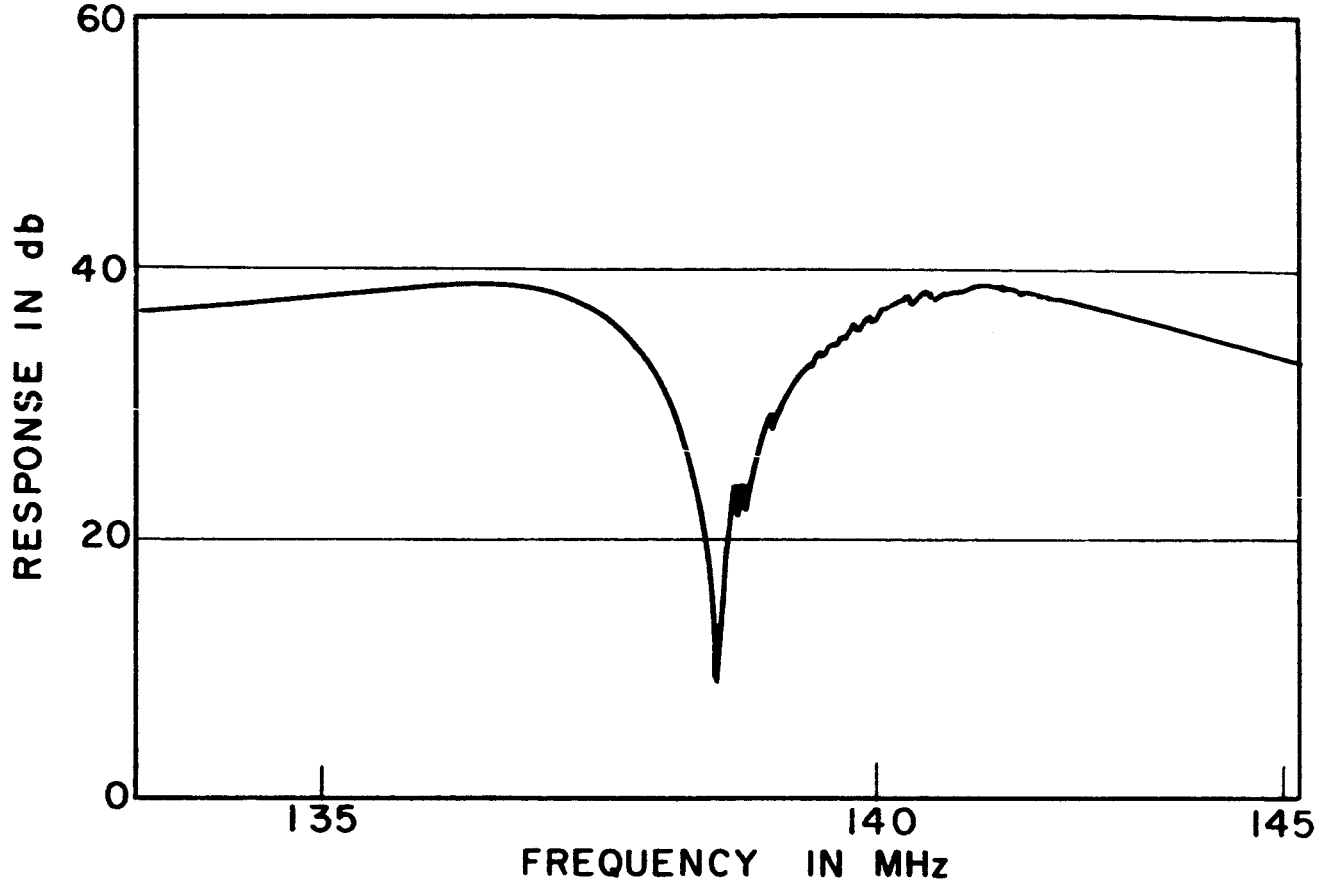

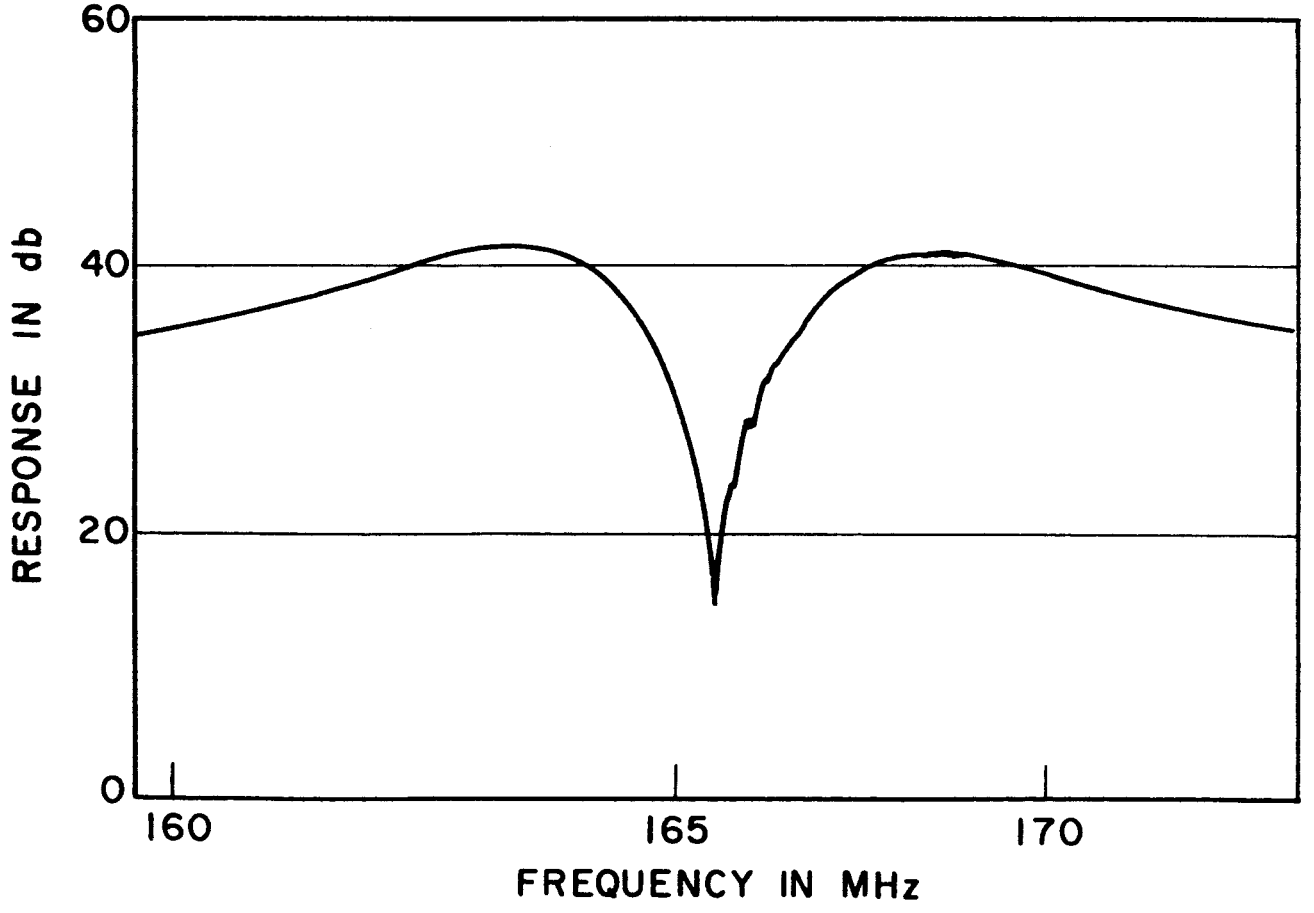

FIG. 35. FIFTH AND SIXTH OVERTONE RESPONSES OF SAMPLE 026R-A.

ERD 7225